8-2016

Mathematical Models of Ebola Virus Disease and Vaccine Preventable Diseases

Yinqiang Zheng
Purdue University

Graduate School Form
30 Updated 12/26/2015

PURDUE UNIVERSITY
GRADUATE SCHOOL
Thesis/Dissertation Acceptance

This is to certify that the thesis/dissertation prepared

By Zheng, Yiqiang

Entitled

MATHEMATICAL MODELS OF EBOLA VIRUS DISEASE AND VACCINE PREVENTABLE DISEASES

For the degree of Doctor of Philosophy

Is approved by the final examining committee:

Zhilan Feng
Chair

John Glasser

Gregery Buzzard

Aaron Yip

To the best of my knowledge and as understood by the student in the Thesis/Dissertation Agreement, Publication Delay, and Certification Disclaimer (Graduate School Form 32), this thesis/dissertation adheres to the provisions of Purdue University's "Policy of Integrity in Research" and the use of copyright material.

Approved by Major Professor(s): Zhilan Feng

Approved by: David Goldberg 5/12/2016

Head of the Departmental Graduate Program Date

MATHEMATICAL MODELS OF EBOLA VIRUS DISEASE AND VACCINE PREVENTABLE DISEASES

A Dissertation

Submitted to the Faculty

of

Purdue University

by

Yiqiang Zheng

In Partial Fulfillment of the

Requirements for the Degree

of

Doctor of Philosophy

August 2016

Purdue University

West Lafayette, Indiana

To my family.

ACKNOWLEDGMENTS

First and foremost, I would like to express my sincere gratitude to my advisor Professor Zhilan Feng, for your continuous guidance and tremendous support through my Ph.D. studies at Purdue University. I have learned a lot from your unique perspective on research and your persistent enthusiasm towards work.

I would like to express my special thanks to Dr. John Glasser and Dr. Andrew Hill at C.D.C., Professor Guang Lin and Henry Zhao at Purdue University and Dr. Nancy Hernandez-Ceron at University of Michigan for your valuable discussions and insightful advice on this work. I really appreciate our collaboration.

I would also like to thank Professors Gregory Buzzard and Nung Kwan Yip for being on my dissertation committee and for your inspiring comments on the thesis work.

I also thank Professor Yulin Zhao and Dr. Xiuli Cen for collaboration and discussion on other projects while you visited Purdue University. I have learned many things from you.

My sincere thanks go to Professor Carlos Castillo-Chavez for taking me into the MTBI summer program at Arizona State University. The experience helped me see more topics on Mathematical Biology. Meanwhile, I have learned a lot from Professors Baojun Song, Erika Camacho, Steve Wirkus, Jose Flores, and Dr. Romie Morales, Anarina Murillo and many others.

My grateful thanks also go to my parents Zhonghan Zheng and Li Sui for your love, understanding and support. Being a medical doctor, my father grows my interests in Mathematical modeling of infectious diseases and inspires me all the way in my PhD study.

Finally, I want to thank all members in our MathBio Group and all my friends at Purdue. I am grateful to have all of you in this journey. The following list is by

no means complete: Jorge Alfaro-Murillo, Christina Alvey, Katia Vogt Geisse, Nancy Hernandez-Ceron, Kyle Dahlin, Qing Han, Gayane Poghotanyan, Joan Ponce.

TABLE OF CONTENTS

Page

Page

LIST OF TABLES

LIST OF FIGURES

ABSTRACT

Zheng, Yiqiang PhD, Purdue University, August 2016. Mathematical Models of Ebola Virus Disease and Vaccine Preventable Diseases. Major Professor: Zhilan Feng.

This thesis focuses on applying mathematical models to studies on the transmission dynamics and control interventions of infectious diseases such as Ebola virus disease and vaccine preventable diseases.

Many models in studies of Ebola transmission are based on the model by Legrand et al. (2007). However, there are potential issues with the Legrand model. First, the model was originally formulated in a complex form, leading to confusion and hindering its uses in practice. To overcome the difficulty, the Legrand model is reformulated in a much simpler but equivalent form in this thesis. The reformulated model also provides an intuitive understanding of its parameterization. Second, the underlying assumptions of the Legrand model are not mathematically clear for researchers, which might lead to inadvertent misuse of the model. The assumptions are clearly identified through comparison with three models developed with clear assumptions in this thesis, one of which simplifies to the Legrand model. This three models are also built with more realistic sojourns of epidemiological processes. The comparison among these models also demonstrates the importance of the underlying assumptions as they may provide different implications on control strategies.

In addition, a concern about current Ebola models is that many of them consider only infections with typical symptoms, but Ebola presents clinically in a more complicated way. To account crudely for the wide spectrum of clinical symptoms that characterizes Ebola infection, a model is developed including asymptomatic, mild and severe infections. Comparing to the model with only typical symptoms, it shows that modeling the spectrum is important as it could affect estimation of the reproduction

number and effectiveness of interventions. Possible effective control strategies are also evaluated. We show that the spectrum of Ebola infection is important in modeling as it has implications for policy-making.

In many parts of the world, people seasonally migrate between rural and urban/peri-urban patches for economic opportunities. Migration meanwhile changes the immunity levels of patches and might increase the chance of recurrent outbreaks of vaccine preventable diseases. A three-patch meta-population model is developed that incorporates spatially explicit migration of individuals. The model is used to evaluate vaccination strategies to mitigate outbreaks. It suggests that rural-urban migration is an important factor in designing public health policies to mitigate vaccine-preventable diseases.

1. INTRODUCTION AND BACKGROUND

The 2014-15 Ebola outbreak in West Africa presents a serious threat to the public health world wide [1] and is the largest and longest since the first identification of the disease [2]. Ebola virus disease (EVD), also known as Ebola haemorrhagic fever, is a potentially severe illness with high case fatality rate in human [3, 4]. The first recorded Ebola outbreak dates to 1976 in a remote village Zaire [5, 6], and its name is from the Ebola River close to the village [7]. Since then, 24 Ebola outbreaks have been recorded in different African countries [3, 8]. It is believed that Ebola virus originated from wild animals, which transmit the pathogen to humans [9–11]. The Ebola virus is transmitted among humans through close contact with bodily fluids of infected ill and dead persons, including blood, secretions, semen [12], breast milk [13], etc. Symptoms of Ebola infection start from 3 to 21 days and commonly include, fever, fatigue, loss of appetite, vomiting, diarrhea, headache, etc, as well as specific hemorrhagic symptoms, unexplained bleeding at different organs, etc [14]. The 2014-15 Ebola outbreak in West Africa was caused by the strain called Zaire, one of three strains (Zaire, Bundibugyo, Sudan) linked to large outbreaks in Africa [8]. This outbreak started in Guinea in December 2013, and then propagated to its neighbors Liberia and Sierra Leone [2, 15]. Later, many other countries were affected, including Nigeria, Senegal, United States, Spain, Mali, United Kingdom and Italy [2]. A total of 28647 suspected cases and 11322 deaths were reported to WHO by March 27, 2016 [16].

Ebola transmission, unlike most other infectious diseases, contains three major components, including their community, hospital and post-death transmission [17–20]. Transmission among people in community is the major component in Ebola outbreaks. Absent awareness of the disease, Ebola cases grow exponentially without any prevention and intervention [2]. Most of time, people are infected by Ebola virus without

accurate diagnosis, or are wrongly diagnosed as other prevalent infectious diseases, for instance, Malaria or flu, even though they seek for medical care in these developing Africa countries [3]. Without properly handling the EVD cases, transmission in hospitals occurs widely. Hospital visitors and other non-Ebola patients are infected by Ebola virus in hospital [3]. Many healthcare workers are also infected and die of EVD, which poses further difficulties to contain the disease due to the lack of experienced healthcare workers [2]. Those deceased from EVD still have the infectious viruses in their bodily fluids, and can transmit the disease if they are not properly buried. Some traditional customs in funerals also promote the spreading, including washing, touching and kissing the deceased [19]. Thus, post-death transmission of the deceased yet not buried is also important in Ebola virus transmission.

Many mathematical models have been applied to the recent and previous Ebola outbreaks in Africa. Some of contain transmission in only community [21], in both community and hospital [22], and in community and at funerals [23]. However, few models include the three transmission components together. Legrand et al. (2007) [20] developed a model that captures Ebola virus transmission in the community, at hospital and at funerals. Although it was devoted to studies of the 1995 Congo and 2000 Uganda outbreaks [20], the Legrand model was applied to the first recorded outbreak [24] and recently to the 2014-15 outbreak in West Africa [25]. Many other models are built on ideas of Legrand et al. (for example, [26]). Thus, the Legrand model is widely used for Ebola outbreaks. However, the formulation of the Legrand model involves many intermediate parameters of no particular biological meanings that poses difficulties in understanding and applying the model to practice (see the online discussions in [25]). Further, similar to most ordinary differential equation models, the Legrand model assumes exponential sojourns implicitly for different biological states. When more than one process is considered, it seems even difficult to understand the relationship among them and how they are modeled mathematically. An investigation of these underlying assumptions is of great practical value in model verification for further application in practice.

Chapter 2 unveils the underlying assumptions of the Legrand model and provides three alternative models with more realistic assumptions. First, the Legrand model is reformulated in an equivalent form. The reformulated model is much simpler, and it does not rely on intermediate parameters as does the original formulation. Thus, it is much easier to understand and to compute the reproduction number. Second, the relationship among the epidemiological processes (recovery, death, and hospitalization) is also investigated by comparing with three models developed in Chapter 2. One of them simplifies to the Legrand model. The three models have clear assumptions and more realistic distributions of the sojourns in the epidemiological states. They are built from the basic assumptions of the relationship among the three processes of recovery, death and hospitalization using integro-differential equations. Basic and control reproduction numbers are also derived for these general models based on an understanding of stochastic processes. In addition, a detailed proof is shown of how the integro-differential equations are reduced to ordinary differential equations when the sojourns are assumed to follow Gamma distributions using so called "linear chain trick". The linear chain trick is introduced later in Section 1.2 of this chapter. Comparison among these models demonstrate that different underlying assumptions have distinct implications about control strategies.

Ebola virus disease presents clinically in a complicated way, as infected individuals report various symptoms. Symptoms of Ebola infection vary widely, including flu-like nonspecific symptoms, as well as specific hemorrhagic symptoms [14]. For the 2014-15 West Africa Ebola outbreak, even the most common symptom, fever, is not experienced by 13% of patients. There are even rare cases reported with hemorrhagic symptoms ($< 5.7\%$) [14]. This suggests that infected individuals experience a spectrum of symptoms, from mild to severe. Asymptomatic infections are quite possible, as shown in previous Ebola outbreaks [27, 28].

Chapter 3 develops a compartmental model including asymptomatic(mild), moderate and severe symptoms to account crudely for the wide spectrum of clinical symptoms that characterizes Ebola infection. The model is based on Model II in Chapter 2,

which is augmented by including asymptomatic and moderately symptomatic infection to susceptible, exposed, infectious, hospitalized and deceased (not yet buried) and recovered compartments. The model captures the dynamics of the 2014-15 Liberia outbreak when calibrated to the case data. Our estimate of the basic reproduction number is 1.83 (CI: 1.73, 1.95), consistent with the WHO response team's estimate using early outbreak case data. We also estimate the effectiveness of interventions using case data before and after their introduction. As the final epidemic size is linked to the timing of interventions in an exponential fashion, a simple empirical formula is provided to guide policy-making. It suggests that early implementation could significantly decrease final size. We also compare our model to one with typical symptoms by disabling mild and moderate symptoms. The model with only typical symptoms overestimates the basic reproduction number and effectiveness of control measures, and exaggerates changes in final size attributable to the timing of interventions. In addition, uncertainty about asymptomatic or mild and moderate symptoms affects the variability of the basic reproduction number. Sources of variability are quantified by Sobol indices, which suggest the need for further study. Possible control strategies are evaluated through sensitivity analyses, indicating that simultaneously strengthening contact tracing and effectiveness of isolation in hospital would be most effective. In this chapter, we show that the spectrum of Ebola symptoms is important in modeling as it has implications for policy-making.

Chapter 4 develops models to evaluate public health policies for vaccine-preventable diseases. Unlike other models assuming homogeneous mixing, the model in this chapter explicitly includes urban, peri-urban and rural patches. A deterministic discrete model is used to determine the immunity levels of patches in the long term, in which models the rural patch has lower immunity than the urban/peri-urban patches. Thus, seasonal migration of rural residents between rural to urban/peri-urban patches possibly changes the immunity levels of patches dynamically. This increases chances of recurrent outbreaks. A short term stochastic model is developed to capture migration as well as disease transmission. Stochastic simulations evaluate the effects of alterna-

tive vaccination strategies on preventing disease outbreaks, examine the distribution of possible outcomes, and compare the likelihood of outbreak mitigation and prevention across immunization policies. The results may help public health officials to ensure the best possible use of available vaccines. They also suggest that the spatial structure is an important factor in designing the public health policies of vaccination.

The remainder of this chapter is organized as follows. Section 1.1 includes a brief summary of mathematical models applied to Ebola outbreaks. Section 1.2 introduces the linear chain trick to reduce integro-differential equations to ordinary differential equations. Sections 1.3 and 1.4 includes some commonly used parameter estimation techniques and uncertainty quantification techniques can be found. These sections are closely connected to the work presented in the following chapters.

1.1 Ebola models

This section reviews some of the Ebola models that have been applied to Ebola outbreaks in Africa. SEIR models in Chowell et al. [29] and [30] were applied to study the 1995 and 2000 outbreaks in Congo and Uganda. However, the SEIR does not capture the transmission in hospital and post-death transmission, which are important components in the transmission chain for EVD. Legrand et al. [20] extended the SEIR model by including compartments for hospitalized individuals and those deceased yet not buried. They applied their model to the Congo and Uganda outbreaks in 1995 and 2000. It has become a widely used model for Ebola outbreaks, having been applied to first known 1976 outbreak in Congo [24] and recent 2014-15 outbreak in West Africa [25, 31, 32]. Many other models are based on the idea in the Legrand model, for example, [26], which contains a more complex model with 36 compartments.

In this section, the Legrand model [20] is explained. The model includes: the susceptible S, the latent (exposed) E , the infectious I, the hospitalized H, and the disease-induced death and not sanitarily buried D as well as the recovered R and the total population $N = S + E + I + H + R$.

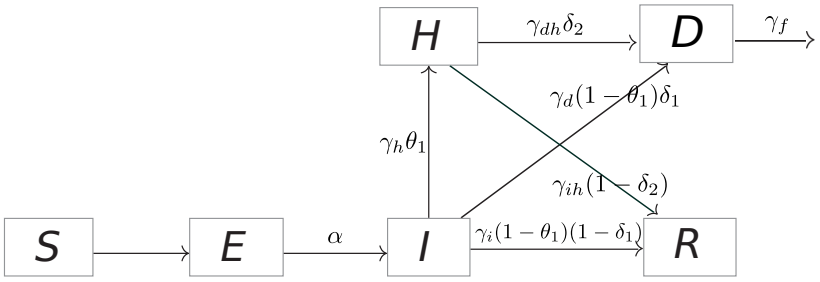

Fig. 1.1. Diagram of the Legrand Model [20].

Based on the diagram, the model in [20] is as follows,

$$\begin{aligned}
\frac{dS}{dt} &= -\frac{1}{N}(\beta_I SI + \beta_H SH + \beta_D SD), \\
\frac{dE}{dt} &= \frac{1}{N}(\beta_I SI + \beta_H SH + \beta_D SD) - \alpha E, \\
\frac{dI}{dt} &= \alpha E - (\gamma_h\theta_1 + \gamma_i(1-\theta_1)(1-\delta_1) + \gamma_d(1-\theta_1)\delta_1)I, \\
\frac{dH}{dt} &= \gamma_h\theta_1 I - (\gamma_{dh}\delta_2 + \gamma_{ih}(1-\delta_2))H, \\
\frac{dD}{dt} &= \gamma_d(1-\theta_1)\delta_1 I + \gamma_{dh}\delta_2 H - \gamma_f D, \\
\frac{dR}{dt} &= \gamma_i(1-\theta_1)(1-\delta_1)I + \gamma_{ih}(1-\delta_2)H,
\end{aligned} \tag{1.1}$$

where β_I, β_H and β_D are the transmission rates for community, hospital and funerals, $1/\alpha$ is the duration of the incubation period, $1/\gamma_h$ is the time from onset to hospitalization, $1/\gamma_d$ is the time from onset to death, $1/\gamma_i$ is the time from onset to end of infectiousness for survivors, and $1/\gamma_f$ is the time from death to traditional burial.

The parameters θ_1, δ_1 and δ_2 are defined through the probability of hospitalization p and case-fatality ratio f based on the following expressions [20],

$$\theta_1 = \frac{p[\gamma_i(1-\delta_1) + \gamma_d\delta_1]}{p[\gamma_i(1-\delta_1) + \gamma_d\delta_1] + (1-p)\gamma_h} \tag{1.2}$$

and

$$\begin{aligned}
\delta_1 &= \frac{f\gamma_i}{f\gamma_i + (1-f)\gamma_d}, \\
\delta_2 &= \frac{f\gamma_{ih}}{f\gamma_{ih} + (1-f)\gamma_{dh}}.
\end{aligned} \tag{1.3}$$

Remark that the parameters θ_1, δ_1 and δ_2 are intermediate parameters without particular biological meanings. The Legrand model also imposes the constraints [20]

$$\gamma_{ih} = \frac{1}{\frac{1}{\gamma_i} - \frac{1}{\gamma_h}} \quad \text{and} \quad \gamma_{dh} = \frac{1}{\frac{1}{\gamma_i} - \frac{1}{\gamma_h}}. \tag{1.4}$$

From complex expressions, it is difficult to understand the formulation, parametrization, and underlying assumptions about the epidemiological processes, including hospitalization, recovery and death. In more detail, exponential sojourns of disease stages are commonly assumed in ODEs models. For example, if infected individuals are assumed to recover at a constant per-capita rate γ, then the infectious period is assumed to follow exponential distribution, i.e. the probability that an individual is still infectious $s > 0$ time since onset is

$$P_I(s) = e^{-\gamma s},$$

in which case the mean of infectious period is

$$D_I = \frac{1}{\gamma}.$$

It becomes complicated for the Legrand model because once an individual enters the infectious class I, he or she can leave due either to hospitalization (entering the H class) or recovery without being hospitalized (entering the R class from I) or death without being hospitalized (entering the D class from I) with mean durations $1/\gamma_h$, $1/\gamma_i$, $1/\gamma_d$, respectively. This is equivalently assumed that individuals after onset enters the H, R and D classes at constant rates γ_h, γ_i, γ_d, respectively. From the I equation, the model assumes that the overall rate of leaving the I class is a combination of the rates γ_h, γ_i, γ_d as

$$\Delta = \theta_1\gamma_h + (1-\theta_1)\delta_1\gamma_d + (1-\theta_1)(1-\delta_1)\gamma_i. \tag{1.5}$$

However, it is not clear what underlying assumptions have been made about the relationship of the three epidemiological processes, i.e. hospitalization, recovery without hospitalization, and death without hospitalization. Let IH, IR and ID denote the

events of the three processes. At first, it may seem that the waiting times of IR, IH and ID are assumed to be independent and all follows exponential distributions with mean durations $1/\gamma_h$, $1/\gamma_i$, $1/\gamma_d$, respectively. If so, the mean overall rate of exiting the I compartment would be different from Δ in (1.5). Let random variables T_P, T_L and T_M represent the waiting times associated with events IR, IH and ID and denote their survival functions by $P(t) = e^{-\gamma_i t}$, $L(t) = e^{-\gamma_h t}$ and $M(t) = e^{-\gamma_d t}$, respectively, then the overall waiting time in I has survival functions defined as

$$\begin{aligned} \mathbb{P}\left(\min\left\{T_P, T_L, T_M\right\} > t\right) &= \mathbb{P}\left(\left\{T_P > t\right\} \cap \left\{T_L > t\right\} \cap \left\{T_M > t\right\}\right) \\ &= \mathbb{P}\left(T_P > t\right)\mathbb{P}\left(T_L > t\right)\mathbb{P}\left(T_M > t\right). \end{aligned} \tag{1.6}$$

Thus, the mean overall duration of the I compartment is

$$\mathbb{E}\Big(\min\left\{T_P, T_L, T_M\right\}\Big) = \int_0^\infty P(t)L(t)M(t)dt = \frac{1}{\gamma_i + \gamma_h + \gamma_d}.$$

It follows that the overall exiting rate of I is $\gamma_i + \gamma_h + \gamma_d$, which is inconsistent with Δ in (1.5). Similarly, for hospitalized individuals, there are two possible events, recovery or death, denoted by HR and HD. Therefore, a natural question is what the assumptions are made underlying the three events IH, IR and ID and the two events HR and HD.

The complex formulation also leads to an unnecessarily complex expression for the reproduction number. The reproduction number [20] is computed using next generation matrix approach [33],

$$R_0 = \frac{\beta_I}{\Delta} + \frac{\frac{\gamma_h \theta_1}{\gamma_{dh}\delta_2 + \gamma_{ih}(1-\delta_2)}\beta_H}{\Delta} + \frac{\delta\beta_D}{\Delta}. \tag{1.7}$$

This expression (1.7) is complex and hard to interpret biologically.

In Chapter 2, a reformulated model is provided to better understand the model formulation and parameterization. The reformulated model is shown to be equivalent to its original formulation, but much cleaner and simpler, and it provides an intuitive interpretation of the Legrand model. The reproduction number for the reformulated model is a much simpler expression. It is of essential importance to accurately identify

the underlying assumptions behind models so that they closely approximate biological systems of interest. The underlying assumptions of the Legrand model are identified through comparison to three models, which are developed in Chapter 2. The three alternatives have clear assumptions and they are formulated from the stochastic processes of hospitalization, recovery and death using integro-differential equations. The integro-differential equations are then reduced to ordinary differential equations using the "linear chain trick" (see the following section for more detail), when the sojourns are assumed to follow more realistic Gamma distributions. One of the three model simplifies to Legrand model so that the underlying assumptions are identified.

1.2 Linear chain trick

A common underlying assumption of ordinary differential equation based epidemiological models is about exponentially distributed sojourns of disease stages (e.g. the exponentially distributed infectious period). However, exponentially distributed durations might provide biased or misleading estimates (for example, [34]). Similarly, for discrete models, geometrically distributed sojourns are equivalent to exponentially ones (for examples, [35, 36]). Many works [34, 37–39], therefore, adopt more general distributions for sojourns, which result in integro-differential equations. When general distributions are specified as Gamma distributions, the integro-differential equations can be reduced to ordinary differential equations with multiple sub-stages, which is known as "linear chain trick". This linear chain trick is also used for delayed differential equations [40]. This technique is used for complex models in Chapter 2.

In this section, I provide a simple example using "linear chain trick" to reduce a SEIR with generally distributed infectious period to a set of ordinary differential equations when the general distribution is assumed as Gamma. The technique relies on the expression of the Gamma survival function. For a Gamma distribution with

shape and rate parameter $(n, n\gamma)$ (where $n \geq 1$ is an integer), the probability density function $g(t)$ is

$$g(t) = \frac{n\gamma(n\gamma t)^{n-1}}{(n-1)!}e^{-n\gamma t}, \tag{1.8}$$

and the survival fuction $G(t)$ is given by

$$G(t) = \sum_{j=1}^{n} \frac{(n\gamma t)^{j-1}e^{-n\gamma t}}{(j-1)!}. \tag{1.9}$$

This form of Gamma survival function is derived based on the property that sum of independently and identically distributed exponential random variables follows Gamma distribution and these exponential random variables can be viewed as waiting times in a Poisson process (see Section 5.6.1 of Ross (2002) [41]). In more detail, denote by W the waiting time until the n-th event in the Poisson process with rate $n\gamma$. If $n = 1$, it is known that W is exponentially distributed. If $n \geq 1$, then W follows Gamma distribution with shape and rate parameter $(n, n\gamma)$. Denote by $F(t)$ the cumulative distribution function of W. Then

$$\begin{aligned}
F(t) &= 1 - \mathbb{P}(W < t), \\
&= 1 - \mathbb{P}(\text{fewer than } n \text{ events in } [0,t]), \\
&= 1 - \mathbb{P}(0 \text{ events or } 1 \text{ event or } \ldots \text{ or } n-1 \text{ events in } [0,t]), \\
&= 1 - \sum_{k=0}^{n-1} \frac{(n\gamma t)^k e^{-n\gamma t}}{k!} \text{ or } 1 - \sum_{j=1}^{n} \frac{(n\gamma t)^{j-1}e^{-n\gamma t}}{(j-1)!},
\end{aligned}$$

where the probability of the event $\{k \text{ events in } [0,t]\}$ is $(n\gamma t)^k e^{-n\gamma t}/k!$ based on the Poisson process with rate $n\gamma$.

A standard SEIR model with generally distributed infectious period is

$$\begin{aligned}
\frac{dS}{dt} &= -\beta SI/N, \\
\frac{dE}{dt} &= \beta SI/N - \alpha E, \\
I(t) &= \int_0^t \alpha E(s)P(t-s)ds + I(0)P(t), \\
R(t) &= \int_0^t \left[\int_0^\tau \alpha E(s) g_P(\tau - s)ds + I(0)g_P(\tau) \right] d\tau,
\end{aligned} \tag{1.10}$$

where P is the survival function for the infectious period, i.e., the probability that an individual is still infectious $s > 0$ time since onset, and g_P is the negative derivative of the survival function. In more detail, $I = I(t)$ is the total number of infectious individuals at time t, including the individuals who became infectious $t - s$ units of time ago ($0 < s < t$) and have not recovered yet, as well as those individuals who were infectious at time 0 and are still in the I class at time t. Then differentiating $I(t)$, it gives

$$I'(t) = \alpha E(t) - \left[\int_0^t \alpha E(s) g_P(t-s) ds + I(0) g_P(t)\right] \tag{1.11}$$

where the first term $\alpha E(t)$ is the inflow to I class and the second term is the outflow from I class to R class at time t. Therefore, $R = R(t)$ equation is an integral equation as in equations (1.10), which is the total number of the recovered individuals leaving from I class at τ from time 0 to t.

Next, the integro-differential equations can be shown to reduced to ordinary differential equations, if the survival distribution is Gamma with shape and rate parameter $(n, n\gamma)$ as (1.9). In this case, the I equation in (1.10) becomes

$$\begin{aligned} I(t) &= \int_0^t \alpha E(s) \sum_{j=1}^{n} \frac{(n\gamma(t-s))^{j-1} e^{-n\gamma(t-s)}}{(j-1)!} ds + I(0) \sum_{j=1}^{n} \frac{(n\gamma t)^{j-1} e^{-n\gamma t}}{(j-1)!}, \\ &\doteq \sum_{j=1}^{n} I_j(t) \end{aligned}$$

where

$$I_j(t) = \int_0^t \alpha E(s) \frac{(n\gamma(t-s))^{j-1} e^{-n\gamma(t-s)}}{(j-1)!} ds + I(0) \frac{(n\gamma t)^{j-1} e^{-n\gamma t}}{(j-1)!},$$

for $j = 1, \cdots, n$. Differentiating each $I_j(t)$ equations, it gives

$$\begin{aligned} \frac{dI_1}{dt} &= \alpha E - n\gamma I_1, \\ \frac{dI_j}{dt} &= n\gamma I_{j-1} - n\gamma I_j, \text{ for } j = 2, \cdots, n. \end{aligned}$$

Differentiating $R(t)$ equation, gives

$$\frac{dR}{dt} = n\gamma I_n,$$

Therefore, model (1.10) becomes a system of ordinary differential equations

$$\begin{aligned}
\frac{dS}{dt} &= -\beta SI/N, \\
\frac{dE}{dt} &= \beta SI/N - \alpha E, \\
\frac{dI_1}{dt} &= \alpha E - n\gamma I_1, \\
\frac{dI_j}{dt} &= n\gamma I_{j-1} - n\gamma I_j, \text{ for } j = 2, \cdots, n, \\
\frac{dR}{dt} &= n\gamma I_n.
\end{aligned} \tag{1.12}$$

Remark that the substages I_j's are not only for the mathematical convenience, but also may represent the individuals with typical symptoms shown in the j-th sub-stage. Although the infectious compartment is stratified into n sub-stages, it does not necessarily mean that every individual spends the same amount of time in each sub-stage or have the same total infectious period. It only describes the average behaviors of infectious individuals, so some individuals could progress through the sub-stages faster than others.

1.3 Parameter estimation

In this section, parameter estimation methods are introduced as the basis for the data fitting in Chapter 4. Commonly used data fitting techniques include least squares and maximum likelihood estimation [42]. I will provide an example that is adapted from [21] and [29]. The example is based on a SEIR model that has been applied to Ebola breaks of Congo (1995) and Uganda (2000) as well as Guinea, Liberia, Sierra Leone of West Africa (2014)

$$\begin{aligned}
\frac{dS}{dt} &= -\beta SI/N, \\
\frac{dE}{dt} &= \beta SI/N - \alpha E, \\
\frac{dI}{dt} &= \alpha E - \gamma I, \\
\frac{dR}{dt} &= \gamma I,
\end{aligned}$$

where S, E, I and R denote the population of susceptible, exposed, infectious, and removed individuals, β is the tranmission rate, $1/\alpha$ is the average duration of incubation, and $1/\gamma$ is the average infectious period.

The basic reproduction number for this model is simply given by

$$R_0 = \beta/\gamma,$$

which is the quantity to be estimated.

To connect the model and observed case data, an auxiliary equation is defined as

$$\frac{dC}{dt} = \alpha E,$$

where C represents the cumulative number of Ebola cases.

The reported cumulative numbers of cases for the 2014-15 West Africa outbreak are available through the WHO website. Here we used the case data presented in [21] for Liberia as an example. The parameters $1/\alpha = 5.3$ days and $1/\gamma = 5.61$ days are assumed in the example, which are estimates from the 1995 Congo outbreak [29]. The population at risk is assumed to be 1 million [21]. Denote by O_i and C_i the observed cases and the model predicted cases at time t_i for $i = 1, \cdots, n$. In this example, the transmission rate β is to be estimated.

The method of least squares estimation is to minimize the sum of squared errors

$$SSE = \sum_{i=1}^{n} (C_i - O_i)^2$$

to obtain the best fitting parameters, where n is the number of observations.

The method of maximum likelihood is a statistical inference method that maximizes the likelihood (or probability) of the observed data. Count data are commonly assumed to follow Poisson distribution, i.e. $O_i \sim Poisson(C_i)$. Then, to obtain the best fitting parameters, maximize the likelihood or log likelihood function,

$$log(\text{Likelihood}) = \sum_{i=1}^{n} log(f_{Poisson}(O_i; C_i))$$

where $f_{Poisson}(\cdot; C_i)$ is the probability mass function of the Poisson distribution with mean C_i. In addition to Poisson distribution, other distributions, for example, Normal distribution, Binomial and Negative Binomial distributions are also used.

Remark that least squares and maximum likelihood estimation are equivalent, given that observed cases follow Normal distribution of model predicted cases C_i (See Chapter 4 in [42]). This is because the Normal log likelihood is $log(f_{Normal}(O_i; C_i, \sigma^2) = a(C_i - O_i)^2 + b$, where $f_{Normal}(\cdot; C_i, \sigma^2)$ is the probability density function of Normal distribution with mean C_i and variance σ^2, and a, b are constants independent of C_i and O_i. Therefore, the two methods provide the same estimates.

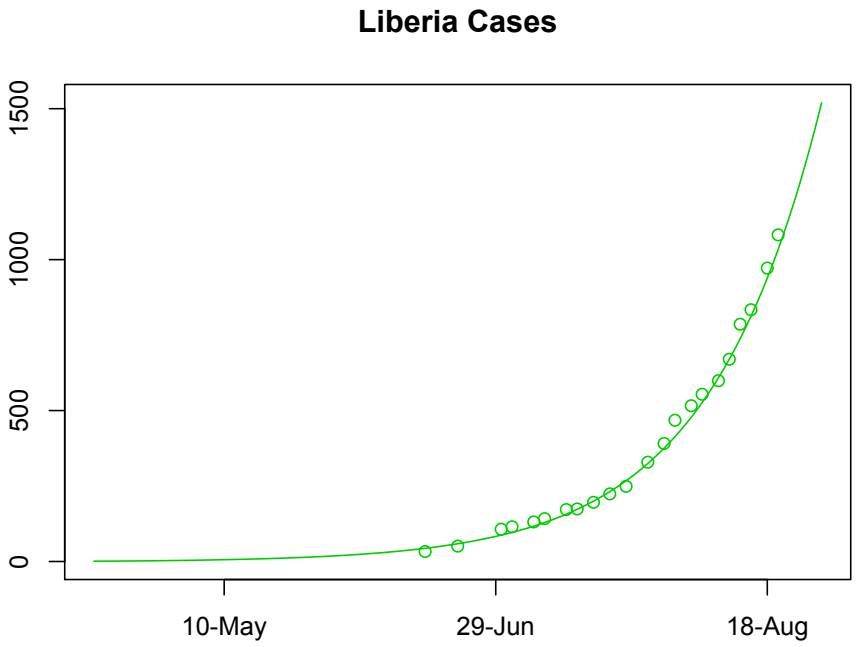

Fig. 1.2. Fitting an SEIR model to Liberia Cases as an example. Estimated R_0 is 1.59.

These two methods can be implemented in R using packages bbmle and deSolve [21, 43]. The specified ODE model is numerically sovled by the ODE solver package deSolve. To ensure that the parameters to be estimated are in the correct ranges, those

to-be-estimated parameters are transformed if they are assumed positive $(0, \infty)$ or in the range of $(0, 1)$ using log or logistic transformation, respectively. Implementation has four major parts: 1) a function that specifies a model, 2) a function that calculates the negative log-likelihood or the sum of squared errors , 3) a call to a function that does the optimization to search best parameter values, and 4) analyzing the results.

1.4 Sensitivity analysis

In this section, some useful sensitivity and uncertainty analysis techniques are shown as the basis for Chapter 4. Sensitivity analysis is routinely employed to evaluate how and to what extents model outputs are affected by model inputs [44], which is divided into local and global analyses. Denote by u a scaler output and by $\boldsymbol{x} = (x_1, \cdots, x_n)$ an n-dimensional input, then a function $u = f(\boldsymbol{x})$ defines the relationship between the output and the input. Local sensitivity analysis is about evaluation of the partial derivatives $(\partial u/\partial x_k)_{\boldsymbol{x}=\boldsymbol{x}^*}$ that describes the sensitivity of $u^* = f(\boldsymbol{x}^*)$ with respect to x_k locally at $\boldsymbol{x} = \boldsymbol{x}^*$. Sometimes elasticity is defined as the proportional changes in u with respect to proportional changes in x_k, i.e., $[(\partial u/u^*)/(\partial x_k/x_k^*)]_{\boldsymbol{x}=\boldsymbol{x}^*}$. Therefore, local sensitivity and elasticity analyses by definition study the local linear dependence between the output and inputs.

The global sensitivity approach does not need to specify the particular input $\boldsymbol{x} = \boldsymbol{x}^*$ but considers the output $u = f(\boldsymbol{x})$ for all $\boldsymbol{x}$ in the possible range. Thus, global sensitivity analysis is used to study the overall dependence between the output and its inputs instead of their dependence at a given point. Two popular and widely used global sensitivity analysis methods are illustrated, partial rank correlation coefficients (PRCC) and Sobol indices. Both methods involve the sampling of inputs in their ranges, for which a method called Latin hypercube sampling (LHS) is widely used.

Latin hypercube sampling is a stratified sampling method that controls how random samples are drawn from a probability distribution of an input. A distribution is assigned to each input variables, which specifies the range of possible values and the

probability of each value. Two popular distributions in global sensitivity analysis are triangular and uniform. The triangular distribution is used when a most likely value and range of the input are estimable, while the uniform distribution is used when only the range is estimable. For each input, the probability density function (PDF) is divided into `N` equiprobable partitions and samples are obtained in each partition. The `N` sample values for one parameter are generated and then are randomly combined with samples for other parameters through shuffling. This process forms length `N` vectors of sampled parameter values, called Latin hypercube samples.

The global sensitivity analysis applies partial rank correlation coefficients (PRCC) to assessing pairwise relations between inputs and the output after removing the influence of other input variables [45,46]. In detail, a rank transformation is performed for the samples of each input variable as well as the output variable. In rank transformation, sample values are replaced by their ranks (or orders) for each input and the output. The rank transformed samples are then used to compute partial correlation coefficients. To compute the partial rank correlation coefficient for a given input and the output, two linear regression models are fitted to the rank transformed samples. In detail, the rank transformed samples denoted by $\{(X_1^{(j)}, X_2^{(j)}, \cdots, X_n^{(j)}, U^{(j)})\}_{j=1,\cdots,\mathtt{N}}$ are obtained through replacing $x_i^{(j)}$ in the sample $\{x_i^{(j)}\}_{j=1,\cdots,\mathtt{N}}$ by its order denoted by $X_i^{(j)}$ for $i = 1, \cdots, n$ and replacing $u^{(j)}$ in the sample $\{u^{(j)}\}_{j=1,\cdots,\mathtt{N}}$ by its order denoted by $U^{(j)}$. Two linear regression models are

$$X_i = b_0 + \sum_{j=1, j\neq i}^{n} b_j X_j + \varepsilon_i$$

and

$$U = c_0 + \sum_{j=1, j\neq i}^{n} c_j X_j + \eta_i$$

where ε_i and η_i are the residuals of the two linear models.

The first linear model treats the input of interest as the dependent variable and other inputs as independent variables. Similarly, the other regression model is fitted to the same independent variables with the output variable as dependent variable. The residuals from the two linear regression models can be interpreted as the remaining

association between the input and output after removing the influences of other input variables. Then the residual vectors from the two regression models are used to compute a Pearson correlation coefficient,

$$\rho_{\varepsilon_i,\eta_i} = \frac{\sum_{j=1}^{\mathtt{N}}(\varepsilon_i^{(j)} - \bar{\varepsilon}_i)(\eta_i^{(j)} - \bar{\eta}_i)}{\sqrt{\sum_{j=1}^{\mathtt{N}}(\varepsilon_i^{(j)} - \bar{\varepsilon}_i)^2 \sum_{j=1}^{\mathtt{N}}(\eta_i^{(j)} - \bar{\eta}_i)^2}},$$

where $\bar{\varepsilon}_i$, $\bar{\eta}_i$ are the means of $\varepsilon_i^{(j)}{}_{j=1,\cdots,\mathtt{N}}$ and $\eta_i^{(j)}{}_{j=1,\cdots,\mathtt{N}}$, respectively, and $\rho_{\varepsilon_i,\eta_i}$ is the PRCC value of x_i and u. Therefore, PRCC identifies and measures the statistical influence, specifically the monotonicity, of the inputs on the output, even though the relationship between the input and output may be nonlinear.

The Sobol method is a variance-based global sensitivity analysis method [44, 47], which is different from the correlation-based method using partial rank correlation coefficients. It decomposes the variance of the output and quantifies the sources of variability for inputs and interactions by Sobol indices. In detail, the ANOVA (Analysis of Variances) representation [47] of $u = f(\boldsymbol{x})$ is

$$u = f(\boldsymbol{x}) = f_0 + \sum_{i=1}^{n} f_i(x_i) + \sum_{j>i}^{n} f_{ij}(x_i, x_j) + \cdots + f_{1,\cdots,n}(x_1, \cdots, x_n),$$

where f_0, $f_i(x_i)$, ... $f_{1,\cdots,n}(x_1, \cdots, x_n)$ are defined as follows

$$\begin{aligned}
\int f(\boldsymbol{x}) d\boldsymbol{x} &= f_0, \\
\int f(\boldsymbol{x}) \prod_{k\neq i} dx_k &= f_0 + f_i(x_i), \\
\int f(\boldsymbol{x}) \prod_{k\neq i,j} dx_k &= f_0 + f_i(x_i) + f_j(x_j) + f_{ij}(x_i, x_j),
\end{aligned}$$

and so on, where the integrals have bounds of the input ranges. Then define variances [47] by

$$V = \int f^2 d\boldsymbol{x} - f_0^2, \qquad V_{i_1,\cdots,i_s} = \int f_{i_1,\cdots,i_s}^2 dx_{i_1} \cdots dx_{i_s},$$

and

$$V = \sum_{s=1}^{n} \sum_{i_1<\cdots<i_s}^{n} V_{i_1,\cdots,i_s}.$$

Define Sobol indices [47] by

$$S_{i_1,\cdots,i_s} = \frac{V_{i_1,\cdots,i_s}}{V},$$

and

$$\sum_{s=1}^{n} \sum_{i_1<\cdots<i_s}^{n} S_{i_1,\cdots,i_s} = 1.$$

Therefore, Sobol indices are the percentages of variability attributed to inputs, and can be directly interpreted as measures of sensitivity. The Sobol method can be also applied to nonlinear relationship between inputs and the output.

2. EBOLA MODELS - CONSEQUENCES OF UNDERLYING ASSUMPTIONS

The chapter presents the work in collaboration with Feng, Hernandez-Ceron, Zhao, Glasser and Hill. Most of the results and ideas in this chapter have been accepted for publication in the journal of Mathematical Biosciences [48]. I contribute several parts of the manuscript but not exclusively, including model formulation and analysis as well as the writing of the manuscript.

2.1 Introduction

The Legrand model [20] is widely used model for many Ebola outbreaks. However, its complex expression makes it difficult to understand the formulation, parameterization, and underlying assumptions about the epidemiological processes including hospitalization, recovery and death, which are discussed in Section 1.1 in Chapter 1. This chapter focuses on unveiling the underlying assumptions used in the Legrand model. We simplify the Legrand model by reformulating it, which helps us to gain more insights into its formulation and parameterization. We also specifies the underlying assumptions of the Legrand model by comparing it with three alternative models developed in this chapter with more realistic assumptions. Through comparison, it also demonstrates that different underlying assumptions have distinct implications about control strategies.

We first provide a simpler (but equivalent) formulation of the Legrand model in Section 2.2. In particular, we define the overall waiting time in the I class to be the

weighted combination of waiting times $D_{IH} = 1/\gamma_{IH}$, $D_{IR} = 1/\gamma_{IR}$ and $D_{ID} = 1/\gamma_{ID}$ in the following form:

$$T_I = p\frac{1}{\gamma_{IH}} + (1-p)f\frac{1}{\gamma_{ID}} + (1-p)(1-f)\frac{1}{\gamma_{IR}}, \tag{2.1}$$

or equivalently using parameters in Legrand model:

$$T_I = p\frac{1}{\gamma_h} + (1-p)f\frac{1}{\gamma_d} + (1-p)(1-f)\frac{1}{\gamma_i}, \tag{2.2}$$

where p and f denote the probability of hospitalization and case-fatality, respectively. Using this assumption, as shown in Section 2.2, we obtain a much simpler formulation of the Legrand model. This facilitates identification of its underlying assumptions, as illustrated in Sections 2.3 and 2.4.

To fully understand the underlying assumptions used in the Legrand model, we develop three models based on general distributions for the waiting times of key processes and consider various assumptions about their relationships. We demonstrate that, when specific stage distributions are considered, one of these general models reduces to the Legrand model. The models that we develop in this chapter under arbitrarily distributed disease stages consist of integro-differential equations. It has been asserted that, when the arbitrary distributions are replaced by Gamma distributions, the so-called "linear chain trick" (see Section 1.2 for more detail) can be applied to reduce the integral equations to ordinary differential equations (ODEs) [37, 49, 50]. However, apart from a proof of the linear chain trick in a simpler setting by Smith in [40], a rigorous derivation of this fact for more complex epidemic models, such as the one in this chapter, is lacking. In this chapter, we provide a derivation (see Section 2.3).

This chapter is organized as follows. In Section 2.2, we present an equivalent Legrand model with a simpler formulation. Section 2.3 is devoted to the derivation of three models with arbitrarily distributed disease stages under various assumptions about the relationships between the overall waiting time in the I class and those for recovery, hospitalization and death. It is shown that these integro-differential equa-

Table 2.1.
Definition of quantities commonly used in models in Chapter 2.

Symbol	**Definition**
D_{IR}	Mean duration from onset to recovery (absent intervention) or infectious period
γ_{IR} (γ_i)	$= 1/D_{IR}$
D_{ID}	Mean duration between onset and death (absent intervention)
γ_{ID} (γ_d)	$= 1/D_{ID}$
D_{IH}	Mean duration from onset to hospitalization (given hospitalized)
γ_{IH} (γ_h)	$= 1/D_{IH}$
D_{HR}	Mean duration from hospitalization to recovery
ω_{HR} (γ_{ih})	$= 1/D_{HR}$
D_{HD}	Mean duration from hospitalization to death
ω_{HD} (γ_{dh})	$= 1/D_{HD}$
p	Proportion hospitalized (dependent on control effort)
f	Probability of death (with or without hospitalization)

Note: the symbols in parentheses are the corresponding quantities used in the Legrand model (1.1).

tions models reduce to ODE models when the distributions are Gamma or exponential. One of these ODE models is shown to be equivalent to the Legrand model. Basic and control reproduction numbers for these general models are derived in Section 2.4. The three models and the Legrand model are compared in Section 2.5. Discussions of the results are included in Section 2.6. The Appendix is given in Section 2.7 and collects the detailed proofs of results.

2.2 An equivalent and simpler formulation of the Legrand model

The Ebola model (1.1) studied by Legrand et al. (2007) [20] has been widely cited (see Section 1, Chapter 1). Their model consists of a system of ordinary differential equations with six compartments representing the epidemiological classes of susceptible (S), exposed (E), infectious (I), hospitalized (H), dead but not yet buried (D) and recovered (R). We can show (Section 2.7.2) that the Legrand model given by system (1.1) is equivalent to the following system

$$\begin{aligned}
\frac{dS}{dt} &= -\frac{1}{N}S(\beta_I I + \beta_H H + \beta_D D),\\
\frac{dE}{dt} &= \frac{1}{N}S(\beta_I I + \beta_H H + \beta_D D) - \alpha E,\\
\frac{dI}{dt} &= \alpha E - \gamma I,\\
\frac{dH}{dt} &= p\gamma I - \omega H,\\
\frac{dD}{dt} &= (1-p)f\gamma I + f\omega H - \gamma_f D,\\
\frac{dR}{dt} &= (1-p)(1-f)\gamma I + (1-f)\omega H,
\end{aligned} \tag{2.3}$$

where γ is the overall rate of leaving the I compartment (and $1/\gamma$ is the overall waiting time in I) and ω is the the average rate of leaving H (and $1/\omega$ is the overall waiting time in the H), which are *defined* as

$$\begin{aligned}
\frac{1}{\gamma} &= p\frac{1}{\gamma_{IH}} + (1-p)f\frac{1}{\gamma_{ID}} + (1-p)(1-f)\frac{1}{\gamma_{IR}},\\
\frac{1}{\omega} &= f\frac{1}{\omega_{HD}} + (1-f)\frac{1}{\omega_{HR}},
\end{aligned} \tag{2.4}$$

or equivalently, using the notation in Legrand model (see Table 2.1 for the biological meanings of γ's):

$$\begin{aligned}
\frac{1}{\gamma} &= p\frac{1}{\gamma_h} + (1-p)f\frac{1}{\gamma_d} + (1-p)(1-f)\frac{1}{\gamma_i},\\
\frac{1}{\omega} &= f\frac{1}{\gamma_{dh}} + (1-f)\frac{1}{\gamma_{ih}}.
\end{aligned} \tag{2.5}$$

From the above expressions, the intermediate parameters θ_1, δ_1 and δ_2 of the Legrand model (1.1) in (1.2) and (1.3) are determined by the fraction of infectious people hospitalized is

$$p = \frac{\gamma_h \theta_1}{\gamma_h \theta_1 + \gamma_i(1-\theta_1)(1-\delta_1) + \gamma_d(1-\theta_1)\delta_1}, \tag{2.6}$$

and the probabilities of death with (f_h) and without hospitalization (f_i) are given by

$$f_h = \frac{\gamma_{dh}\delta_2}{\gamma_{dh}\delta_2 + \gamma_{ih}(1-\delta_2)} \quad \text{and} \quad f_i = \frac{\gamma_d \delta_1}{\gamma_i(1-\delta_1) + \gamma_d \delta_1}. \tag{2.7}$$

Moreover, the Legrand model (1.1) and model (2.3) impose the following constraints (see also (1.4))

$$\begin{aligned} &f_i = f_h \doteq f, \\ &\frac{1}{\gamma_i} = \frac{1}{\gamma_h} + \frac{1}{\gamma_{ih}} \quad \Big(\text{or equivalently} \quad \frac{1}{\gamma_{IR}} = \frac{1}{\gamma_{IH}} + \frac{1}{\omega_{HR}}\Big), \\ &\frac{1}{\gamma_d} = \frac{1}{\gamma_h} + \frac{1}{\gamma_{dh}} \quad \Big(\text{or equivalently} \quad \frac{1}{\gamma_{ID}} = \frac{1}{\gamma_{IH}} + \frac{1}{\omega_{HD}}\Big). \end{aligned} \tag{2.8}$$

and assumes that hospitalization does not affect the time from onset to recovery or from onset to death.

We show in the Section 2.7.1 that model (2.3) is equivalent to the Legrand model (1.1). However, the presentation of the model formulation (2.3) is much simpler and easier to follow than that of (1.1). Moreover, the system (2.3) facillatates derivation of the control reproduction number $\mathcal{R}_c$, which (based on the next generation matrix approach) is

$$\mathcal{R}_c = \frac{\beta_I}{\gamma} + p\frac{\beta_H}{\omega} + f\frac{\beta_D}{\gamma_f}. \tag{2.9}$$

We remark that the computation from model (2.3) does not require any of the γ_j in Table 2.1, or the intermediate parameters, such as θ_1, δ_1 and δ_2, used in Legrand model.

2.3 Models with general distributions for disease stages

To examine the underlying assumptions in the Legrand (1.1) or equivalent model (2.3), and to provide more accurate evaluations of disease control strategies, we de-

velop models using more realistic assumptions about the disease stage distributions. In this section, we formulate three models based on different assumptions about the relationship between the overall waiting time in the I class and the waiting times from onset to hospitalization, recovery without hospitalization, and death without hospitalization. We illustrate that these various assumptions lead to different models. We will adopt probabilistic terminology to facilitate the interpretation of our deterministic model, and focus on the following three scenarios:

(I). Assume that the three events IR, IH and ID are *independent* and the waiting times are described by the survival functions $P_1(s)$, $L_1(s)$ and $M_1(s)$, respectively, where s represents the time-since-onset. It is also assumed that hospitalization does not affect the time from onset to recovery or death.

(II). The two events IR and ID are *combined* and described by a single distribution $P_2(s)$, with a fraction $1-f$ of the exiting individuals recovering (and the fraction f dying). The event IH is independent of IR and ID and the waiting time is described by distribution $L_2(s)$. Similar to Model I, it is also assumed that hospitalization does not affect the time from onset to recovery or probability of death.

(III). All three events (IH, IR, and ID) are combined and described by a single distribution $P_3(s)$, with a fraction p of the exiting individuals being hospitalized and a fraction $1-f$ (respectively, f) of the non-hospitalized individuals recovering (respectively, dying). The two events HR and HD are combined and the waiting time is described by a single distribution $Q_3(s)$ with a fraction $1-f$ (or f) of the exiting individuals recovering (or dying). P_3 and Q_3 are assumed to be independent. Unlike in Models I and II, in which the time from onset to hospitalization is tracked due to the independent stage distributions, in Model III a constraint must be imposed so that the time between onset and hospitalization plus the time beween hospitalization and recovery (or death) equals the time between onset and recovery (or death).

Because we focus on the general waiting time for the infectious stage and its influence on model formulation when hospitalization is considered, we assume simpler distributions for other stages including the latent stage and the duration between death and burial. That is, the E and D stages are assumed to have exponential distributions with constant rates α and γ_f. As the models are derived under arbitrary distributions for the waiting times of key disease stages, they consist of systems of integro-differential equations. We show that these systems reduce to ODEs systems when the arbitrary stage distributions are replaced by Gamma distributions.

We introduce the following notation for two conditional probabilities, which will be used later in the following section. Let s denote the time of disease onset. The conditional probability of being still infectious at time t, given that the individual was hospitalized at time τ is as

$$P_1(t-s|\tau-s) := \frac{\mathbb{P}[T_{P_1} > t-s]}{\mathbb{P}[T_{P_1} > \tau-s]} = \frac{P_1(t-s)}{P_1(\tau-s)}. \tag{2.10}$$

Similarly, the assumption that hospitalization does not affect the time from onset to death implies that the conditional probability of being still alive at time t given being alive and hospitalized at τ $(s < \tau < t)$ is

$$M_1(t-s|\tau-s) := \frac{\mathbb{P}[T_{M_1} > t-s]}{\mathbb{P}[T_{M_1} > \tau-s]} = \frac{M_1(t-s)}{M_1(\tau-s)}. \tag{2.11}$$

2.3.1 Model I

The model associated to (**I**) is described in this section. For the three independent events IR, IH, and ID, the waiting times are described respectively by the survival functions

- $P_1(s)$: Probability that a living individual remains infectious s units of time since onset (governing both IR and HR events).
- $L_1(s)$: Probability of a living individual not being hospitalized s units of time since onset (governing the IH event).

- $M_1(s)$: Probability of surviving the disease s units of time since onset (governing ID and HD events).

Figure 2.3.1 depicts the transitions between epidemiological classes for the model under scenario (I). All variables and parameters have the same meanings as before unless otherwise stated. The diagram in (a) depicts transitions between compartments when stage durations for the IR, IH, and ID events are arbitrary described by probability distributions $P_1(t)$, $L_1(t)$ and $M_1(t)$. The dotted rectangle around the I and H compartments indicates that individuals in these two compartments are being tracked for their time-since-onset using the distribution $P_1(t)$; i.e., the time elapsed in I before entering H is taken into account when determining the time between entering H and recovery R. The diagram in (b) illustrates the effect of the 'linear chain trick' when $P_1(t)$ is a Gamma distribution, and $L_1(t)$ and $M_1(t)$ are exponential survival functions. More details about the parameters for these distributions are given later (see also Remark 2.1 for explanations about the multiple compartments for the I and H classes).

The equations for the S and E classes are ODEs given by

$$\frac{dS}{dt} = -\lambda(t)S, \quad \frac{dE}{dt} = \lambda(t)S - \alpha E, \tag{2.12}$$

where $\lambda(t)$ denotes the force of infection (or hazard rate) given by

$$\lambda(t) = \frac{\beta_I I + \beta_H H + \beta_D D}{N}, \tag{2.13}$$

and $I = I(t)$ is the total number of infectious individuals given by

$$I(t) = \int_0^t \alpha E(s) P_1(t-s) L_1(t-s) M_1(t-s) ds + I(0) P_1(t) L_1(t) M_1(t). \tag{2.14}$$

The first term in (2.14) represents the total number of individuals at time t who became infectious $t - s$ units of time ago ($0 < s < t$) and have not recovered, or been hospitalized or died by time t. The second term in (2.14) represents those individuals who were infectious at time 0 and are still in the I class at time t. Assume that the number of initially infected individuals $I(0)$ is small and, for simplicity, that these individuals all have stage age 0 in I.

Let $g_{P_1} = -P_1'$, $g_{L_1} = -L_1'$ and $g_{M_1} = -M_1'$ denote the probability density functions of P_1, L_1 and M_1 respectively. These functions also give the rates of entering the R, H and D classes, respectively. Differentiating the I equation (2.14) will generate inflow terms from I to R, H and D classes:

$$\begin{aligned} I'(t) = \alpha E(t) &- \left[\int_0^t \alpha E(s) P_1(t-s) g_{L_1}(t-s) M_1(t-s) ds + I(0) P_1(t) g_{L_1}(t) M_1(t)\right] \\ &- \left[\int_0^t \alpha E(s) P_1(t-s) L_1(t-s) g_{M_1}(t-s) ds + I(0) P_1(t) L_1(t) g_{M_1}(t)\right] \\ &- \left[\int_0^t \alpha E(s) g_{P_1}(t-s) L_1(t-s) M_1(t-s) ds + I(0) g_{P_1}(t) L_1(t) M_1(t)\right]. \end{aligned}$$

If an infectious individual entered the H class $\tau - s$ $(0 < s < \tau < t)$ units after becoming infectious, then based on the conditional probabilities $P_1(t-s|\tau-s)$ and $M_1(t-s|\tau-s)$ shown in (2.10) and (2.11), the H equation can be written as

$$\begin{aligned} H(t) &= \int_0^t \left[\int_0^\tau \alpha E(s) P_1(\tau-s) M_1(\tau-s) g_{L_1}(\tau-s) P_1(t-s|\tau-s) M_1(t-s|\tau-s) ds \right. \\ &\quad \left. + I(0) P_1(\tau) M_1(\tau) g_{L_1}(\tau) P_1(t-\tau|\tau) M_1(t-\tau|\tau)\right] d\tau, \\ &= \int_0^t \left[\int_0^\tau \alpha E(s) P_1(t-s) M_1(t-s) g_{L_1}(\tau-s) ds + I(0) P_1(t) M_1(t) g_{L_1}(\tau)\right] d\tau, \\ &= \int_0^t \alpha E(s) P_1(t-s) M_1(t-s) \int_s^t g_{L_1}(\tau-s) d\tau ds + I(0) P_1(t) M_1(t) \int_0^t g_{L_1}(\tau) d\tau, \\ &= \int_0^t \alpha E(s) P_1(t-s) M_1(t-s)(1 - L_1(t-s)) ds + I(0) P_1(t) M_1(t)(1 - L_1(t)). \end{aligned}$$

For the inflows to the D class, in addition to the term from the I equation there is also a term from the H equation. Differentiating the H equation, we have

$$\begin{aligned} H'(t) &= \int_0^t \alpha E(s) P_1(t-s) M_1(t-s) g_{L_1}(t-s) ds + I(0) P_1(t) M_1(t) g_{L_1}(t) \\ &\quad \underbrace{- \int_0^t \alpha E(s) P_1(t-s) g_{M_1}(t-s)(1 - L_1(t-s)) ds - I(0) P_1(t) g_{M_1}(t)(1 - L_1(t)))}_{\text{to } D \text{ class}} \\ &\quad \underbrace{- \int_0^t \alpha E(s) g_{P_1}(t-s) M_1(t-s)(1 - L_1(t-s)) ds - I(0) g_{P_1}(t) M_1(t)(1 - L_1(t)))}_{\text{to } R \text{ class}} \end{aligned}$$

(a) Arbitrary distributions

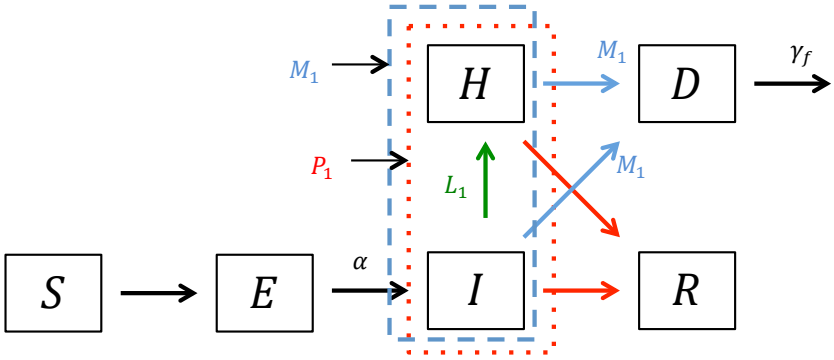

(b) Gamma distributions

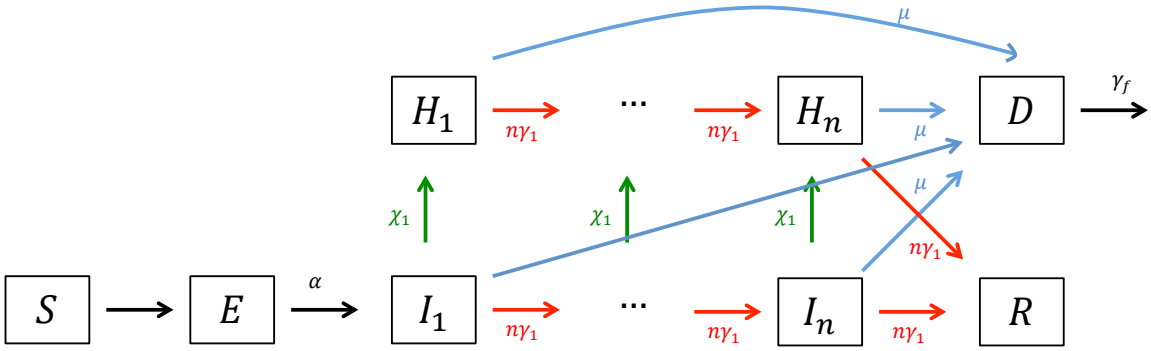

Fig. 2.1. Transition diagram for Model I when distributions $P_1(t)$ (red), $L_1(t)$ (green), and $M_1(t)$ (blue) are arbitrary (a), or Gamma/exponential (b).

From equations (2.3.1) and (2.15), we obtain the equations for D and R:

$$\begin{aligned} D'(t) &= \int_0^\tau \alpha E(s) P_1(\tau - s) g_{M_1}(\tau - s) ds + I(0) P_1(\tau) g_{M_1}(\tau) \\ &\quad -\gamma_f \int_0^t \left[\int_0^\tau \alpha E(s) P_1(\tau - s) g_{M_1}(\tau - s) ds + I(0) P_1(\tau) g_{M_1}(\tau) \right] e^{-\gamma_f (t-\tau)} d\tau. \end{aligned}$$

and

$$\begin{aligned} R(t) &= \underbrace{\int_0^t \left[\int_0^\tau \alpha E(s) g_{p_1}(\tau - s) M_1(\tau - s) L_1(\tau - s) ds + I(0) g_{p_1}(\tau) M_1(\tau) L_1(\tau)\right] d\tau}_{\text{(from } I \text{ class)}} \\ &\quad + \underbrace{\int_0^t \left[\int_0^\tau \alpha E(s) g_{p_1}(\tau - s) M_1(\tau - s)(1 - L_1(\tau - s)) ds + I(0) g_{p_1}(\tau) M_1(\tau)(1 - L_1(\tau))\right] d\tau}_{\text{(from } H \text{ class)}}, \\ &= \int_0^t \left[\int_0^\tau \alpha E(s) g_{p_1}(\tau - s) M_1(\tau - s) ds + I(0) g_{p_1}(\tau) M_1(\tau)\right] d\tau, \end{aligned}$$

Using the equations derived above, we obtain the system of integro-differential equations for Model I:

$$\begin{aligned} \frac{dS(t)}{dt} &= -\lambda(t) S(t), \qquad \frac{dE(t)}{dt} = \lambda(t) S(t) - \alpha E(t), \\ I(t) &= \int_0^t \alpha E(s) P_1(t - s) M_1(t - s) L_1(t - s) ds + I(0) P_1(t) M_1(t) L_1(t), \qquad (2.15) \\ H(t) &= \int_0^t \alpha E(s) P_1(t - s) M_1(t - s)(1 - L_1(t - s)) + I(0) P_1(t) M_1(t)(1 - L_1(t)), \\ D(t) &= \int_0^t \left[\int_0^\tau \alpha E(s) P_1(\tau - s) g_{M_1}(\tau - s) ds + I(0) P_1(\tau) g_{M_1}(\tau)\right] e^{-\gamma_f (t-\tau)} d\tau, \\ R(t) &= \int_0^t \left[\int_0^\tau \alpha E(s) g_{p_1}(\tau - s) M_1(\tau - s) ds + I(0) g_{p_1}(\tau) M_1(\tau)\right] d\tau, \end{aligned}$$

where $\lambda(t)$ is given in (2.13). The initial condition is $(S(0), E(0), I(0), H(0), D(0), R(0)) = (S_0, E_0, I_0, 0, 0, 0)$, where S_0 and E_0 are positive constants.

We remark that, in the system (2.15), the probability distributions P_1, L_1 and M_1 are arbitrary. We show in the next section that when these general distributions are replaced by Gamma distributions, the integral equations can be reduced to ODEs.

Reduction of Model I (2.15) to ODEs

In this section, we show that the system of integro-differential equations (2.15) for Model I can be reduced to a system of ordinary differential equations when P_1, L_1 and M_1 are Gamma distributions. Note that, for a Gamma distribution with shape and

rate parameters $(n, n\alpha)$ (where $n \geq 1$ is an integer), the probability density function $g(t)$ and the survival function $G(t)$ are given, respectively, by

$$g(t) = \frac{n\alpha(n\alpha t)^{n-1}}{(n-1)!}e^{-n\alpha t}, \quad G(t) = \sum_{j=1}^{n} \frac{(n\alpha t)^{j-1}e^{-n\alpha t}}{(j-1)!}. \tag{2.16}$$

A derivation for the survival function $G(t)$ in (2.16) can be found in Section 1.2 of Chapter 1.

Consider the case when $P_1(t)$ is a Gamma distribution with shape and rate parameters $(n, n\gamma_1)$ (where $n \geq 1$ is an integer), and $L_1(t)$ and $M_1(t)$ are exponential distributions with parameters χ_1 and μ, respectively (which are Gamma distributions with shape parameter 1). That is,

$$\begin{aligned} P_1(t) &= G^n_{n\gamma_1}(t) = \sum_{j=1}^{n} \frac{(n\gamma_1 t)^{j-1}e^{-n\gamma_1 t}}{(j-1)!}, \\ L_1(t) &= G^1_{\chi_1}(t) = e^{-\chi_1 t}, \\ M_1(t) &= G^1_{\mu}(t) = e^{-\mu t}. \end{aligned} \tag{2.17}$$

In this case, the I equation in (2.15) becomes

$$\begin{aligned} I(t) &= \int_0^t \alpha E(s)e^{-\mu(t-s)}e^{-\chi_1(t-s)} \sum_{j=1}^{n} \frac{(n\gamma_1(t-s))^{j-1}e^{-n\gamma_1(t-s)}}{(j-1)!}ds \\ &\quad + I(0)e^{-\mu t}e^{-\chi_1 t} \sum_{j=1}^{n} \frac{(n\gamma_1 t)^{j-1}e^{-n\gamma_1 t}}{(j-1)!} \\ &\doteq \sum_{j=1}^{n} I_j(t), \end{aligned}$$

where

$$\begin{aligned} I_j(t) &= \int_0^t \alpha E(s)e^{-\mu(t-s)}e^{-\chi_1(t-s)} \frac{(n\gamma_1(t-s))^{j-1}e^{-n\gamma_1(t-s)}}{(j-1)!}ds \\ &\quad + I(0)e^{-\mu t}e^{-\chi_1 t} \frac{(n\gamma_1 t)^{j-1}e^{-n\gamma_1 t}}{(j-1)!}, \end{aligned}$$

for $j = 1, \cdots, n$. Similarly, the hospitalized class can be written as

$$H(t) = \sum_{j=1}^{n} H_j(t)$$

with $H_j(t)$ being the functions given by

$$\begin{aligned} H_j(t) &= \int_0^t \alpha E(s) e^{-\mu(t-s)} \frac{(n\gamma_1(t-s))^{j-1} e^{-n\gamma_1(t-s)}}{(j-1)!}(1-e^{-\chi_1(t-s)})ds \\ &\quad + I(0)e^{-\mu t}\frac{(n\gamma_1 t)^{j-1}e^{-n\gamma_1 t}}{(j-1)!}(1-e^{-\chi_1 t}) \end{aligned}$$

Then, we can show (see the detailed derivation in Appendix) that the system (2.15) is equivalent to the following system of ODEs:

$$\begin{aligned} \frac{dS(t)}{dt} &= -\lambda(t)S(t), \qquad \frac{dE(t)}{dt} = \lambda(t)S(t) - \alpha E(t), \\ \frac{dI_1(t)}{dt} &= \alpha E(t) - (n\gamma_1 + \chi_1 + \mu)I_1(t), \\ \frac{dI_j(t)}{dt} &= n\gamma_1 I_{j-1}(t) - (n\gamma_1 + \chi_1 + \mu)I_j(t), \text{ for } j = 2, \dots n \\ \frac{dH_1(t)}{dt} &= \chi_1 I_1(t) - (n\gamma_1 + \mu)H_1(t), \\ \frac{dH_j(t)}{dt} &= \chi_1 I_j(t) + n\gamma_1 H_{j-1}(t) - (n\gamma_1 + \mu)H_j(t), \text{ for } j = 2, \dots n \\ \frac{dD(t)}{dt} &= \sum_{j=1}^{n} \mu I_j(t) + \sum_{j=1}^{n} \mu H_j(t) - \gamma_f D(t), \\ \frac{dR(t)}{dt} &= n\gamma_1 I_n(t) + n\gamma_1 H_n(t). \end{aligned} \tag{2.18}$$

Remark 2.1. System (2.18) is consistent with the ODE system obtained by applying the linear chain trick to system (2.15), which implies that the Gamma distributed stage can be considered as a sequence of n sub-stages with equal length, each of which follows an exponential distribution with parameter γ_1 (see, for example, MacDonald, 1978; Hethcote and Tudor, 1980; Lloyd, 2001). However, a rigorous proof for the reduction of integral equations to the ODEs has not been provided. Note that, in this case, the diagram in Fig. 2.3.1(a) becomes the one illustrated in Fig. 2.3.1(b), where the I and H stages are divided into n sub-stages each of which follows an exponential distribution with parameter $n\gamma_1$. In this case, the period between H_i and H_{i+1} is the same as that between I_i and I_{i+1} (due to the memoryless property of exponential distributions).

We observe that the recovery rates from both I_n and H_n, as well as the transition rates from I_j to I_{j+1} and from H_j to H_{j+1} $(j = 1, \cdots n-1)$ are all the same and equal to $n\gamma_1$.

Remark 2.2. When $n = 1$ (i.e., when $P_1(t)$ is an exponential distribution), model (2.18) has a very similar structure to the Legrand model. However, because the exiting rates from I and H due to recovery are the same (γ_1), model (2.18) differs from the Legrand model (see section 2.5.1 for more details).

2.3.2 Model II

In Model I, the three processes IR, IH and ID are assumed to be independent, in which case the three events 'compete' for individuals in the I class. Another scenario is to consider only two independent processes, one being hospitalization and other combining recovery and death for those who are not hospitalized. In this case, we have two survival probability functions:

- $P_2(s)$: Survival probability of recovery and death s time units after onset (governing events IR, ID, HR and HD).
- $L_2(s)$: Probability of not being hospitalized s time units after onset (governing the IH event).

Assume that, for those who exit I without being hospitalized, a fixed fraction $1-f$ (or f) will recover (or die), an assumption of Legrand model. Assume also that individuals in I and H classes have the same probability of death (f), also as assumed in the Legrand model. The transition diagram is depicted in Fig. 2.3.2(a).

Let $g_{P_2} = -P_2'$ and $g_{L_2} = -L_2'$. Note that the I equation in this case is

$$I(t) = \int_0^t \alpha E(s) P_2(t-s) L_2(t-s) ds + I(0) P_2(t) L_2(t).$$

(a) Arbitrary distributions

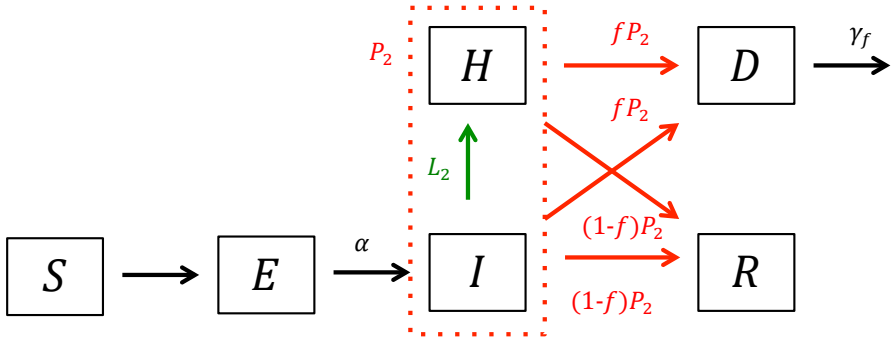

(b) Gamma distributions

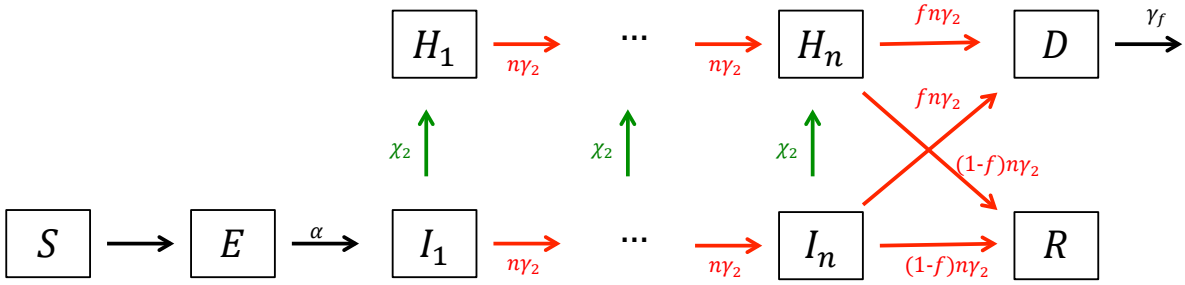

Fig. 2.2. A transition diagram for Model II when P_2 and L_2 are arbitrary distributions (a) and when they are Gamma or exponential (b). In (a), the recovery/death (red) and hospitalization (green) processes are governed by P_2 and L_2. In (b), he recovery/death (red) and hospitalization (green) processes are indicated by the same colors as in (a).

Differentiation yields

$$I'(t) = \alpha E(s) - \underbrace{\left[\int_0^t \alpha E(s) P_2(t-s) g_{L_2}(t-s) ds + I(0) P_2(t) g_{L_2}(t)\right]}_{to\ H}$$
$$- \underbrace{\left[\int_0^t \alpha E(s) g_{P_2}(t-s) L_2(t-s) ds + I(0) g_{P_2}(t) L_2(t)\right]}_{to\ D,R}.$$

For the variable H, we have

$$\begin{aligned} H(t) &= \int_0^t \left[\int_0^\tau \alpha E(s)P_2(t-s)g_{L_2}(\tau-s)\right] ds d\tau + \int_0^t I(0)P_2(t)g_{L_2}(\tau)d\tau, \\ &= \int_0^t \alpha E(s)P_2(t-s)(1-L_2(t-s)) + I(0)P_2(t)(1-L_2(t)), \end{aligned}$$

and

$$\begin{aligned} H'(t) &= \int_0^t \alpha E(s)P_2(t-s)g_{L_2}(t-s)ds + I(0)P_2(t)g_{L_2}(t) \\ &\quad \underbrace{- \int_0^t \alpha E(s)g_{P_2}(t-s)(1-L_2(t-s))ds - I(0)g_{P_2}(t)(1-L_2(t)))}_{\text{to } D,R} \end{aligned}$$

Then, using the assumption of fixed fraction of death (f), we arrive at the system of equations for Model II:

$$\begin{aligned} \frac{dS(t)}{dt} &= -\lambda(t)S(t), \qquad \frac{dE(t)}{dt} = \lambda(t)S(t) - \alpha E(t), \\ I(t) &= \int_0^t \alpha E(s)P_2(t-s)L_2(t-s)ds + I(0)P_2(t)L_2(t), \\ H(t) &= \int_0^t \alpha E(s)P_2(t-s)(1-L_2(t-s)) + I(0)P_2(t)(1-L_2(t)), \\ D'(t) &= f\int_0^t \left[\int_0^\tau \alpha E(s)g_{P_2}(\tau-s)ds + I(0)g_{P_2}(\tau)\right] e^{-\gamma_f(t-\tau)}d\tau - \gamma_f D(t), \\ R'(t) &= (1-f)\int_0^t \left[\int_0^\tau \alpha E(s)g_{p_2}(\tau-s)ds + I(0)g_{p_2}(\tau)\right] d\tau, \end{aligned} \tag{2.19}$$

The function $\lambda(t)$ is the same as in Model I and given in (2.13).

Reduction of Model II to a system of ODEs

If $P_2(t)$ is a Gamma distribution with parameters $(n, n\gamma_2)$ and $L_2(t)$ is an exponential distribution with parameter χ_2, i.e.,

$$\begin{aligned} P_2(t) &= G^n_{n\gamma_2}(t) = \textstyle\sum_{j=1}^n \frac{(n\gamma_2 t)^{j-1}e^{-n\gamma_2 t}}{(j-1)!}, \\ L_2(t) &= G^1_{\chi_2}(t) = e^{-\chi_2 t}, \end{aligned} \tag{2.20}$$

then, similar to the derivation of system (2.18) for Model I, we can reduce the integral equations in (2.19) to the ODEs given below:

$$\begin{aligned}
\frac{dS}{dt} &= -\frac{1}{N}S\Big(\beta_I \sum_{j=1}^{n} I_j + \beta_H \sum_{j=1}^{n} H_j + \beta_D D\Big),\\
\frac{dE}{dt} &= \frac{1}{N}S\Big(\beta_I \sum_{j=1}^{n} I_j + \beta_H \sum_{j=1}^{n} H_j + \beta_D D\Big) - \alpha E,\\
\frac{dI_1}{dt} &= \alpha E - (n\gamma_2 + \chi_2)I_1,\\
\frac{dI_j}{dt} &= n\gamma_2 I_{j-1}(t) - (n\gamma_2 + \chi_2)I_j, \text{ for } j = 2, \dots n\\
\frac{dH_1}{dt} &= \chi_2 I_1 - n\gamma_2 H_1,\\
\frac{dH_j}{dt} &= \chi_2 I_j + n\gamma_2 H_{j-1} - n\gamma_2 H_j, \text{ for } j = 2, \dots n\\
\frac{dD}{dt} &= fn\gamma_2 I_n + fn\gamma_2 H_n - \gamma_f D,\\
\frac{dR}{dt} &= (1-f)n\gamma_2 I_n + (1-f)n\gamma_2 H_n.
\end{aligned} \tag{2.21}$$

Because of the different assumptions made in Model II, the ODE reduction (2.21) differs from the ODE reduction (2.18) for Model I. This is more clearly illustrated in the transition diagram for (2.21) in Fig. 2.3.2(b). For example, we observe in Fig. 2.3.2(b) that transitions to R or D occur only to individuals in the last infectious and hospitalized compartments (I_n and H_n), whereas in Fig. 2.3.1(b), recovery and death can be from all the I_j and H_j ($j = 1, \cdots, n$) compartments. Observe also that the recovery rates from both I_n and H_n, as well as the transition rates from I_j to I_{j+1} and from H_j to H_{j+1} ($j = 1, \cdots n-1$), are all the same and equal to $n\gamma_2$.

Remark 2.3. Note that the distributions $P_1(t)$ and $P_2(t)$ describe two very different processes. Thus, the two parameters γ_1 and γ_2 in the Gamma distributions $P_1 = G^n_{n\gamma_1}$ and $P_2 = G^n_{n\gamma_2}$ have very different meanings. That is, they have different connections with epidemiological parameters such as the infectious period. More detailed discussions of this point can be found in Section 2.5.

Remark 2.4. From the ODEs model (2.21) or the transition diagram 2.3.2(b) we observe that, in the case of $n = 1$, the rates from I to R and from H to R are the same. Therefore, as in the case of Model I, the ODE model (2.21) *cannot* be equivalent to the Legrand model. This suggests that the Legrand model does not assume that the hospitalization process is independent of the (combined) recovery and death processes.

(a) Arbitrary distributions

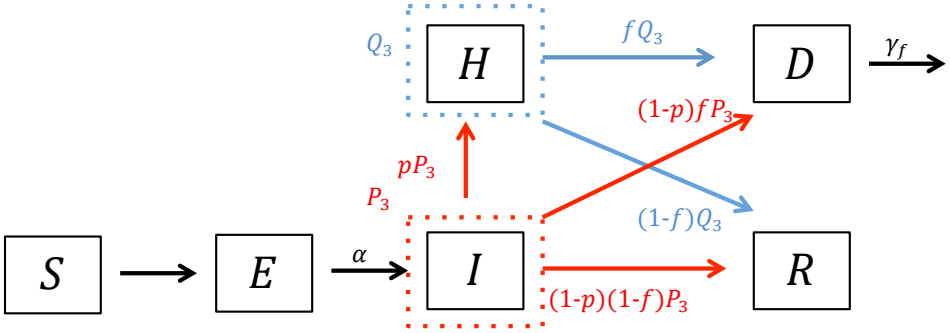

(b) Gamma distributions

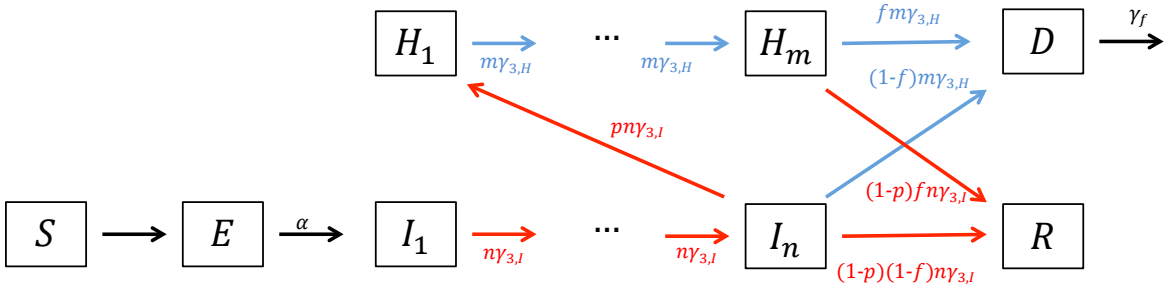

Fig. 2.3. A transition diagram for Model III when P_3 and Q_3 are arbitrary distributions (a) and when they are Gamma or exponential (b).

2.3.3 Model III

Models I and II focus on the three exiting processes from the I class. In Model III, both the processes exiting the I and H classes are considered. Consider two independent distributions for the infectious individuals in I and H classes

- $P_3(s)$: Probability of remaining in the I class s units of time since onset (governing the events IR, IH and ID).
- $Q_3(s)$: Probability remaining in the H class s units of time after being hospitalized (governing the HR and HD events).

Let $p_3(t) = -P_3'(t)$ and $q_3(t) = -Q_3'(t)$ denote the probability density functions. P_3 describes the waiting time for the combined events, IR, IH and ID. Assume that among the individuals exiting the I class, fractions of p, $(1-p)f$, $(1-p)(1-f)$ will be hospitalized, non-hospitalized and dead, and non-hospitalized and recovered, respectively ($0 \leq p, f < 1$). Q_3 describes the waiting time for the combined two events, HR and HD, and we assume that fractions $1-f$ and f of the hospitalized individuals recover or die, respectively.

In this case, Model III consists of the following system of integro-differential equations:

$$
\begin{aligned}
&S'(t) = -\lambda(t)S(t), \qquad E'(t) = \lambda(t)S(t) - \alpha E(t),\\
&I(t) = \int_0^t \alpha E(s)P_3(t-s)ds + I(0)P_3(t),\\
&H(t) = \int_0^t p\left[\int_0^s \alpha E(\tau)p_3(s-\tau)d\tau + I(0)p_3(s)\right] Q_3(t-s)ds\\
&D'(t) = (1-p)f\left[\int_0^t \alpha E(s)p_3(t-s)ds + I(0)p_3(t)\right]\\
&\qquad +f\int_0^t \left[p\int_0^s \alpha E(\tau)p_3(s-\tau)d\tau + pI(0)p_3(s)\right] q_3(t-s)ds - \gamma_f D(t),\\
&R'(t) = (1-p)(1-f)\left[\int_0^t \alpha E(s)p_3(t-s))ds + I(0)p_3(t)\right]\\
&\qquad +(1-f)\int_0^t \left[p\int_0^s \alpha E(\tau)p_3(s-\tau)d\tau + pI(0)p_3(s)\right] q_3(t-s)ds.
\end{aligned}
\tag{2.22}
$$

Note that it is easier in this case to write equations for D' and H' than for D and H.

Reduction of Model III (2.22) **to a system of ODEs**

Assume that P_3 and Q_3 are Gamma distributions with parameters $(n, n\gamma_3)$ and $(m, m\omega_3)$, respectively, i.e.,

$$\begin{aligned} P_3(t) &= G^n_{n\gamma_3}(t) = \sum_{j=1}^{n} \frac{(n\gamma_3 t)^{j-1} e^{-n\gamma_3 t}}{(j-1)!}, \\ Q_3(t) &= G^m_{m\omega_3}(t) = \sum_{j=1}^{m} \frac{(m\omega_3 t)^{j-1} e^{-m\omega_3 t}}{(j-1)!}. \end{aligned} \tag{2.23}$$

Then, the system (2.22) reduces to the following system of ODEs:

$$\begin{aligned} \frac{dS}{dt} &= -\frac{1}{N} S\Big(\beta_I \sum_{j=1}^{n} I_j + \beta_H \sum_{j=1}^{m} H_j + \beta_D D\Big) \\ \frac{dE}{dt} &= \frac{1}{N} S\Big(\beta_I \sum_{j=1}^{n} I_j + \beta_H \sum_{j=1}^{m} H_j + \beta_D D\Big) - \alpha E, \\ \frac{dI_1}{dt} &= \alpha E - n\gamma_3 I_1, \\ \frac{dI_k}{dt} &= I_{k-1} - n\gamma_3 I_k, \qquad k = 2, \ldots, n \\ \frac{dH_1}{dt} &= pn\gamma_3 I_n - m\omega_3 H_1, \\ \frac{dH_k}{dt} &= m\omega_3 H_{k-1} - m\omega_3 H_k, \qquad k = 2, \ldots, m \\ \frac{dD}{dt} &= (1-p) f n\gamma_3 I_n + f m\omega_3 H_n - \gamma_f D, \\ \frac{dR}{dt} &= (1-p)(1-f) n\gamma_3 I_n + (1-f) m\omega_3 H_m. \end{aligned} \tag{2.24}$$

A transition diagram under the Gamma distributions for P_3 and Q_3 and for the ODE model (2.24) is shown in Fig. 2.3.2(b). We observe a major difference between this figure and Fig. 2.3.1(b) or Fig. 2.3.2(b) in the recovery rates from I_n and H_m, which have different values here. A similar difference exists in the transition rates from I_j to I_{j+1} $(j = 1, \cdots, n-1)$ and from H_j to H_{j+1} $(j = 1, \cdots, m-1)$.

Remark 2.5. As pointed out in Remark 2.3, the distributions $P_i(t)$ $(i = 1, 2, 3)$ describe waiting times for three very different processes. Thus, the three parameters γ_i $(i = 1, 2, 3)$ in the Gamma distributions $P_i = G^n_{n\gamma_i}$ have very different meanings and connections with epidemiological parameters such as the infectious period determined by γ_{IR}. More detailed discussions about this can be found in Section 2.5.

Remark 2.6. We observe from the ODE model (2.24) and diagram 2.3.2(b) that, in the case of $n = m = 1$, the transition rates from I to R and from H to R can differ. This is a major difference between Model III and Models I and II. In fact, we show in Section 2.5.3 that with an appropriate definition for γ_3 and ω_3 and the constraints (2.8), model (2.24) when $m = n = 1$ is the same as the model (2.3), which is equivalent to the Legrand model (1.1).

2.4 Reproduction numbers

In this section, we provide formulas for the control reproduction numbers for Models I, II and III. Both the case of arbitrary distributions and the special case of Gamma distribution are considered. These reproduction numbers are derived both using the next generation matrix approach and from biological interpretations. Denote the control reproduction numbers for Models I, II and III by $\mathcal{R}_{C1}$, $\mathcal{R}_{C2}$ and $\mathcal{R}_{C3}$, respectively.

2.4.1 Reproduction number $\mathcal{R}_{C1}$ for Model I

We derive the control reproduction number $\mathcal{R}_{C1}$ using two approaches, one using arguments based on the probabilistic processes behind the integro-differential equations, which provide a formula for $\mathcal{R}_{C1}$ for general distributions. We present the formula under the specific distributions for P_1, L_1 and M_1 used in the ODEs model (2.18). The other approach uses the next generation matrix for the ODE model (2.18).

For the first approach, define three independent waiting times T_{P_1}, T_{L_1} and T_{M_1}, which are random variables distributed according to P_1, L_1 and Q_1 and describe, repectively, the timing of events IR and HR; IH; and ID and HD. The expectations of T_j $(j = P_1, L_1, M_1)$ represent times to recovery, hospitalization or death, respectively. Then, the average time spent in the I compartment is $\mathbb{E}\left(\min\left\{T_{P_1}, T_{L_1}, T_{M_1}\right\}\right)$. Then

$$\begin{aligned}\mathbb{P}\left(\min\left\{T_{P_1}, T_{L_1}, T_{M_1}\right\} > x\right) &= \mathbb{P}\left(\left\{T_{P_1} > x\right\} \cap \left\{T_{L_1} > x\right\} \cap \left\{T_{M_1} > x\right\}\right) \\ &= \mathbb{P}\left(T_{P_1} > x\right)\mathbb{P}\left(T_{L_1} > x\right)\mathbb{P}\left(T_{M_1} > x\right).\end{aligned}$$

Thus,

$$\mathbb{E}\left(\min\left\{T_{P_1}, T_{L_1}, T_{M_1}\right\}\right) = \int_0^\infty P_1(t)L_1(t)M_1(t)dt.$$

Letting p_{M1} denote the probability of death for Model I, which includes two events, death before hospitalization and death during hospitalization, we have

$$p_{M1} = \mathbb{P}(T_{M_1} = \min\left\{T_{P_1}, T_{L_1}, T_{M_1}\right\}) + \mathbb{P}(T_{L_1} < T_{M_1} < T_{P_1}).$$

Note that the average duration in the D compartment is $1/\gamma_f$. Then, based on the biological meaning of $\mathcal{R}_{C1}$, we obtain the following expression for $\mathcal{R}_{C1}$ under general stage distributions:

$$\begin{aligned}\mathcal{R}_{C1} &= \beta_I\mathbb{E}\left(\min\left\{T_{P_1}, T_{L_1}, T_{M_1}\right\}\right) + \beta_H\left[\mathbb{E}\left(\min\left\{T_{P_1}, T_{M_1}\right\}\right) - \mathbb{E}\left(\min\left\{T_{P_1}, T_{L_1}, T_{M_1}\right\}\right)\right] \\ &\quad +\beta_F\frac{1}{\gamma_f}p_M. \qquad (2.25)\end{aligned}$$

The formula (2.25) is convenient to use when specific distribution functions for T_j $(j = P_1, L_1, M_1)$ are given. For example, consider the special case of Model I with $P_1(t) = G^n_{n\gamma_1}(t)$, $L_1(t) = e^{-\chi_1 t}$ and $M_1(t) = e^{-\mu t}$ (see (2.17)). Note that the average time in I is

$$\begin{aligned}\mathbb{E}\left(\min\left\{T_{P_1}, T_{L_1}, T_{M_1}\right\}\right) &= \int_0^\infty \sum_{k=1}^{n} \frac{(n\gamma_1 t)^{k-1}e^{-n\gamma_1 t}}{(k-1)!}e^{-\chi_1 t}e^{-\mu t}dt \\ &= \sum_{k=1}^{n}\int_0^\infty \frac{(n\gamma_1 t)^{k-1}e^{-(n\gamma_1+\chi_1+\mu)t}}{(k-1)!}dt \qquad (2.26) \\ &= \frac{1}{\chi_1+\mu}\left[1-\left(\frac{n\gamma_1}{n\gamma_1+\chi_1+\mu}\right)^n\right],\end{aligned}$$

and the average total time spent in I and H is given by

$$\begin{aligned}\mathbb{E}\left(\min\left\{T_{P_1}, T_{M_1}\right\}\right) &= \int_0^\infty \sum_{k=1}^{n} \frac{(n\gamma_1 t)^{k-1} e^{-n\gamma_1 t}}{(k-1)!} e^{-\mu t} dt \\ &= \sum_{k=1}^{n} \int_0^\infty \frac{(n\gamma_1 t)^{k-1} e^{-(n\gamma_1+\mu)t}}{(k-1)!} dt = \frac{1}{\mu}\left[1 - \left(\frac{n\gamma_1}{n\gamma_1+\mu}\right)^n\right].\end{aligned} \tag{2.27}$$

Thus, the average time spent in H is given by

$$\begin{aligned}&\mathbb{E}\left(\min\left\{T_{P_1}, T_{M_1}\right\}\right) - \mathbb{E}\left(\min\left\{T_P, T_L, T_M\right\}\right) \\ &= \frac{1}{\mu}\left[1 - \left(\frac{n\gamma_1}{n\gamma_1+\mu}\right)^n\right] - \frac{1}{\chi_1+\mu}\left[1 - \left(\frac{n\gamma_1}{n\gamma_1+\chi_1+\mu}\right)^n\right].\end{aligned} \tag{2.28}$$

Note also that

$$p_{M1} = \mathbb{P}(T_{M_1} = \min\left\{T_{P_1}, T_{L_1}, T_{M_1}\right\}) + \mathbb{P}(T_{L_1} < T_{M_1} < T_{P_1}) = 1 - \left(\frac{n\gamma_1}{n\gamma_1+\mu}\right)^n. \tag{2.29}$$

Substituting expressions (2.26)–(2.29) into (2.25), we arrive at the following expression

$$\begin{aligned}\mathcal{R}_{C1} &= \frac{\beta_I}{\chi_1+\mu}\left[1 - \left(\frac{n\gamma_1}{n\gamma_1+\chi_1+\mu}\right)^n\right] \\ &\quad + \frac{\beta_H}{\mu}\left[\frac{\chi_1}{\chi_1+\mu} + \frac{\mu}{\chi_1+\mu}\left(\frac{n\gamma_1}{n\gamma_1+\chi_1+\mu}\right)^n - \left(\frac{n\gamma_1}{n\gamma_1+\mu}\right)^n\right] \\ &\quad + \frac{\beta_F}{\gamma_f}\left[1 - \left(\frac{n\gamma_1}{n\gamma_1+\mu}\right)^n\right].\end{aligned} \tag{2.30}$$

The next generation matrix approach for model (2.18) requires much more involved computations including the inverse of the transition matrix. The expression for $\mathcal{R}_C$ has the following form

$$\mathcal{R}_{C1} = \frac{\beta_I}{n\gamma_1+\chi_1+\mu}\sum_{j=1}^{n} q_{I_j} + \frac{\beta_H}{n\gamma_1+\mu}\sum_{j=1}^{n} q_{H_j} + \frac{\beta_F}{\gamma_f} p_{M1}, \tag{2.31}$$

where q_X denote the probabilities of being in compartment $X = I_j$ or H_j for $j = 1, \cdots, n$; i.e.,

$$q_{I_j} = \left(\frac{n\gamma_1}{n\gamma_1+\chi_1+\mu}\right)^{j-1},$$

$$q_{H_j} = \sum_{i=1}^{j}\left(\frac{n\gamma_1}{n\gamma_1+\chi_1+\mu}\right)^{i-1}\frac{\chi_1}{n\gamma_1+\chi_1+\mu}\left(\frac{n\gamma_1}{n\gamma_1+\mu}\right)^{j-i}, \quad j = 1, \cdots, n,$$

and p_{M1} denotes the probability of death for Model I, given by

$$p_{M1} = \frac{\mu}{n\gamma_1 + \chi_1 + \mu} \sum_{j=1}^{n} q_{I_j} + \frac{\mu}{n\gamma_1 + \mu} \sum_{j=1}^{n} q_{H_j} = 1 - \left(\frac{n\gamma_1}{n\gamma_1 + \mu} \right)^n . \tag{2.32}$$

In p_{M_1}, the first term corresponds to the probability of death without being hospitalized, whereas the second term corresponds to the probability of death after being hospitalized. Note that the average total times in I, H and D are $\sum_{j=1}^{n} \frac{q_{I_j}}{n\gamma_1+\chi_1+\mu}$, $\sum_{j=1}^{n} \frac{q_{H_j}}{n\gamma_1+\mu}$ and p_{M1}/γ_f, respectively. Note also that

$$\begin{aligned} \sum_{j=1}^{n} q_{I_j} &= 1 + \frac{n\gamma_1}{n\gamma_1 + \chi_1 + \mu} + \cdots + \left(\frac{n\gamma_1}{n\gamma_1 + \chi_1 + \mu} \right)^{n-1} = \sum_{j=1}^{n} \left(\frac{n\gamma_1}{n\gamma_1 + \chi_1 + \mu} \right)^{j-1} \\ &= \frac{n\gamma_1 + \chi_1 + \mu}{\chi_1 + \mu} \left[1 - \left(\frac{n\gamma_1}{n\gamma_1 + \chi_1 + \mu} \right)^n \right] \end{aligned}$$

and

$$\begin{aligned} \sum_{j=1}^{n} q_{H_j} &= \underbrace{\sum_{j=1}^{n} \left(\frac{n\gamma_1}{n\gamma_1 + \chi_1 + \mu} \right)^{j-1} \frac{\chi_1}{n\gamma_1 + \chi_1 + \mu}}_{\text{(probability of path } I_1 \to I_j \to H_j)} \\ &\quad + \underbrace{\sum_{j=1}^{n} \sum_{i=1}^{j} \left(\frac{n\gamma_1}{n\gamma_1 + \chi_1 + \mu} \right)^{i-1} \frac{\chi_1}{n\gamma_1 + \chi_1 + \mu} \left(\frac{n\gamma_1}{\gamma_1 + \mu} \right)^{j-i}}_{\text{(probability of path } I_1 \to I_i \to H_i \to H_j)} \\ &= \sum_{k=1}^{n} \left(\frac{n\gamma_1}{n\gamma_1 + \chi_1 + \mu} \right)^{k-1} \frac{\chi_1}{n\gamma_1 + \chi_1 + \mu} \sum_{i=k}^{n} \left(\frac{n\gamma_1}{n\gamma_1 + \mu} \right)^{i} . \end{aligned}$$

Based on the biological meanings of the quantities involved in the expression for $\mathcal{R}_{C1}$ in (2.31), it is clear that the formula (2.31) describes the control reproduction number for the ODE model (2.18).

We repeat that the formula of $\mathcal{R}_{C1}$ for general distributions (2.25) is very helpful and convenient to use when specific stage distributions are considered. The derivation using probabilistic arguments also provides a contrast to the derivation of $\mathcal{R}_{C1}$ using the next-generation matrix approach, which requires intensive algebraic computations including the computation of the inverse of the transition matrix.

2.4.2 Reproduction number $\mathcal{R}_{C2}$ for Model II

As for Model I, we derive the formula for $\mathcal{R}_{C2}$ using two approaches. For the derivation of $\mathcal{R}_{C2}$ using the approach of probabilistic process, define two waiting times T_{P_2} and T_{L_2} corresponding to P_2 and L_2. The expectations of T_{P_2} and T_{L_2} are the infectious period and average time before hospitalization. Let $\mathbb{E}(T_{P_2})$ denote the expected total time spent in the I and H compartments and let $\mathbb{E}(\min\{T_{P_2}, T_{L_2}\})$ denote the expected time in the I compartment. Then the expected time spent in the H compartment is $\mathbb{E}(T_{P_2}) - \mathbb{E}(\min\{T_{P_2}, T_{L_2}\})$. Let $p_{H2} = \mathbb{P}(T_{L_2} < T_{P_2})$, which denotes the probability of being hospitalized. Then, using these general notations we can write the reproduction number $\mathcal{R}_{C2}$ as

$$\begin{aligned}\mathcal{R}_{C2} &= \beta_I \mathbb{E}(\min\{T_{P_2}, T_{L_2}\}) + \beta_H \left[\mathbb{E}(T_{P_2}) - \mathbb{E}(\min\{T_{P_2}, T_{L_2}\})\right] \\ &\quad + \beta_F \frac{1}{\gamma_f}\left[f(1-p_{H2}) + f p_{H2}\right]. \end{aligned} \tag{2.33}$$

Consider the special case when $P_2 = G^n_{n\gamma_2}$ and $L_2 = G^1_{\chi_2}$ (see (2.20)). Note that

$$\begin{aligned}\mathbb{E}(\min\{T_{P_2}, T_{L_2}\}) &= \int_0^\infty \sum_{k=1}^{n} \frac{(n\gamma_2 t)^{k-1} e^{-n\gamma_2 t}}{(k-1)!} e^{-\chi_2 t} dt \\ &= \sum_{k=1}^{n} \int_0^\infty \frac{(n\gamma_2 t)^{k-1} e^{-(n\gamma_2+\chi_2)t}}{(k-1)!} dt = \frac{1}{n\gamma_2+\chi_2} \sum_{k=1}^{n} \left(\frac{n\gamma_2}{n\gamma_2+\chi_2}\right)^{k-1} \\ &= \frac{1}{\chi_2}\left[1 - \left(\frac{n\gamma_2}{n\gamma_2+\chi_2}\right)^n\right].\end{aligned}$$

The time spent in the H compartments is given by

$$\mathbb{E}(T_{P_2}) - \mathbb{E}(\min\{T_{P_2}, T_{L_2}\}) = \frac{1}{\gamma_2} - \frac{1}{\chi_2}\left[1 - \left(\frac{n\gamma_2}{n\gamma_2+\chi_2}\right)^n\right].$$

Note that $f(1-p_{H2}) + f p_{H2} = f$. Substituting these expressions into the general formula (2.33) for $\mathcal{R}_{C2}$, we obtain

$$\mathcal{R}_{C2} = \beta_I \frac{1}{\chi_2}\left[1 - \left(\frac{n\gamma_2}{n\gamma_2+\chi_2}\right)^n\right] + \beta_H \left[\frac{1}{\gamma_2} - \frac{1}{\chi_2}\left[1 - \left(\frac{n\gamma_2}{n\gamma_2+\chi_2}\right)^n\right]\right] + \beta_F \frac{f}{\gamma_f}. \tag{2.34}$$

When using the next generation matrix approach for the ODEs model (2.21), we obtain

$$\mathcal{R}_{C2} = \beta_I \frac{1}{n\gamma_2 + \chi_2} \sum_{k=1}^{n} q_{Ik} + \beta_H \frac{1}{n\gamma_2} \sum_{k=1}^{n} q_{Hk} + \beta_F \frac{1}{\gamma_f} p_{M2}, \tag{2.35}$$

where q_X and p_M are defined in the same way as in section 2.4.1, although they have different expressions from those in Model I. It can be verified that the formula for $\mathcal{R}_{C2}$ is identical to (2.33).

2.4.3 Reproduction number $\mathcal{R}_{C3}$ for Model III

We can derive $\mathcal{R}_{C3}$ using the two approaches as for Models I and II. Because the derivations are similar, we omit the details, and present the formula only for the special case when P_3 and Q_3 are both exponential distributions, i.e., $P_3 = G^1_{\gamma_3}$ and $Q_3 = G^1_{\omega_3}$ (see (2.23)). In this case, the formula for $\mathcal{R}_{C3}$ for the ODEs model (2.24) with $m = n = 1$ is given by

$$\mathcal{R}_{C3} = \frac{\beta_I}{\gamma_3} + p\frac{\beta_H}{\omega_3} + f\frac{\beta_D}{\gamma_f}. \tag{2.36}$$

Remark 2.7. If we compare the $\mathcal{R}_{C3}$ formula with the $\mathcal{R}_C$ formula in (2.9), the two are identical when $\gamma_3 = \gamma$ and $\omega_3 = \omega$. This suggests again that the model (2.24), as the reduction of Model III when P_3 and L_3 are exponential distributions, is equivalent to the Legrand model.

2.5 Connections between the Legrand model and Models I, II and III

In this section, we compare the general Models I, II and III, particularly the ODEs models (2.18), (2.21) and (2.24), which are their reductions when the distributions P, L, M, Q are Gamma or exponential. We investigate the key differences between these models and compare them with the Legrand model, which helps identify its underlying assumptions.

The key difference between Models I, II and III (or between the ODEs models (2.18), (2.21) and (2.24)) is in the parameters that define the stage distributions P,

L, M and Q. Particularly, the parameters γ_j for the Gamma distributions $P_j = G^n_{n\gamma_j}$ $(j = 1, 2, 3)$ have very different connections with other epidemiological parameters. Because the distributions P_1, P_2 and P_3 describe different processes, γ_1, γ_2 and γ_3 have very different meanings. In fact, how γ's are connected to other epidemiological parameters (e.g., the time between onset and recovery absent control, duration of hospitalization, time between onset and death, etc.) can play important role in model structure and outcomes, as well as the meaning of other parameters such as χ and μ.

2.5.1 Parameters in Model I and their connection to other epidemiological parameters

When P_1, L_1 and M_1 are exponential with the respective parameters γ_1, χ_1 and μ, because of the assumption for Model I that the three events IR, IH and ID are independent, the overall waiting time in the I compartment is also exponential with the rate constant $\gamma_1 + \chi_1 + \mu$. From the definition of these parameters, we can link them to those in Table 2.1. For example,

$$\frac{1}{\gamma_1} = (1-p)(1-f)\frac{1}{\gamma_{IR}}, \tag{2.37}$$

It is also convenient sometimes to express the rates χ_1, and μ in terms of γ_{IR}, p and f. Note from (2.37) that

$$\gamma_1 = \frac{\gamma_{IR}}{(1-p)(1-f)}. \tag{2.38}$$

Note that the probability of death (see (2.29) with $n = 1$ and (2.38)) is given by

$$f = p_{M1} = 1 - \left(\frac{n\gamma_1}{n\gamma_1 + \mu}\right)^n = \frac{\mu}{\gamma_1 + \mu}. \tag{2.39}$$

from (2.37) and (2.39) we can solve for μ, i.e.,

$$\mu = \frac{\gamma_{IR} f}{(1-p)(1-f)^2}. \tag{2.40}$$

Notice also that the probability of hospitalization, which occurs before recovery or death, is (see Appendix for a detailed derivation)

$$\begin{aligned} p = p_{H1} &= \mathbb{P}(T_{L_1} = \min\{T_{P_1}, T_{L_1}, T_{M_1}\}) = \int_{T_{P_1}, T_{M_1} > T_{L_1}} g_{P_1}(s) g_{M_1}(u) g_{L_1}(t) du dt ds, \\ &= \int_0^\infty \int_0^t \int_0^u g_{L_1}(s) ds \; g_{M_1}(u) du \; g_{P_1}(t) dt \quad (T_{P_1} \geq T_{M_1} \geq T_{L_1}) \\ &\quad + \int_0^\infty \int_0^u \int_0^t g_{L_1}(s) ds \; g_{P_1}(t) dt \; g_{M_1}(u) du \quad (T_{M_1} \geq T_{P_1} \geq T_{L_1}) \\ &= \frac{\chi_1}{\chi_1 + \mu} \left[1 - \left(\frac{n\gamma_1}{\chi_1 + n\gamma_1 + \mu} \right)^n \right] = \frac{\chi_1}{\gamma_1 + \chi_1 + \mu} \quad (\text{for} \quad n = 1). \end{aligned} \tag{2.41}$$

Using (2.38) and (2.41) we can solve for χ_1, i.e.,

$$\chi_1 = \frac{p\gamma_{IR}}{(1-p)^2(1-f)^2}. \tag{2.42}$$

In this case, the formula for $\mathcal{R}_{C1}$ in (2.25) simplifies to

$$\mathcal{R}_{C1} = \frac{\beta_I}{\gamma_1 + \chi_1 + \mu} + \frac{\beta_H}{\gamma_1 + \mu} \frac{\chi_1}{\gamma_1 + \chi_1 + \mu} + \frac{\beta_D}{\gamma_f} \frac{\mu}{\gamma_1 + \mu} = \frac{\beta_I}{\gamma_1 + \chi_1 + \mu} + \frac{\beta_H p}{\gamma_1 + \mu} + \frac{\beta_D f}{\gamma_f}. \tag{2.43}$$

The formula for p_{H1} for Gamma distributions can also be calculated from the reduced ODE model (2.18) or by looking at all possible paths to enter any of the H_k (Fig. 2.3.1(b)), which leads to

$$p_{H1} = \sum_{k=1}^{n} \frac{\chi_1}{\chi_1 + n\gamma_1 + \mu} \left(\frac{n\gamma_1}{\chi_1 + n\gamma_1 + \mu} \right)^{k-1} = \frac{\chi_1}{\chi_1 + \mu} \left[1 - \left(\frac{n\gamma_1}{\chi_1 + n\gamma_1 + \mu} \right)^n \right].$$

Comparison between Model I and the Legrand model

Consider the ODE formulation (2.18) of Model I. In the special case when P_1 is exponential (i.e., $P_1 = G^1_{\gamma_1}$), the ODE system reduces to

$$\begin{aligned}
\frac{dS}{dt} &= -\frac{1}{N}S(\beta_I I + \beta_H H + \beta_D D),\\
\frac{dE}{dt} &= \frac{1}{N}S(\beta_I I + \beta_H H + \beta_D D) - \alpha E,\\
\frac{dI}{dt} &= \alpha E - (\gamma_1 + \chi_1 + \mu)I,\\
\frac{dH}{dt} &= \chi_1 I - (\gamma_1 + \mu)H,\\
\frac{dD}{dt} &= \mu I + \mu H - \gamma_f D,\\
\frac{dR}{dt} &= \gamma_1 I + \gamma_1 H.
\end{aligned} \tag{2.44}$$

We can compare the system (2.44) with the system (2.3) (which is equivalent to the Legrand model).

First, note that in model (2.44) the per-capita transition rates from I to R and from H to R are both equal to γ_1, which means that the second constraint in (2.8) for model (2.3) cannot be satisfied (note that $\gamma_{IR} = \omega_{HR}$). Thus, Model I cannot be equivalent to the Legrand model. This suggests that Legrand et al. did *not* assume that the three processes of IR, IH and ID were independent exponential distributions and that the overall waiting time in the I compartment was the minimum of these three exponential waiting times.

Second, note that the exiting rate γ from I in (2.3) corresponds to the sum of rates $\gamma_1+\chi_1+\mu$ from I in (2.44). Note also that the condition (2.4) defines γ in terms of the common parameters γ_{IR}, γ_{IH}, γ_{ID}, p and f (see Table 2.1). To examine if this condition holds in model (2.44), we note from (2.37) that $\gamma_{IR} = (1-f)(1-p)\gamma_1$, $\gamma_{IH} = p\chi_1$ and $\gamma_{ID} = f(1-p)\mu$. Thus, The left- and right-hand-sides of the $1/\gamma$ equation in (2.4) are

$$\frac{1}{\gamma_1 + \chi_1 + \mu} \quad \text{and} \quad \frac{1}{\gamma_1} + \frac{1}{\chi_1} + \frac{1}{\mu},$$

respectively. Therefore, the condition (2.4) does not hold for model (2.44).

2.5.2 Parameters in Model II and their connection to other epidemiological parameters

The key difference between Model I and Model II may become more transparent by examining how the parameters such as γ_i and χ_i, which determine the stage distributions $P_i(t)$ and $L_i(t)$ $(i = 1, 2)$, are connected to the common parameters listed in Table 2.1. For example, for Model I, when the stage distributions are Gamma (P_1 and L_1) and exponential (M_1), the parameters γ_1, χ_1 and μ are linked to the common parameters as given in (2.37). For Model II, consider model (2.21) in which $P_2(t) = G^n_{n\gamma_2}(t)$ and $L_2(t) = G^1_{\chi_2}(t) = e^{-\chi_2 t}$, with the fraction $1 - f$ of the individuals exiting I recovering and the fraction f dying. Then, one way to link the parameter γ_2 to common parameters is to assume that the duration in I before recovery or death $(1/\gamma_2)$ is the weighted average of the durations D_{IR} and D_{ID} given not being hospitalized (see Table 2.1),

$$\frac{1}{\gamma_2} = (1-p)\Big[(1-f)\frac{1}{\gamma_{IR}} + f\frac{1}{\gamma_{ID}}\Big]. \tag{2.45}$$

From (2.45) and the fact that the probability of death is $\gamma_{ID}/(\gamma_{ID} + \gamma_{IR}) = f$, we can also solve for γ_2 and get

$$\gamma_2 = \frac{\gamma_{IR}}{2(1-p)(1-f)}. \tag{2.46}$$

From (2.37) and (2.45) we can observe the difference between γ_1 and γ_2 in terms of their connections with the common parameters listed in Table 2.1, particularly p, f and γ_{IR}.

Because P_2 and L_2 are independent, similar to the definition of χ_1 in Model I, we can link χ_2 to common parameters as

$$\frac{1}{\chi_2} = p\frac{1}{\gamma_{IH}}. \tag{2.47}$$

Similar to the derivation of $p = p_{H1}$ for Model I, we can also get $p = p_{H2} = \chi_2/(\gamma_2 + \chi_2)$. Then, for the ODE model (2.49), the formula for $\mathcal{R}_{C2}$ in (2.33) simplifies to

$$\mathcal{R}_{C2} = \frac{\beta_I}{\gamma_2 + \chi_2} + \frac{\beta_H p}{\gamma_2} + \frac{\beta_D f}{\gamma_f}. \tag{2.48}$$

Comparison of Model II with the Legrand model

In the special case when P_2 is exponential (i.e., $n = 1$), the ODE system (2.21) becomes

$$\begin{aligned}
\frac{dS}{dt} &= -\frac{1}{N}S(\beta_I I + \beta_H H + \beta_D D),\\
\frac{dE}{dt} &= \frac{1}{N}S(\beta_I I + \beta_H H + \beta_D D) - \alpha E,\\
\frac{dI}{dt} &= \alpha E - (\gamma_2 + \chi_2)I,\\
\frac{dH}{dt} &= \chi_2 I - \gamma_2 H,\\
\frac{dD}{dt} &= f\gamma_2 I + f\gamma_2 H(t) - \gamma_f D(t),\\
\frac{dR}{dt} &= (1-f)\gamma_2 I + (1-f)\gamma_2 H.
\end{aligned} \tag{2.49}$$

For the same reason as in Model I (i.e., equal rates of recovery from I and H compartments in (2.49) and the constraint (2.8) in Legrand model), Model II or (2.49) cannot be the same as the Legrand model.

In addition, similar to the case of Model I, we can examine whether or not the condition (2.4) for γ in model (2.3) also holds for model (2.49). Note, from the I equations in the two models, that the γ in (2.4) corresponds to the sum of rates $\gamma_2 + \chi_2$ in (2.49), which implies that

$$\frac{1}{\gamma} = \frac{1}{\gamma_2 + \chi_2}. \tag{2.50}$$

However, condition (2.4) implies (see (2.45) and (2.47)) that

$$\frac{1}{\gamma} = \frac{1}{\gamma_2} + \frac{1}{\chi_2},$$

which is not the same as (2.50). Therefore, the condition (2.4) does not hold in model (2.49).

2.5.3 Parameters in Model III and its equivalence to Legrand model

Recall that the ODE model (2.24), as the reduction of Model III, assumed that the distributions of overall times in the I and H compartments were two independent

Gamma distributions $P_3 = G^n_{n\gamma_3}$ and $Q_3 = G^m_{m\omega_3}$. Consider the special case when $n = m = 1$ (i.e., P_3 and Q_3 are exponential). The ODE model (2.24) simplifies to

$$\begin{aligned}
\frac{dS}{dt} &= -\frac{1}{N}S(\beta_I I + \beta_H H + \beta_D D),\\
\frac{dE}{dt} &= \frac{1}{N}S(\beta_I I + \beta_H H + \beta_D D) - \alpha E,\\
\frac{dI}{dt} &= \alpha E - \gamma_3 I,\\
\frac{dH}{dt} &= p\gamma_3 I - \omega_3 H,\\
\frac{dD}{dt} &= (1-p)f\gamma_3 I + f\omega_3 H - \gamma_f D,\\
\frac{dR}{dt} &= (1-p)(1-f)\gamma_3 I + (1-f)\omega_3 H.
\end{aligned} \tag{2.51}$$

Notice that, if we ignore the last term in the R equation in the equivalent Legrand model (2.3) (this term indicates that the R class includes those buried), the the model (2.51) is identical to the model (2.3) when the subscript "3" is dropped; that is, when γ_3 and ω_3 are defined as the follows:

$$\begin{aligned}
\frac{1}{\gamma_3} &= \frac{p}{\gamma_{IH}} + \frac{(1-p)f}{\gamma_{ID}} + \frac{(1-p)(1-f)}{\gamma_{IR}},\\
\frac{1}{\omega_3} &= \frac{f}{\omega_{HD}} + \frac{1-f}{\omega_{HR}},
\end{aligned} \tag{2.52}$$

together with the constraints

$$\begin{aligned}
\frac{1}{\gamma_{IR}} &= \frac{1}{\gamma_{IH}} + \frac{1}{\omega_{HR}},\\
\frac{1}{\gamma_{ID}} &= \frac{1}{\gamma_{IH}} + \frac{1}{\omega_{HD}}.
\end{aligned} \tag{2.53}$$

Remark 2.8. Note that the main difference between Models I, II and III lies in the assumptions on the underlying biological processes, particulaly the sojourn distributions for various stage transitions, which are described by functions $L(t)$, $P(t)$, $M(t)$ and $Q(t)$. The fact that the Legrand model can only be obtained from Model III, not from Models I and II, makes it transparent to identify the specific model assumptions made in the Legrand model in terms of these sojourn distributions. For example, our analyses suggest the following assumptions made in Legrand model:

(a) The overall sojourn in the I stage is assumed to be exponentially distributed with the average duration $1/\gamma$, which is further assumed to be the specific weighted average of $1/\gamma_{IR}$, $1/\gamma_{IH}$ and $1/\gamma_{ID}$ as given in (2.4), where $1/\gamma_{IR}$, $1/\gamma_{IH}$ and $1/\gamma_{ID}$ are the respective average stage durations of the IR, IH and ID events. However, from Model I we see that if the IR, IH and ID events follow independent exponential distributions with parameters γ_{IR}, γ_{IH} and γ_{ID}, then the overall sojourn in the I stage is exponentially distributed with the parameter $\gamma = \gamma_{IR} + \gamma_{IH} + \gamma_{ID}$ with the average duration

$$\frac{1}{\gamma} = \frac{1}{\gamma_{IR} + \gamma_{IH} + \gamma_{ID}},$$

which differs from (2.4).

(b) The distributions for the I and H stages are independent (see distributions $P_3(t)$ and $Q_3(t)$). This implies that the average time spent in the H stage before recovery or death ($1/\omega_3$) does not depend on the average time spent in the I stage before recovery or being hospitalized or dying ($1/\gamma_3$). Under this assumption, the time spent in H before recovery ($1/\gamma_{HR}$) does not take into consideration the time spent in I before being hospitalized ($1/\gamma_{IH}$) . Because of this independence, the model needs to impose a constraint to link these two durations (see (2.8)).

2.6 Discussion

The objective of this chapter is to investigate the underlying assumptions made in the Legrand model. Our approach is to develop three models with general distributed waiting times (e.g., $P(s), L(s)$, $M(s)$ and Q) for the processes associated with recovery, hospitalization, and death (referred to as events IR, IH and ID) under different assumptions about the connections between these processes. These models (see Models I, II and III in Sections 2.3.1, 2.3.2 and 2.3.3) are systems of integro-differential equations, but we show that they can be reduced to systems of ordinary differential

equations when sojourns are Gamma or exponential. Particularly, when these distribution are exponential, we can compare the resulting ODE models with the Legrand model, which allows us to identify the assumptions under which the general model reduces to the Legrand model.

Among the three ODE models (2.44), (2.49) and (2.51), which are reduced from the Models I, II and III with general distributions, the only model that can match the Legrand model is (2.51), for which the assumptions include: (i) The waiting times of the three events IR, IH and ID are *not* independent and (ii) the overall waiting time in the I compartment is a weighted average of the mean durations ($1/\gamma_{IR}$, $1/\gamma_{IH}$ and $1/\gamma_{ID}$) for the three events with weights determined by the probabilities of hospitalization p and death f, as described in (2.4) or (2.5). By examining ODE model (2.44), we found that, if the waiting times of three events IR, IH and ID are independent and exponentially distributed (with parameters γ_1, χ_1 and μ), then the overall waiting time from I should be an exponential distribution with the parameter $\gamma_1 + \chi_1 + \mu$. That is, the average overall waiting time should be $1/(\gamma_1 + \chi_1 + \mu)$, *not* a weighted average such as the ones in (2.4) or (2.5).

Control reproduction numbers $\mathcal{R}_{Ci}$ $(i = 1, 2, 3)$ for the three general models are derived, as well as their expressions when the general distributions are replaced by Gamma or exponential distributions. These formulas for $\mathcal{R}_{Ci}$ provide a means of examining the influence of assumptions on model outcomes. For example, consider the three control reproduction numbers $\mathcal{R}_{Ci}$ $(i = 1, 2, 3)$, which are given in (2.43), (2.48), and (2.36) corresponding to the three ODE models (2.44), (2.49), and (2.51), respectively. In the absence of hospitalization (i.e., $p = 0$), these $\mathcal{R}_{Ci}$ reduce to the corresponding basic reproduction numbers $\mathcal{R}_{0i}$ $(i = 1, 2, 3)$. Figure 2.4 illustrates the difference between the basic and control reproduction numbers of the three models for a given set of parameter values. Most of these parameter values are based on the Ebola outbreak in West Africa in 2014. We fix all parameters except β_i $(i = 1, 2, 3)$ and f. Then, for a fixed value of $f_0 = 0.7$, we estimate β_i $(i = 1, 2, 3)$ from a given value of $\mathcal{R}_0$ (assumed to be the same for all three models). Once we have the

value of β_i, we have three functions of f, $\mathcal{R}_{0i}(f)$ $(i = 1, 2, 3)$. For Figure 2.4(A), we used the common value of $\mathcal{R}_0(f_0) = 1.8$. The three curves are for Model I (the thin solid curve), Model II (the thick dashed curve), and Model III (the thick solid curve). The decreasing property of these curves represents the fact that higher disease morality decreases $\mathcal{R}_{0i}(f)$, which is expected because the assumption that $\beta_D < \beta_I$. An interesting observation is that the dependence of the basic reproduction number on disease death f is more dramatic in Model I than Models II and III, particularly for smaller f values. For smaller values f, Model I tends to generate the highest $\mathcal{R}_0$, while for larger f values, Model III provides higher $\mathcal{R}_0$. Other parameter values used are (time in days): $1/\gamma_{IR} = 18, 1/\gamma_f = 2, 1/\alpha = 9$. Parameters such as μ, χ_i $(i = 1, 2)$ are calculated based on their relationships with the common parameters (e.g., (2.38), (2.40) and (2.42) for γ_1, μ and χ_1, respectively, (2.46) for γ_2, and (2.52) for γ_3 and ω_3, etc.).

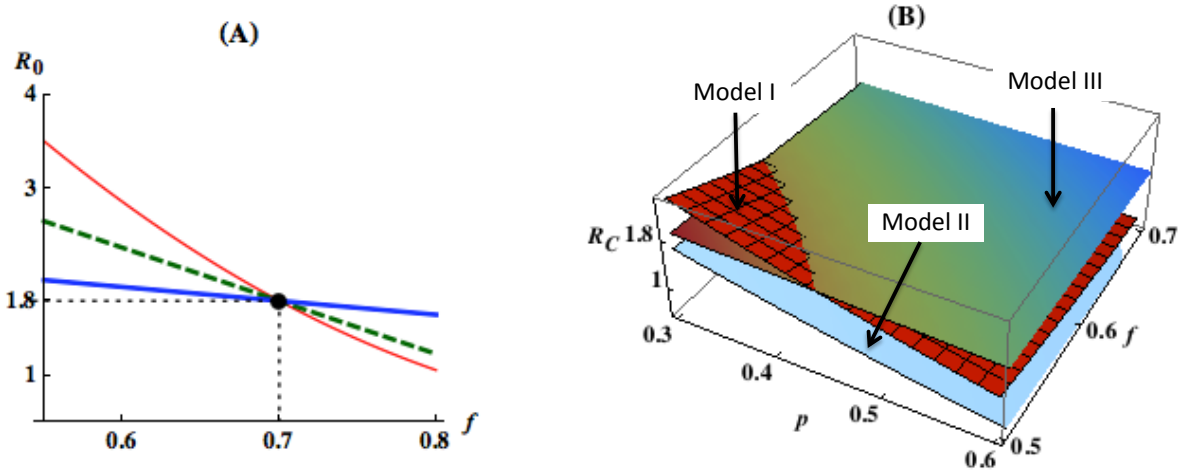

Fig. 2.4. Plots of the basic reproduction numbers (A) and control reproduction numbers (B) for the three models. In (A), $\mathcal{R}_0$ is plotted as a function of f for Model I (thin solid), Model II (thick dashed), and Model III (thick solid). The parameter values are chosen such that all three $\mathcal{R}_{0i}$ have the same value 1.8 at $f = 0.7$. In (B), $\mathcal{R}_{Ci}$ is plotted as a function of p and f for Models I, II, and III. Other parameter values are given in the text.

When control is considered ($p > 0$), the dependence of $\mathcal{R}_{Ci}$ on p and f is illustrated in Figure 2.4(B). We observe that, for the given set of parameter values, Model I (the darker surfce with mash) generates the highest $\mathcal{R}_C$ value than Models II (the lighter surface) and III (the darker surface with no mash) for smaller p and f, while Model III provides the highest for larger values of p and/or f. The differences in $\mathcal{R}_0$ and $\mathcal{R}_C$ between the three models indicate that model predictions about and evaluations of the effectiveness of control measures could be very different as well. Such an example is demonstrated in Figure 2.5. It shows the numerical simulation results of the three ODE models (2.44), (2.49) and (2.51), which are reduced from the Models I, II and III, and presented in columns 1 , 2, and 3, respectively. The A, B, and C panels correspond to three sets of (p, f) values: $(p, f) = (0, 0.7)$ (top panel), $(p, f) = (0.3, 0.5)$ (middle panel), $(p, f) = (0.2, 0.7)$ (bottom panel). The top panel (A1–A3) is for the case of no hospitalization ($p = 0$). We observe that the three models generate similar epidemic curve (fraction of infected individuals $(E + I + H)/N$), including peak sizes, times to peak, durations of epidemic (which lead to similar final epidemic sizes). From the middle panel (B1–B3), we observe that Model I has the highest peak size while Model II has the lowest. This is in agreement with the relative magnitudes of the control reproduction numbers $\mathcal{R}_{Ci}$, as the point $(p, f) = (0.3, 0.5)$ lies in the region where $\mathcal{R}_{C1} > \mathcal{R}_{C3} > \mathcal{R}_{C2}$ (see Figure 2.4). For the bottom panel (C1–C3), because the point $(p, f) = (0.2, 0.7)$ lies in the region where $\mathcal{R}_{C3} > \mathcal{R}_{C1} > \mathcal{R}_{C2}$, we observe that Model III generates the highest peak size while Model II has again the lowest.

Another interesting observation from Figure 2.5 is that Model 3 generated very similar epidemic curves for all three sets of (p, f) values (see A3, B3 and C3), whereas Model I (and II) produced vary different epidemic curves (A1, B1 and C1). This suggests that these three models may provide very different evaluations of the effects of control.

One of the main contributions of this study is to provide an equivalent (but simpler) formulation of the Legrand model (see Section 2.2). This simpler formulation not only makes the model presentation much clearer (due to a large reduction in the

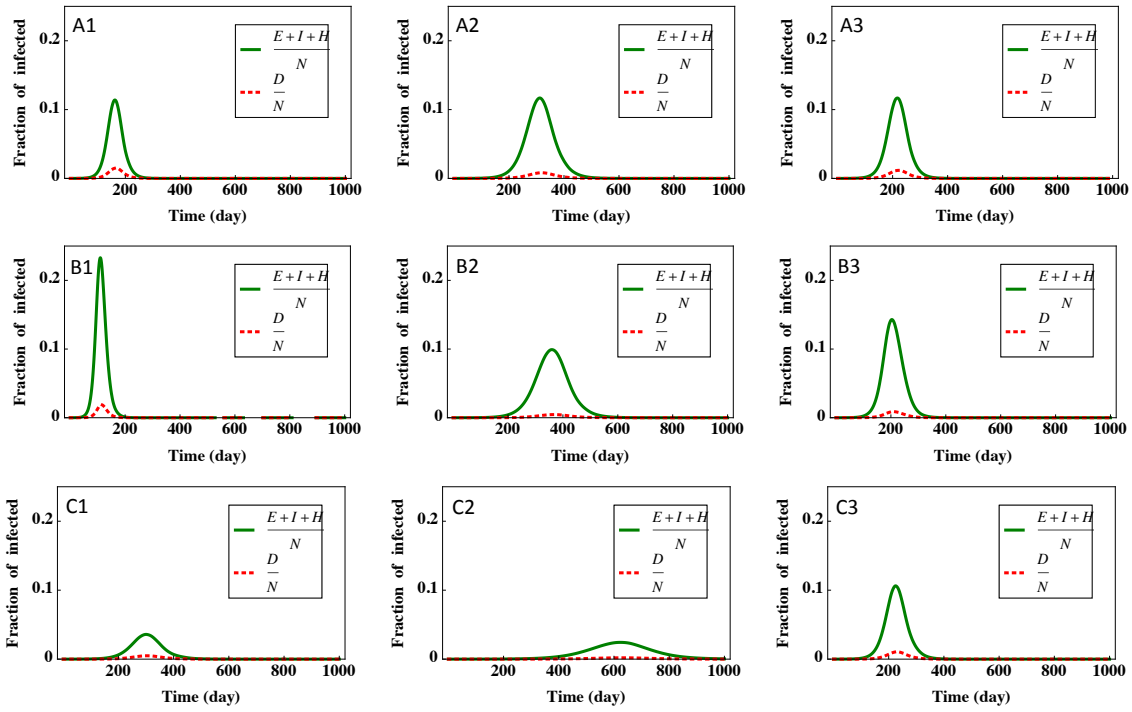

Fig. 2.5. Numerical simulations of the three ODE models (2.44), (2.49) and (2.51), which are reduced from the Models I (column 1) , II (column 2) and III (column 3), respectively. The fractions of infected individuals $(E + I + H)/N$) and death (D/N) are plotted over a time period of 1000 days. Three sets of (p, f) values are used: $(p, f) = (0, 0.7)$ (top row), $(p, f) = (0.3, 0.5)$ (middle row), $(p, f) = (0.2, 0.7)$ (bottom row). All other parameter values are the same as in Figure 2.4.

number of parameters involved), particularly when its extensions are considered, but also makes the computation of $\mathcal{R}_C$ much easier. More importantly, the simpler formulation makes it possible to compare the Legrand model with our three new models and to identify underlying assumptions used in the Legrand model.

Another significant contribution of this study is a detailed proof showing that the systems of integro-differential equations under arbitrarily-distributed stage durations can be reduced to systems of ODEs under Gamma distributions. Although such

reductions have been used in the literature (the so called "linear chain trick"), there has not heretofore been a rigorous proof for epidemiological models.

In this chapter, we focused only on identifying assumptions in the Legrand model. We have started to explore possible differences in the outcomes of Models I, II and III as well as their ODE reductions, both under Gamma- and exponentially-distributed stage durations, particularly which model would better capture the observed epidemics. Results will be published elsewhere.

2.7 Appendix

In this appendix, we provide a detailed proof showing that the simpler formulation of model (2.3) is equivalent to the Legrand model (1.1). We also provide the detailed derivation showing that the general integro-differential equations model (2.15) can be reduced to the ODE model (2.18) under gamma distribution for $P_1 = G^n_{n\gamma_1}$ and exponential distributions for $L_1 = G^1_{\chi_1}$ and $M_1 = G^1_{\mu}$, as given in (2.17).

2.7.1 Equivalence of model (2.3) to the Legrand model (1.1)

In this section, we show that model (2.3) is equivalent to the Legrand model (1.1), by showing that the coefficients in corresponding terms in the two models are equal. Note that the model (2.3) involves fewer parameters than the Legrand model (1.1). In addition to the two common parameters, p and f, the model equations involve two more parameters, γ and ω, which are defined by using only the common parameters listed in Table 2.1 (see (2.4) or (2.5)).

Our derivation is for the general case in which f_i and f_h can be different, which simplifies if $f_i = f_h = f$. Define γ and ω as

$$\frac{1}{\gamma} = p\frac{1}{\gamma_h} + (1-p)f_i\frac{1}{\gamma_d} + (1-p)(1-f_i)\frac{1}{\gamma_i}, \tag{2.54}$$

$$\frac{1}{\omega} = f_h\frac{1}{\gamma_{dh}} + (1-f_h)\frac{1}{\gamma_{ih}}, \tag{2.55}$$

which simplifies to (2.5) when $f_i = f_h = f$. Notice that, in Legrand et al. (2007) [20],

$$\delta_1 = \frac{\gamma_i f_i}{\gamma_i f_i + \gamma_d(1-f_i)}, \quad \delta_2 = \frac{\gamma_{ih} f_h}{\gamma_{ih} f_h + \gamma_{dh}(1-f_h)}, \quad \theta_1 = \frac{p(\gamma_d\delta_1 + \gamma_i(1-\delta_1))}{p\big[\gamma_d\delta_1 + \gamma_i(1-\delta_1)\big] + (1-p)\gamma_h}, \tag{2.56}$$

with $p = \theta$ and $f_i = f_h = \delta$, from which we have that

$$f_i = \frac{1}{\gamma_d\delta_1 + \gamma_i(1-\delta_1)}, \ f_h = \frac{1}{\gamma_{dh}\delta_2 + \gamma_{ih}(1-\delta_2)}, \ p = \frac{1}{\gamma_h\theta_1 + \gamma_i(1-\theta_1)(1-\delta_1) + \gamma_d(1-\theta_1)\delta_1}. \tag{2.57}$$

Substituting (2.57) into (2.55), we obtain

$$\gamma = \gamma_h\theta_1 + \gamma_i(1-\theta_1)(1-\delta_1) + \gamma_d(1-\theta_1)\delta_1, \tag{2.58}$$

$$\omega = \gamma_{dh}\delta_2 + \gamma_{ih}(1-\delta_2). \tag{2.59}$$

Next, we match other coefficients in the H, D, and R equations of the model (2.3) to the corresponding ones in the model (1.1). This includes (note that $f_i = f_h = f$) $p\gamma$ in the H equations:

$$\begin{aligned} p\gamma &= \frac{\gamma_h\theta_1}{\gamma_h\theta_1 + \gamma_i(1-\theta_1)(1-\delta_1) + \gamma_d(1-\theta_1)\delta_1} \cdot (\gamma_h\theta_1 + \gamma_i(1-\theta_1)(1-\delta_1) + \gamma_d(1-\theta_1)\delta_1) \\ &= \gamma_h\theta_1, \end{aligned}$$

$(1-p)f_i\gamma$ and $f_h\omega$ in the D equation (with $f_i = f_h = f$):

$$\begin{aligned} (1-p)f_i\gamma &= \frac{\gamma_i(1-\theta_1)(1-\delta_1) + \gamma_d(1-\theta_1)\delta_1}{\gamma_h\theta_1 + \gamma_i(1-\theta_1)(1-\delta_1) + \gamma_d(1-\theta_1)\delta_1} \\ &\quad \cdot \frac{\gamma_d(1-\theta_1)\delta_1}{\gamma_i(1-\theta_1)(1-\delta_1) + \gamma_d(1-\theta_1)\delta_1} \cdot (\gamma_h\theta_1 + \gamma_i(1-\theta_1)(1-\delta_1) + \gamma_d(1-\theta_1)\delta_1) \\ &= \gamma_d(1-\theta_1)\delta_1, \end{aligned}$$

and

$$f_h\omega = \frac{\gamma_{dh}\delta_2}{\gamma_{dh}\delta_2 + \gamma_{ih}(1-\delta_2)} \cdot (\gamma_{dh}\delta_2 + \gamma_{ih}(1-\delta_2)) = \gamma_{dh}\delta_2,$$

$(1-p)(1-f_i)\gamma$ and $(1-f_h)w$ in the R equation (with $f_i = f_h = f$):

$$\begin{aligned} (1-p)(1-f_i)\gamma &= \frac{\gamma_i(1-\theta_1)(1-\delta_1) + \gamma_d(1-\theta_1)\delta_1}{\gamma_h\theta_1 + \gamma_i(1-\theta_1)(1-\delta_1) + \gamma_d(1-\theta_1)\delta_1} \\ &\quad \cdot \frac{\gamma_i(1-\theta_1)(1-\delta_1)}{\gamma_i(1-\theta_1)(1-\delta_1) + \gamma_d(1-\theta_1)\delta_1} \\ &\quad \cdot (\gamma_h\theta_1 + \gamma_i(1-\theta_1)(1-\delta_1) + \gamma_d(1-\theta_1)\delta_1) \\ &= \gamma_i(1-\theta_1)(1-\delta_1), \end{aligned}$$

and

$$(1-f_h)\omega = \frac{\gamma_{ih}(1-\delta_2)}{\gamma_{dh}\delta_2+\gamma_{ih}(1-\delta_2)}\cdot(\gamma_{dh}\delta_2+\gamma_{ih}(1-\delta_2)) = \gamma_{ih}(1-\delta_2).$$

It follows that all corresponding coefficients in the two models, (1.1) and (2.3), are the same. Thus, these two models are equivalent.

2.7.2 Derivation of the ODE formulation for Model I

In this section, we show that ODE system (2.18) can be derived from the general Model I (2.15) under Gamma and exponential distributions. For ease of notation, we omit the subscripts in P, L, M, γ and χ.

Consider the I equation in (2.17). From the I equation in (2.15), we have

$$\begin{aligned}
I(t) &= \int_0^t \alpha E(s) G_\mu^1(t-s) G_\chi^1(t-s) G_{n\gamma}^n(t-s) ds + I(0) G_\mu^1(t) G_\chi^1(t) G_{n\gamma}^n(t), \\
&= \int_0^t \alpha E(s) e^{-\mu(t-s)} e^{-\chi(t-s)} \sum_{j=1}^{n} \frac{(n\gamma(t-s))^{j-1} e^{-n\gamma(t-s)}}{(j-1)!} ds + I(0) e^{-\mu t} e^{-\chi t} \sum_{j=1}^{n} \frac{(n\gamma t)^{j-1} e^{-n\gamma t}}{(j-1)!}, \\
&= \sum_{j=1}^{n} \left(\int_0^t \alpha E(s) e^{-\mu(t-s)} e^{-\chi(t-s)} \frac{(n\gamma(t-s))^{j-1} e^{-n\gamma(t-s)}}{(j-1)!} ds + I(0) e^{-\mu t} e^{-\chi t} \frac{(n\gamma t)^{j-1} e^{-n\gamma t}}{(j-1)!} \right), \\
&\doteq \sum_{j=1}^{n} I_n(t),
\end{aligned}$$

where

$$I_j(t) = \int_0^t \alpha E(s) e^{-\mu(t-s)} e^{-\chi(t-s)} \frac{(n\gamma(t-s))^{j-1} e^{-n\gamma(t-s)}}{(j-1)!} ds + I(0) e^{-\mu t} e^{-\chi t} \frac{(n\gamma t)^{j-1} e^{-n\gamma t}}{(j-1)!},$$

for $j = 1, \cdots, n$. Note that for $j = 1$,

$$I_1(t) = \int_0^t \alpha E(s) e^{-\mu(t-s)} e^{-\chi(t-s)} e^{-n\gamma(t-s)} ds + I(0) e^{-\mu t} e^{-\chi t} e^{-n\gamma t}.$$

Differentiation of this $I_1(t)$ equation yields

$$\begin{aligned}
I_1'(t) &= \alpha E(t) - (n\gamma + \chi + \mu) \left(\int_0^t \alpha E(s) e^{-\mu(t-s)} e^{-\chi(t-s)} e^{-n\gamma(t-s)} ds + I(0) e^{-\mu t} e^{-\chi t} e^{-n\gamma t} \right), \\
&= \alpha E(t) - (n\gamma + \chi + \mu) I_1(t),
\end{aligned}$$

which is the I_1' equation in (2.18). Differentiation of the $I_j(t)$ equation for $j > 1$ leads to

$$\begin{aligned}
I_j'(t) &= \alpha E(t)e^{-\mu\cdot 0}e^{-\chi\cdot 0}\frac{(n\gamma\cdot 0)^{j-1}e^{-n\gamma\cdot 0}}{(j-1)!} \\
&\quad + \int_0^t \alpha E(s)\frac{d}{dt}\left(e^{-\mu(t-s)}e^{-\chi(t-s)}\frac{(n\gamma(t-s))^{j-1}e^{-n\gamma(t-s)}}{(j-1)!}\right)ds \\
&\quad + I(0)\frac{d}{dt}\left(e^{-\mu t}e^{-\chi t}\frac{(n\gamma t)^{j-1}e^{-n\gamma t}}{(j-1)!}\right), \\
&= \int_0^t \alpha E(s)e^{-\mu(t-s)}e^{-\chi(t-s)}\left(n\gamma\frac{(n\gamma(t-s))^{j-2}e^{-n\gamma(t-s)}}{(j-2)!} - n\gamma\frac{(n\gamma(t-s))^{j-1}e^{-n\gamma(t-s)}}{(j-1)!}\right)ds \\
&\quad -(\mu+\chi)\int_0^t \alpha E(s)e^{-\mu(t-s)}e^{-\chi(t-s)}\frac{(n\gamma(t-s))^{j-1}e^{-n\gamma(t-s)}}{(j-1)!}ds \\
&\quad + I(0)e^{-\mu t}e^{-\chi t}\left(n\gamma\frac{(n\gamma t)^{j-2}e^{-n\gamma t}}{(j-2)!} - n\gamma\frac{(n\gamma t)^{j-1}e^{-n\gamma t}}{(j-1)!}\right) \\
&\quad -(\mu+\chi)I(0)e^{-\mu t}e^{-\chi t}\frac{(n\gamma t)^{j-1}e^{-n\gamma t}}{(j-1)!}, \\
&= \int_0^t \alpha E(s)e^{-\mu(t-s)}e^{-\chi(t-s)}\left(n\gamma\frac{(n\gamma(t-s))^{j-2}e^{-n\gamma(t-s)}}{(j-2)!}\right)ds \\
&\quad + I(0)e^{-\mu t}e^{-\chi t}\left(n\gamma\frac{(n\gamma t)^{j-2}e^{-n\gamma t}}{(j-2)!}\right) \\
&\quad + \int_0^t \alpha E(s)e^{-\mu(t-s)}e^{-\chi(t-s)}\left(-n\gamma\frac{(n\gamma(t-s))^{j-1}e^{-n\gamma(t-s)}}{(j-1)!}\right)ds \\
&\quad + I(0)e^{-\mu t}e^{-\chi t}\left(-n\gamma\frac{(n\gamma t)^{j-1}e^{-n\gamma t}}{(j-1)!}\right) \\
&\quad -(\mu+\chi)\int_0^t \alpha E(s)e^{-\mu(t-s)}e^{-\chi(t-s)}\frac{(n\gamma(t-s))^{j-1}e^{-n\gamma(t-s)}}{(j-1)!}ds \\
&\quad -(\mu+\chi)I(0)e^{-\mu t}e^{-\chi t}\frac{(n\gamma t)^{j-1}e^{-n\gamma t}}{(j-1)!}, \\
&= n\gamma I_{j-1}(t) - (n\gamma+\chi+\mu)I_j(t),
\end{aligned}$$

which is the same as the I_j' equation in (2.18).

From the H equation in (2.15),

$$\begin{aligned}
H(t) &= \int_0^t \alpha E(s)P(t-s)M(t-s)(1-L(t-s))ds + I(0)P(t)M(t)(1-L(t)), \\
&= \int_0^t \alpha E(s)e^{-\mu(t-s)} \sum_{j=1}^{n} \frac{(n\gamma(t-s))^{j-1}e^{-n\gamma(t-s)}}{(j-1)!}(1-e^{-\chi(t-s)})ds \\
&\quad + I(0)e^{-\mu t} \sum_{j=1}^{n} \frac{(n\gamma t)e^{-n\gamma t}}{(j-1)!}(1-e^{-\chi t}), \\
&= \sum_{j=1}^{n} \left[\int_0^t \alpha E(s)e^{-\mu(t-s)} \frac{(n\gamma(t-s))^{j-1}e^{-n\gamma(t-s)}}{(j-1)!}(1-e^{-\chi(t-s)})ds \right. \\
&\quad \left. + I(0)e^{-\mu t} \frac{(n\gamma t)e^{-n\gamma t}}{(j-1)!}(1-e^{-\chi t}) \right], \\
&\doteq \sum_{j=1}^{n} H_j(t).
\end{aligned}$$

Thus, for $j = 1$

$$H_1(t) = \int_0^t \alpha E(s)e^{-\mu(t-s)}e^{-n\gamma(t-s)}(1-e^{-\chi(t-s)})ds + I(0)e^{-\mu t}e^{-n\gamma t}(1-e^{-\chi t}).$$

Differentiating this H_1 equation we have

$$\begin{aligned}
H_1'(t) &= \chi \left[\int_0^t \alpha E(s)e^{-\mu(t-s)}e^{-n\gamma(t-s)}e^{-\chi(t-s)}ds + I(0)e^{-\mu t}e^{-n\gamma t}e^{-\chi t} \right] \\
&\quad -(n\gamma+\mu) \left[\int_0^t \alpha E(s)e^{-\mu(t-s)}e^{-n\gamma(t-s)}\chi e^{-\chi(t-s)}ds + I(0)e^{-\mu t}e^{-n\gamma t}\chi e^{-\chi t} \right], \\
&= \chi I_1(t) - (n\gamma+\mu)H_1(t).
\end{aligned}$$

which is the H_1' equation in (2.18).

For $j > 1$,

$$\begin{aligned}
H_j(t) &= \int_0^t \alpha E(s)e^{-\mu(t-s)} \frac{(n\gamma(t-s))^{j-1}e^{-n\gamma(t-s)}}{(j-1)!}(1-e^{-\chi(t-s)})ds \\
&\quad + I(0)e^{-\mu t} \frac{(n\gamma t)e^{-n\gamma t}}{(j-1)!}(1-e^{-\chi t}).
\end{aligned}$$

Thus,

$$\begin{aligned}
H_j'(t) &= \chi \left[\int_0^t \alpha E(s)e^{-\mu(t-s)} \frac{(n\gamma(t-s))^{j-1}e^{-n\gamma(t-s)}}{(j-1)!}e^{-\chi(t-s)}ds + I(0)e^{-\mu t} \frac{(n\gamma t)^{j-1}e^{-n\gamma t}}{(j-1)!}e^{-\chi t} \right] \\
&\quad + \left[\int_0^t \alpha E(s)e^{-\mu(t-s)} \frac{d}{dt} \left(\frac{(n\gamma(t-s))^{j-1}e^{-n\gamma(t-s)}}{(j-1)!} \right) e^{-\chi(t-s)}ds \right. \\
&\quad \left. + I(0)e^{-\mu t} \frac{d}{dt} \left(\frac{(n\gamma t)^{j-1}e^{-n\gamma t}}{(j-1)!} \right) e^{-\chi t} \right] \\
&\quad -\mu \left[\int_0^t \alpha E(s)e^{-\mu(t-s)} \frac{(n\gamma(t-s))^{j-1}e^{-n\gamma(t-s)}}{(j-1)!}\chi e^{-\chi(t-s)}ds \right. \\
&\quad \left. + I(0)e^{-\mu t} \frac{(n\gamma t)^{j-1}e^{-n\gamma t}}{(j-1)!}\chi e^{-\chi t} \right], \\
&= \chi I_j(t) + n\gamma H_{j-1}(t) - n\gamma H_j(t) - \mu H_j(t),
\end{aligned}$$

which is the H_j' $(j > 1)$ equation in (2.18).

For the D equation

$$\begin{aligned}
D(t) &= \int_0^t \left[\int_0^\tau \alpha E(s)P(\tau-s)g_M(\tau-s)ds + I(0)P(\tau)g_M(\tau)\right] e^{-\gamma_f(t-\tau)}d\tau, \\
&= \int_0^t \left[\int_0^\tau \alpha E(s)\sum_{j=1}^n \frac{(n\gamma(\tau-s))^{j-1}e^{-n\gamma(\tau-s)}}{(j-1)!}\mu e^{-\mu(\tau-s)}ds \right. \\
&\qquad \left. + I(0)\sum_{j=1}^n \frac{(n\gamma\tau)^{j-1}e^{-n\gamma\tau}}{(j-1)!}\mu e^{-\mu\tau}\right] e^{-\gamma_f(t-\tau)}d\tau, \\
&= \sum_{j=1}^n \int_0^t \left[\int_0^\tau \alpha E(s)\frac{(n\gamma(\tau-s))^{j-1}e^{-n\gamma(\tau-s)}}{(j-1)!}\mu e^{-\mu(\tau-s)}ds \right. \\
&\qquad \left. + I(0)\frac{(n\gamma\tau)^{j-1}e^{-n\gamma\tau}}{(j-1)!}\mu e^{-\mu\tau}\right] e^{-\gamma_f(t-\tau)}d\tau.
\end{aligned}$$

and thus,

$$\begin{aligned}
D'(t) &= \mu\sum_{j=1}^n \left[\int_0^t \alpha E(s)e^{-\mu(t-s)}\frac{(n\gamma(t-s))^{j-1}e^{-n\gamma(t-s)}}{(j-1)!}e^{-\chi(t-s)}ds + I(0)e^{-\mu t}\frac{(n\gamma t)e^{-n\gamma t}}{(j-1)!}e^{-\chi t}\right] \\
&\quad +\mu\sum_{j=1}^n \left[\int_0^t \alpha E(s)e^{-\mu(t-s)}\frac{(n\gamma(t-s))^{j-1}e^{-n\gamma(t-s)}}{(j-1)!}(1-e^{-\chi(t-s)})ds \right. \\
&\qquad \left. + I(0)e^{-\mu t}\frac{(n\gamma t)e^{-n\gamma t}}{(j-1)!}(1-e^{-\chi t})\right] \\
&\quad -\gamma_f\sum_{j=1}^n \int_0^t \left[\int_0^\tau \alpha E(s)\frac{(n\gamma(\tau-s))^{j-1}e^{-n\gamma(\tau-s)}}{(j-1)!}\mu e^{-\mu(\tau-s)}ds \right. \\
&\qquad \left. + I(0)\frac{(n\gamma\tau)^{j-1}e^{-n\gamma\tau}}{(j-1)!}\mu e^{-\mu\tau}\right] e^{-\gamma_f(t-\tau)}d\tau, \\
&= \sum_{j=1}^n \mu I_j(t) + \sum_{j=1}^n \mu H_j(t) - \gamma_f D(t),
\end{aligned}$$

which is the D' equation in (2.18).

Finally, for the R equation,

$$\begin{aligned}
R(t) &= \int_0^t \left[\int_0^\tau \alpha E(s)g_p(\tau-s)M(\tau-s)ds + I(0)g_p(\tau)M(\tau)\right] d\tau \\
&= \int_0^t \left[\int_0^\tau \alpha E(s)\frac{(n\gamma(\tau-s))^{n-1}n\gamma e^{-n\gamma(\tau-s)}}{(n-1)!}e^{-\mu(\tau-s)}ds + I(0)\frac{(n\gamma\tau)^{n-1}n\gamma e^{-n\gamma\tau}}{(n-1)!}e^{-\mu\tau}\right] d\tau,
\end{aligned}$$

which leads to the R' equation in (2.18):

$$\begin{aligned}
R'(t) &= \int_0^t \alpha E(s)\frac{(n\gamma(t-s))^{n-1}n\gamma e^{-n\gamma(t-s)}}{(n-1)!}e^{-\mu(t-s)}ds + I(0)\frac{(n\gamma t)^{n-1}n\gamma e^{-n\gamma t}}{(n-1)!}e^{-\mu t}, \\
&= n\gamma I_n(t) + n\gamma H_n(t).
\end{aligned}$$

This completes the proof.

The probability of hospitalization p_{H1} for Model I

Consider the model (2.18), which is Model I in the case when $P_1(t) = G^n_{n\gamma_1}$, $L_1(t) = G^1_{\chi 1}$ and $M_1(t) = G^1_\mu$. The proportion of infected individuals that are hospitalized (see (2.41)) is given by smaller

$$\begin{aligned}
p_{H1} &= \int_0^\infty \int_0^t \int_0^u \chi e^{-\chi s} ds\ \mu e^{-\mu u} du\ \frac{(n\gamma)^n t^{n-1} e^{-n\gamma t}}{n!} dt \\
&\quad + \int_0^\infty \int_0^u \int_0^t \chi e^{-\chi s} ds\ \frac{(n\gamma)^n t^{n-1} e^{-n\gamma t}}{n!} dt\ \mu e^{-\mu u} du, \\
&= \int_0^\infty \int_0^t \left(1 - e^{-\chi u}\right) \mu e^{-\mu u} du\ \frac{(n\gamma)^n t^{n-1} e^{-n\gamma t}}{n!} dt \\
&\quad + \int_0^\infty \int_0^u \left(1 - e^{-\chi t}\right) \frac{(n\gamma)^n t^{n-1} e^{-n\gamma t}}{n!} dt\ \mu e^{-\mu u} du, \\
&= \int_0^\infty \int_0^t \left(1 - e^{-\chi u}\right) \mu e^{-\mu u} du\ \frac{(n\gamma)^n t^{n-1} e^{-n\gamma t}}{n!} dt \\
&\quad + \int_0^\infty \int_t^\infty \mu e^{-\mu u} du\ \left(1 - e^{-\chi t}\right) \frac{(n\gamma)^n t^{n-1} e^{-n\gamma t}}{n!} dt, \\
&= \int_0^\infty \left[1 - e^{-\mu t} - \frac{\mu}{\chi + \mu}\left(1 - e^{-(\chi+\mu)t}\right)\right] \frac{(n\gamma)^n t^{n-1} e^{-n\gamma t}}{n!} dt \\
&\quad + \int_0^\infty e^{-\mu t}\left(1 - e^{-\chi t}\right) \frac{(n\gamma)^n t^{n-1} e^{-n\gamma t}}{n!} dt, \\
&= \left[1 - \frac{(n\gamma)^n}{(n\gamma+\mu)^n} - \frac{\mu}{\chi+\mu}\left(1 - \frac{(n\gamma)^n}{(n\gamma+\chi+\mu)^n}\right)\right] \\
&\quad + \left[\frac{(n\gamma)^n}{(n\gamma+\mu)^n} - \frac{(n\gamma)^n}{(n\gamma+\chi+\mu)^n}\right], \\
&= \left(1 - \frac{\mu}{\chi+\mu}\right)\left(1 - \frac{(n\gamma)^n}{(n\gamma+\chi+\mu)^n}\right), \\
&= \frac{\chi}{\chi+\mu}\left[1 - \left(\frac{n\gamma}{\chi+n\gamma+\mu}\right)^n\right].
\end{aligned}$$

3. EBOLA MODELS - THE SPECTRUM OF EBOLA SYMPTOMS

The work presented in this chapter was done in collaboration with Lin, Glasser and Hill. Most of the results and ideas in this chapter will be submitted to a Mathematical Biology related journal. I contribute several parts of the manuscript but not exclusively, including model formulation and analysis as well as the writing of the manuscript.

3.1 Introduction

Many mathematical models have been applied to the 2014-15 Ebola outbreak in West Africa to estimate the basic reproduction number and evaluate control measures [20–22, 25, 32, 51–53]. Most of these models do not consider the spectrum of Ebola infection symptoms. However, Ebola virus disease presents clinically in a complicated way, as infected individuals report various symptoms. For the 2014-15 West Africa Ebola outbreak, even the most common symptom, fever, is not experienced by 13% of patients. There are even rare cases reported with hemorrhagic symptoms ($< 5.7\%$) [14]. This suggests that infected individuals experience a spectrum of symptoms, from mild to severe. Asymptomatic infections are quite possible, as shown in previous Ebola outbreaks [27, 28]. There are few exceptions [26, 54], but these studies do not consider asymptomatic or moderately symptomatic infections.

Some of the spectrum of Ebola symptoms might be explained through immunological responses to Ebola infection [55–57]. Following the infection of some naive individuals, Ebola virus could evade the innate immune response by interfering with or disabling the detection and signaling functions of immune cells, for instance, dendritic cells and macrophages, etc. This evasion could lead to systemic virus replication

and increase the chance of disease-induced death due to multiple organ failures. For those infected whose innate responses to infection are successful, the initial replication of Ebola virus may be limited or even contained [28]. Successful adaptive immune responses to the virus could lead to full recovery from infection. Variable immune response processes might be the ultimate source of the wide range of symptoms. As similar Ebola viruses circulated in Africa previously (the earliest outbreak caused by Ebola virus was traced back to 1976 [5]), however, people infected before might have partial immunity against the new strain [58] and their adaptive immune response work quickly enough after infection to contain initial viral replication, resulting in few or mild symptoms. In addition, the immunological responses may be related to host genetics. Host genetic studies [59] show that genetic background determines susceptibility and resistance to many infectious diseases, including the strain Ebola virus recently circulating in West Africa [60]. Thus, host genetics may determine if individuals are resistant or susceptible to severe hemorrhagic fever [61].

This chapter aims to account crudely for the spectrum of clinical symptoms that characterizes Ebola infection by modeling mild, moderate and severe infections explicitly through a compartmental model. We augment Model II in Chapter 2 by adding mild and moderately symptomatic to susceptible, exposed, infectious, hospitalized and deceased (not buried yet) and recovered compartments. Furthermore, in modeling mild and moderate symptoms, two possible pathways are considered based on possible outcomes of the initial replication of Ebola virus due to host biological processes. If replication of the virus is limited by genetic resistance or partial immunity, infected people are routed from the susceptible to mild or asymptomatic compartment. If Ebola virus replicates, but is contained by a strong innate immune response, the resulting moderate symptoms are captured by moving people from the exposed compartment to the moderately infectious compartment. Based on their viral load, those becoming asymptomatic directly probably are not infectious, while moderately symptomatic individuals from the exposed class probably are infectious, but less so than those with severe symptoms.

This chapter demonstrates the importance of modeling asymptomatic and moderately symptomatic people in modeling applications. For example, early outbreak data from Liberia are used to estimate the basic reproduction number (there were limited effects of control measures before the middle of September, 2014 [14, 26]). Using this model, the basic reproduction number is estimated as 1.83 for Liberia, consistent with the WHO estimate via a different approach. If mild and moderate symptoms are disabled, however, the estimated reproduction number is 1.97, which is 7.6% higher. This shows that models without the full range of symptoms might overestimate the basic reproduction number. In addition, after international interventions began ([62], the outbreak shows a significant reduction in admissions to hospitals by mid-September, 2014). Based on estimation results, the model without mild and moderately symptomatic infections overestimates the reduction in transmission rates in the community, hospitals and after death. This means that credit given to control measures actually is due to asymptomatic or moderately symptomatic infections as those people also contribute to herd immunity.

This chapter is organized as follows: Section 3.2 elaborates the model, derives the reproduction number, and calibrates the model to the Liberia outbreak. Section 3.3 studies the effectiveness of possible controls from the perspectives of the basic reproduction number and final size. Section 3.4 is devoted to discussion.

3.2 Models and data fitting

The objective of the chapter is to enhance our understanding of the effects of infections with mild and moderate symptoms on Ebola modeling. A compartmental model is developed based on Model II in Chapter 2 by including mildly (or asymptomatic) and moderately symptomatic compartments. This model is fitted to case reports from the 2014-2015 Liberia outbreak. The basic reproduction number is estimated based on the method of maximum likelihood using the early data. The case

counts are assumed to be Poisson distributed. The control effects are estimated using the data after inventions were implemented.

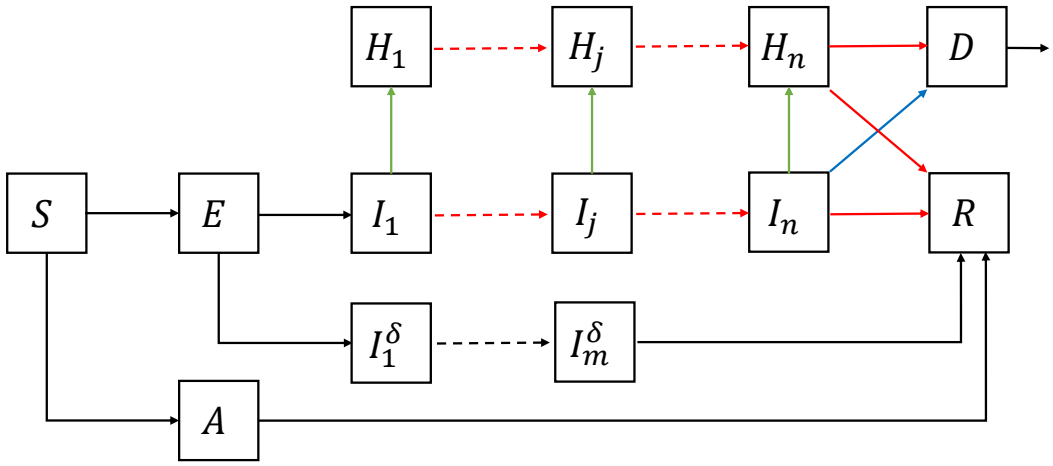

Fig. 3.1. Model Diagram of Chapter 3.

3.2.1 Compartmental model and basic reproduction number

The model developed in this chapter considers different possible outcomes of Ebola infection, including asymptomatic, moderate and severe symptoms, to crudely account for the spectrum of disease reported by Ebola patients. For new infections, individuals might become asymptomatic directly from susceptible, if the initial virus replication is contained due to genetic resistance or partial immunity due to previous exposure. Individuals could also go through the exposed period if the virus replicates and symptoms appear. Depending on the outcome of viral replication and host immunological response, individuals could be mildly infectious with moderate symptoms or fully infectious with severe symptoms. The infectious periods of moderate and severe symptoms are assumed to have different distributions. Those with moderate symptoms have an infectious period following a Gamma distribution with shape parameter m and rate parameter $m\gamma_\delta$, i.e., on average $1/\gamma_\delta$ infectious period. Once

their infectious period ends, these individuals recover. They could be hospitalized, but have limited infectivity, so the reduction in their transmission rate by virtue of isolation is negligible. Thus, the hospitalization of moderately symptomatic people is ignored for simplicity. Individuals with severe symptoms have an infectious period following another Gamma distribution with shape parameter n and rate parameter $n\gamma$, i.e., on average $1/\gamma$ infectious period. During their infectious period, individuals could be hospitalized at each sub-stage. The infectious period ends due either to recovery or disease-induced death if individuals are not hospitalized. These individuals could only die during the last sub-stage of their infectious periods when symptoms become severe, for example, internal bleeding and organ failures. The total infections contain σ mild (or asymptomatic), $(1-\sigma)\delta$ moderate and $(1-\sigma)(1-\delta)$ severe symptoms. Model II in Chapter 2 is used as the base model for severe symptoms. One advantage of this base model is that it allows infection histories to carry over after hospitalization. This advantage arises from its underlying assumption that the transitions to hospitalization and disease progression are independent. Intuitively, the waiting times of these transitions are measured by independent clocks. If the hospitalization clock rings, individuals are hospitalized before they progress. The clock of disease progression continues running even after the hospitalization of these individuals and rings due either to their recovery or disease-induced death. This underlying assumption is explained in more detail in [48] through integral-differential equations, which are reduced to ordinary differential equations (ODEs) when waiting times follow Gamma distributions.

The ODE models contain compartments: susceptible S, mild (or asymptomatic) infected A, latent (exposed) E, infectious with moderate symptoms I_k^δ, $k = 1, \ldots, m$, infectious with severe symptoms I_j, $j = 1, \ldots n$, hospitalized H_j, $j = 1, \ldots n$, and disease-induced death and not safely buried D as well as recovered R, where the shape parameters of the gamma distributions are integers m and n for the infectious with moderate and severe symptoms. The total population is $N(t) = S(t) + A(t) +$

$E(t) + I(t) + I_\delta(t) + H(t) + R(t)$, where $I_\delta(t) = \sum_{k=1}^{m} I_k^\delta(t)$, $I(t) = \sum_{j=1}^{n} I_j(t)$, and $H(t) = \sum_{l=1}^{n} H_l(t)$.

The model is as follows,

$$\begin{aligned}
\frac{dS(t)}{dt} &= -\lambda(t)S(t), \qquad \lambda(t) = \frac{\beta_I(I(t) + \varepsilon I_\delta(t)) + \beta_H H(t) + \beta_D D(t)}{N(t)} \\
\frac{dA(t)}{dt} &= \sigma\lambda(t)S(t) - \nu A(t), \\
\frac{dE(t)}{dt} &= (1-\sigma)\lambda(t)S(t) - \alpha E(t), \\
\frac{dI_1^\delta(t)}{dt} &= \delta\alpha E(t) - m\gamma_\delta I_1^\delta(t), \\
\frac{dI_k^\delta(t)}{dt} &= m\gamma_\delta I_{k-1}^\delta(t) - m\gamma_\delta I_k^\delta(t), \text{ for } k = 2, \ldots, m \\
\frac{dI_1(t)}{dt} &= (1-\delta)\alpha E(t) - (n\gamma + \chi)I_1(t), \\
\frac{dI_j(t)}{dt} &= n\gamma I_{j-1}(t) - (n\gamma + \chi)I_j(t), \text{ for } j = 2, \ldots, n \\
\frac{dH_1(t)}{dt} &= \chi I_1(t) - n\gamma H_1(t), \\
\frac{dH_j(t)}{dt} &= \chi I_j(t) + n\gamma H_{j-1}(t) - n\gamma H_j(t), \text{ for } j = 2, \ldots, n \\
\frac{dD(t)}{dt} &= fn\gamma I_n(t) + fn\gamma H_n(t) - \gamma_f D(t), \\
\frac{dR(t)}{dt} &= (1-f)n\gamma I_n(t) + (1-f)n\gamma H_n(t) + m\gamma_\delta I_m^\delta(t) + \nu A.
\end{aligned} \tag{3.1}$$

where $\lambda(t)$ is the force of infection, β_I, β_H and β_D are transmission rates in the community, hospital and at funerals (deceased but not yet safely buried), σ is the fraction mildly symptomatic, δ is the fraction moderately symptomatic from exposed, $1/\nu$ is the duration of asymptomatic (or mildly symptomatic) infections, $1/\gamma_\delta$ and $1/\gamma$ are the average infectious periods for moderate and severe symptoms, $1/\alpha$ is the latent period, $1/\chi$ is the time from disease onset to hospitalization, and f is the case fatality. In addition, the infectious period $1/\gamma$ can be parameterized by the weighted average

$$\frac{1}{\gamma} = f\frac{1}{\gamma_{ID}} + (1-f)\frac{1}{\gamma_{IR}}, \tag{3.2}$$

where $1/\gamma_{ID}$ is the period from disease onset to death and $1/\gamma_{IR}$ is the period from onset to recovery. (See Table 3.1). This is because disease progression is in fact the

coupled process of recovery and disease-induced death, as when either of these two events occurs the infectious period ends.

The basic reproduction number is the average number of secondary infections caused by an infected individual while infectious. The reproduction number may be computed based on the underlying stochastic processes modeled. This provides an alternative to the next generation matrix approach that is more intuitive and simpler. There are four infectious compartments for moderately and severely symptomatic people. For an infectious person with severe symptoms, there are stochastic waiting times for disease progression and hospitalization denoted, respectively, by T_P and T_L. The expectations of T_P and T_L are the infectious period and time from disease onset to hospitalization denoted by $\mathbb{E}(T_P)$ and $\mathbb{E}(T_L)$. Then $\mathbb{E}(min\{T_P, T_L\})$ is the expected time in the I compartment before infectious individuals leave I due to disease progression or hospitalization, and further $\mathbb{E}(T_P) - \mathbb{E}(min\{T_P, T_L\})$ is the expected time in H compartment. Moderately symptomatic individuals have only a waiting time for disease progression denoted by T_δ and their duration moderately infectious is $\mathbb{E}(T_\delta)$. Remember that the probability of being moderately symptomatic is $(1-\sigma)\delta$ and of severely symptomatic is $(1-\sigma)(1-\delta)$. Thus, the basic reproduction number is the weighted average of the reproduction number of severely and moderately symptomatic,

$$\mathcal{R}_0 \;=\; (1-\sigma)(1-\delta)\mathcal{R}_{10} + (1-\sigma)\delta\mathcal{R}_{20},$$

where $\mathcal{R}_{10}$ is the reproduction number if there are only severe symptoms and no mild or moderate symptoms, i.e.

$$\mathcal{R}_{10} = \beta_I \mathbb{E}(min\{T_P, T_L\}) + \beta_H \left[\mathbb{E}(T_P) - \mathbb{E}(min\{T_P, T_L\})\right] + \beta_D \frac{f}{\gamma_f},$$

and $\mathcal{R}_{20}$ is the reproduction number if there are only moderate symptoms and no mild or severe symptoms, i.e.

$$\mathcal{R}_{20} = \varepsilon\beta_I \mathbb{E}(T_\delta).$$

Biologically, $\mathcal{R}_{10}$ and $\mathcal{R}_{20}$ are the sums of transmission rates times the corresponding expected durations of severe and moderate symptoms.

To compute the expectations, we assume Gamma distributed sojourns, i.e., the distributions of these waiting times T_P, T_L and T_δ follow Gamma distributions as is implicitly assumed by the multiple sub-stages of the compartmental ordinary differential equation model. The waiting times T_P, T_L and T_δ have the Gamma survival functions

$$G^n_{n\gamma}(t) = \sum_{j=1}^{n} \frac{(n\gamma t)^{j-1} e^{-n\gamma t}}{(j-1)!}, \quad G^1_\chi = e^{-\chi t}, \quad G^m_{m\gamma_\delta}(t) = \sum_{j=1}^{n} \frac{(m\gamma_\delta t)^{j-1} e^{-m\gamma_\delta t}}{(j-1)!}.$$

Then $\mathbb{E}(T_P) = 1/\gamma$, $\mathbb{E}(T_L) = 1/\chi$, $\mathbb{E}(T_\delta) = 1/\gamma_\delta$ and

$$\begin{aligned} \mathbb{E}(min\{T_P, T_L\}) &= \int_0^\infty \sum_{j=1}^{n} \frac{(n\gamma t)^{j-1} e^{-n\gamma t}}{(j-1)!} e^{-\chi t} dt = \sum_{j=1}^{n} \int_0^\infty \frac{(n\gamma t)^{j-1} e^{-(n\gamma+\chi)t}}{(j-1)!} dt \\ &= \frac{1}{n\gamma+\chi} \sum_{j=1}^{n} \left(\frac{n\gamma}{n\gamma+\chi}\right)^{j-1} = \frac{1}{\chi}\left[1 - \left(\frac{n\gamma}{n\gamma+\chi}\right)^n\right], \end{aligned}$$

and

$$\mathbb{E}(T_P) - \mathbb{E}(min\{T_P, T_L\}) = \frac{1}{\gamma} - \frac{1}{\chi}\left[1 - \left(\frac{n\gamma}{n\gamma+\chi}\right)^n\right].$$

Therefore,

$$\begin{aligned} \mathcal{R}_0 &= (1-\sigma)(1-\delta)\beta_I \frac{1}{\chi}\left[1 - \left(\frac{n\gamma}{n\gamma+\chi}\right)^n\right] \\ &\quad + (1-\sigma)(1-\delta)\beta_H \left[\frac{1}{\gamma} - \frac{1}{\chi}\left[1 - \left(\frac{n\gamma}{n\gamma+\chi}\right)^n\right]\right] \\ &\quad + (1-\sigma)(1-\delta)\beta_D \frac{f}{\gamma_f} + \frac{(1-\sigma)\delta\varepsilon\beta_I}{\gamma_\delta}. \end{aligned}$$

It is shown that the basic reproduction number given in this way is equivalent to the next generation matrix in previous chapter. We also denote the components of $\mathcal{R}_0$ associated with I, H and D by $\mathcal{R}_0^I$, $\mathcal{R}_0^H$ and $\mathcal{R}_0^D$, and to I_δ by $\mathcal{R}_0^{I_\delta}$, respectively, and $\mathcal{R}_0 = \mathcal{R}_0^I + \mathcal{R}_0^H + \mathcal{R}_0^D + \mathcal{R}_0^{I_\delta}$ with

$$\begin{aligned} \mathcal{R}_0^I &= (1-\sigma)(1-\delta)\beta_I \frac{1}{\chi}\left[1 - \left(\frac{n\gamma}{n\gamma+\chi}\right)^n\right], \\ \mathcal{R}_0^H &= (1-\sigma)(1-\delta)\beta_H \left[\frac{1}{\gamma} - \frac{1}{\chi}\left[1 - \left(\frac{n\gamma}{n\gamma+\chi}\right)^n\right]\right], \\ \mathcal{R}_0^D &= (1-\sigma)(1-\delta)\beta_D \frac{f}{\gamma_f}, \qquad \mathcal{R}_0^{I_\delta} = \frac{(1-\sigma)\delta\varepsilon\beta_I}{\gamma_\delta}. \end{aligned}$$

It is helpful to find the contributions from all infectious compartments in the model, as they shed light on how to mitigate each part.

Remark that in case of no asymptomatic or mildly symptomatic infections $\sigma = 0$ and no moderately symptomatic ones $\delta = 0$, the reproduction number $\mathcal{R}_0 = \mathcal{R}_{10}$ is the same as the reproduction number for Model II in Chapter 2.

3.2.2 Estimation of the reproduction number

Data from the Liberia outbreak were obtained through the CDC's website [63], which are extracted from WHO situation reports [16]. Observations before September 12, 2014 are suitable for estimating the reproduction number because interventions had not yet altered the epidemic curve [14]. Though there were some local efforts to curtail the outbreak from the middle of August 2014, their effects were not significant [26]. To have an accurate estimate, we used the data from June 6, 2014 to September 12, 2014 to calibrate the models and estimate the reproduction number [14, 26].

In estimation, the reported cases from Liberia are assumed to be Poisson samples from the model. We implement maximum likelihood estimation using the R package bbmle for estimation and the package deSolve for solving ODEs similar to [21]. We estimate the transmission rate and use estimates of the WHO Ebola Response Team [14] and others (see Table 3.3) for other parameters. Given the estimated transmission rate, the basic reproduction number is computed. The confidence intervals are computed through bootstrapping. The method firstly reassembles the data by combining predictions and residuals randomly. Second, the model is refitted to the reassembled data. Then confidence intervals are based on estimates of the refitted model. We used Bellan et al.'s estimate [54] that 50% of infections are asymptomatic with a lower bound of 20%. The proportions of infections that are asymptomatic and moderately symptomatic are assumed to be 20% and 30% with 50% of infected people having severe symptoms, i.e., $\sigma = 0.2$, $(1 - \sigma)\delta = 0.3$, to which we refer as combination (a). Three other combinations are also considered: 50% of infections

Table 3.1.
Model parameters in Chapter 3.

Symbol	Definition	Value (Range)	References
β_I	community transmission rate	0.433 (0.35, 0.45)	estimated
β_H	hospital transmission rate	0.6 (0.55, 0.65)β_I	[22]
β_D	traditional burial transmission rate	1.2 (0.9, 1.3)β_I	[18, 26]
ε	the ratio of mild relative to typical infectivity	0.1 (0, 0.3)	assumed
$1/\gamma_{IH}$	time from disease onset to hospitalization	4.9 (4.8, 5.3) days	[8, 14, 20]
$1/\gamma_{ID}$	duration from disease onset to death	7.9 (7.5, 8.5)days	[8, 20]
$1/\gamma_{IR}$	duration from disease onset to recovery	9 (8.5, 9.5)days	[26]
$1/\nu$	duration of asymptomatic infection	3 days	assumed
$1/\gamma_\delta$	duration of mild symptoms	7 (3, 9) days	assumed
$1/\alpha$	duration of the latent (exposed) period for symptomatic infection	9.5 (9, 12)days	[9, 14, 26]
$1/\gamma_f$	duration of the diseased	2 (1.5, 2.5) days	[8, 20, 26]
σ	probability of asymptomatic infection	0.2 (0.2, 0.5)	[54]
δ	conditional probability of having mild symptoms	0.375 (0, 0.375)	[54]
f	probability of disease induced death for the infected with typical symptoms (case fatality rate)	0.723 (0.69, 0.73)	[9, 14]

Table 3.2.
Estimated reproduction number using the data from June 8, 2014 until September 12, 2014. (a) 20% (σ) asymptomatic and 30% $(1-\sigma)\delta$ moderately symptomatic, (b) 0% asymptomatic and 50% moderately symptomatic, (c) 50% asymptomatic and 0% moderately symptomatic (d) 0% asymptomatic and 0% moderately symptomatic.

	$\mathcal{R}_0$	$\mathcal{R}_0^I$	$\mathcal{R}_0^H$	$\mathcal{R}_0^D$	$\mathcal{R}_0^{I_\delta}$
(a)	1.83	0.75	0.62	0.38	0.09
	(1.73, 1.95)	(0.70, 0.79)	(0.58,0.66)	(0.35, 0.40)	(0.08, 0.10)
(b)	1.77	0.70	0.58	0.35	0.14
	(1.70, 1.83)	(0.67, 0.72)	(0.55, 0.60)	(0.33, 0.36)	(0.13, 0.15)
(c)	1.972	0.85	0.70	0.43	0.00
	(1.88, 2.13)	(0.81, 0.91)	(0.67, 0.76)	(0.40, 0.46)	
(d)	1.97	0.85	0.70	0.43	0.00
	(1.84, 2.17)	(0.79, 0.93)	(0.65, 0.77)	(0.40, 0.47)	

with severe symptoms; (b) no asymptomatic (or mild) infections but 50% moderate symptoms, i.e. $\sigma = 0$, $(1-\sigma)\delta = 0.5$; (c) 50% asymptomatic and no moderate symptoms, i.e. $\sigma = 0.5$, $(1-\sigma)\delta = 0$; (d) no asymptomatic or moderate symptoms, i.e., $\sigma = (1-\sigma)\delta = 0$. The estimates of the basic reproduction number are listed in Table 3.2. The estimate from (1), i.e., $\mathcal{R}_0 = 1.83$, is consistent with the estimate from WHO response team using other statistical methods. We estimate that community transmission $\mathcal{R}_0^I = 0.747$ contributes the largest proportion 41% of the basic reproduction number. The hospital transmission $\mathcal{R}_0^H = 0.618$ contributes 34% and the deceased yet not buried transmission $\mathcal{R}_0^D = 0.375$ contributes 20%. The transmission from the moderate symptoms $\mathcal{R}_0^{I_\delta} = 0.091$ accounts for 5%. To control the outbreak in Liberia, community transmission is critical and controlling post-death transmission alone is not sufficient, consistent with results from [26]. All other estimates of (b), (c) and (d) are also in the range of existing estimates [8,9]. From the estimation results, combina-

tion (b) with 50% moderate symptoms provides the lowest estimate, possibly because of the limited infectivity of individuals with moderate symptoms. Combinations (c) and (d) provide similar estimates of the reproduction number because asymptomatic (or mildly symptomatic) infections are a small fraction from the very large susceptible population and thus these people have little impact on disease dynamics. The estimates of (c) and (d) are higher than (a) and (b) because asymptomatic (or mildly symptomatic) infections have little effect on transmission at the beginning, and they do not account explicitly for infected individuals with moderate symptoms, who have lower infectivity than those with severe symptoms. Comparison of reports and model fits are shown in Figure 3.2. All models capture the initial growth of the outbreak, though it is observed that the exponential curves are steeper for higher $\mathcal{R}_0$.

3.2.3 Uncertainty analysis of asymptomatic and moderately symptomatic infection

Uncertainty concerning mild (or asymptomatic) and moderately symptomatic infections could account for variability in reproduction number estimates. Thus, we implement the Sobol method by R package sensitivity and compute Sobol indices. The Sobol method [47] quantifies sources of variability due to different parameters. Sobol indices are the decomposed variance due to related parameters. We focus on asymptomatic and moderately symptomatic related parameters, which are drawn using the Latin hypercube sampling method from their ranges as follows: σ is the fraction asymptomatic and its range is (0.2, 0.5), δ is the fraction moderately symptomatic and its range is (0, 0.375), ε is the discounted ratio of transmission of infected people with moderate and typical symptoms (0, 0.3), and $1/\gamma_\delta$ is the infectious period of those moderately symptomatic with range (3, 9) days. Then the variability of the reproduction number is stratified according to uncertainty of the parameters. The proportions of variability due to each are shown in a pie chart and a histogram of the

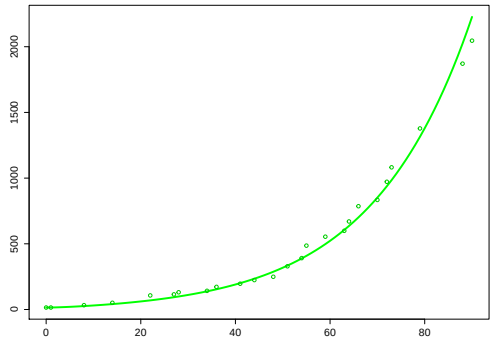

(a) 20% asymptomatic, 30% moderately symptomatic, i.e. $\sigma = 0.2$, $(1-\sigma)\delta = 0.3$.

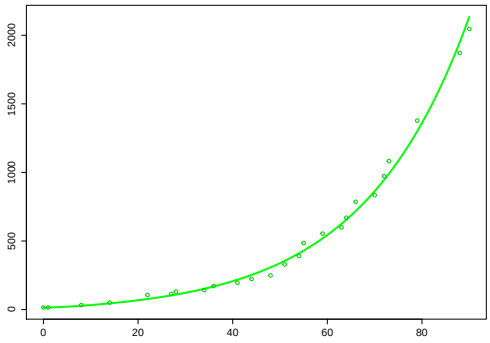

(b) 0% asymptomatic, 50% moderately symptomatic, i.e. $\sigma = 0$, $(1-\sigma)\delta = 0.5$.

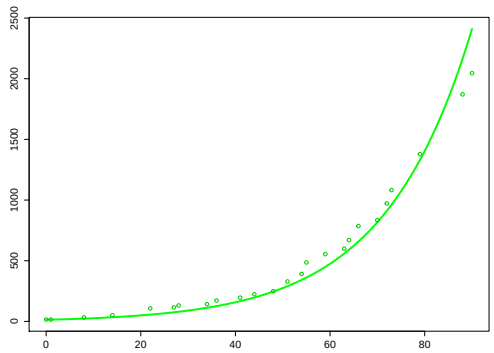

(c) 50% asymptomatic, 0% moderately symptomatic, i.e. $\sigma = .5$, $(1-\sigma)\delta = 0.0$.

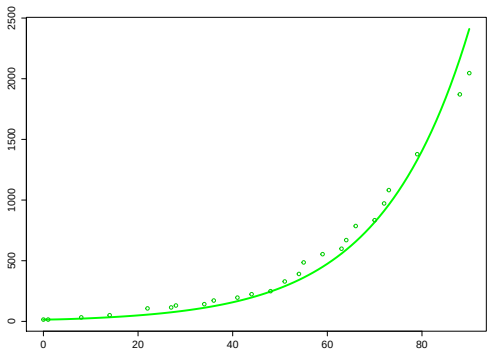

(d) 0% asymptomatic, 0% moderately symptomatic, i.e. $\sigma = 0$, $(1-\sigma)\delta = 0$.

Fig. 3.2. Fitting results based on the data from June 8th 2014 until September 12th 2014.

reproduction number is also shown in Figure 3.3. The reproduction number ranges from 1.32 at 2.5% quantile to 2.57 at 97.5% quantile.

3.2.4 Impact of the control measures

In the countries with widespread and intense spreading, containment of the West Africa Ebola outbreak relied on non-pharmaceutical interventions due to the lack

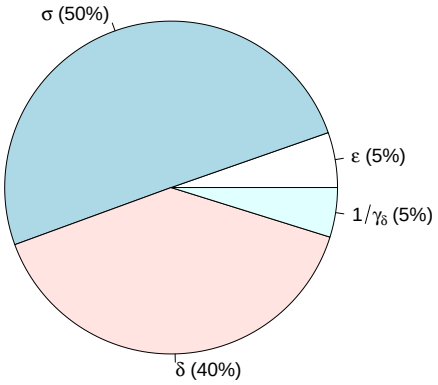

(a) Pie Chart of Sobol indices of the parameters related to mild and moderatesymptoms.

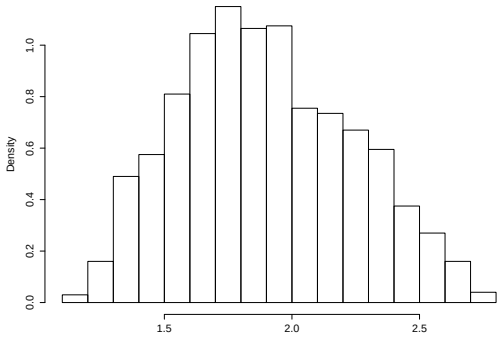

(b) Histogram of the reproduction number with uncertainty of mild and moderate symptoms. 95% CI (1.32, 2.57)

Fig. 3.3. Uncertainty analysis of the basic reproduction number with respect to parameters related to mild and moderate symptoms.

of effective medicines. These interventions include social mobilization, use of personal protective equipment (PPE) in healthcare facilities, safe and dignified burials, and contact-tracing and quarantine. Social mobilization activities include raising the population's awareness of mode of transmission, social distancing with infectious people, timely seeking of medical care and proper handling of deceased persons. Widely used, personal protective equipment (PPE) can lower infections in hospitals and other healthcare facilities. Social and dignified burials conducted by trained teams can reduce transmission from deceased people. Contact-tracing helps to promptly identify and hospitalize suspected and isolate probable cases. All of these interventions are associated with one or multiple parameters in the model. A natural question is whether considering mild and moderate symptoms affects the estimated effectiveness of these interventions.

Table 3.3.
Estimates of reduction in transmission rates. (a) 20%(σ) mild and 30% $(1-\sigma)\delta$ moderate symptoms, (b) 0% mild and 50% moderate symptoms, (c) 50% mild and 0% moderate symptoms (d) 0% mild and 0% moderate symptoms.

	Biological definition	(a)	(b)	(c)	(d)
z_I	Percentage reduction in β_I	0.274	0.265	0.293	0.293
z_H	Percentage reduction in β_H	0.823	0.796	0.880	0.881
z_D	Percentage reduction in β_D	0.548	0.530	0.587	0.587

We assume that the transmission rates for community (β_I), hospital (β_H) and funeral (β_D) and the time from disease onset to hospitalization ($1/\chi$) are piecewise functions of time [20]. For example,

$$\beta_I(t) = \begin{cases} \beta_I & \text{for } t < t_0, \\ \beta_I(1-z_I) & \text{for } t \geq t_0, \end{cases}$$

where t_0 corresponds to September 12, 2014 and z_I is the reduced transmission rate in the community due to interventions. Before September 12, 2014, these parameters remain the same as in the section on estimating the basic reproduction number. After September 12, 2014, there are reductions (i.e., z_I, z_H, z_D and z_χ) that are to be estimated. To focus on estimating the effects of interventions on transmission rates, the reduction z_χ is assumed 0.25, which is around 1.2 days earlier hospitalization than before [32]. The estimated reductions in the transmission rates are shown in Table 3.3. From the table, the reduction in transmission rates for (a) and (b) are smaller than for (c) and (d), which means that interventions seem more effective if only severe symptoms are considered. The reason that (c) and (d) are similar is probably that any herd immunity contributed by asymptomatic (or mildly symptomatic) infections has not yet taken effect as these infections are only a small proportion of the total population (for Liberia, the population is more than 4 million, and the observed final

cumulative cases are around 11000.) The results of the data fitting for the control time-series are shown in Figure 3.4, which also includes the early fitting results from Figure 3.2 before September 12, 2014. These results suggest that considering the full spectrum of symptoms is necessary in estimating the effects of interventions for policy-making.

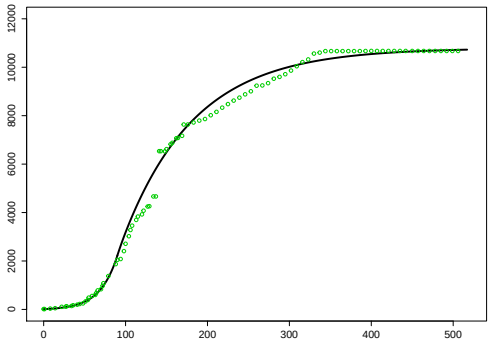

(a) 20% asymptomatic infections, 30% moderate symptoms, i.e. $\sigma = 0.2$, $(1-\sigma)\delta = 0.3$.

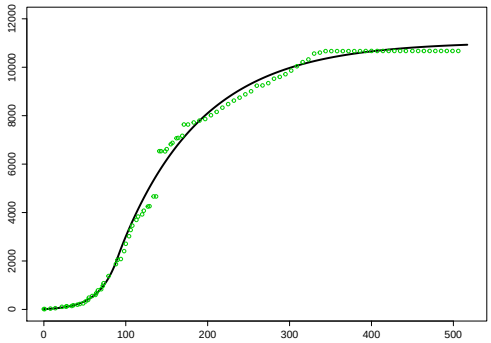

(b) 0% asymptomatic infections, 50% moderate symptoms, i.e. $\sigma = 0$, $(1-\sigma)\delta = 0.5$.

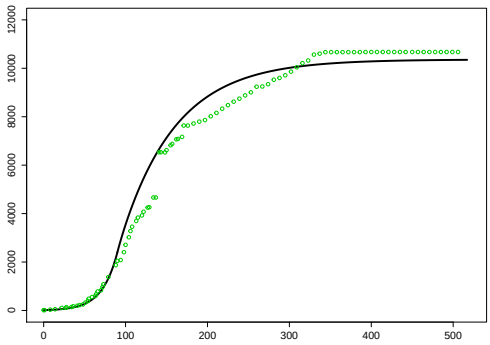

(c) 50% asymptomatic infections, 0% moderate symptoms, i.e. $\sigma = .5$, $(1-\sigma)\delta = 0.0$.

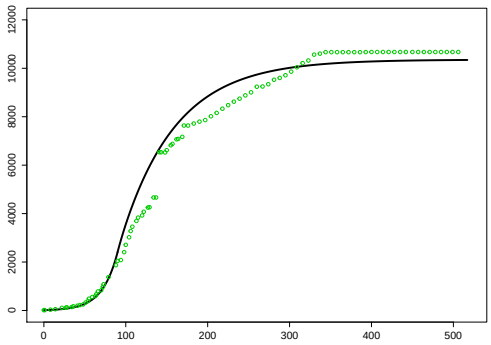

(d) 0% asymptomatic infection, 0% moderate symptoms, i.e. $\sigma = 0$, $(1-\sigma)\delta = 0$.

Fig. 3.4. Fitting results based on the data from June 8th 2014 until September 12th 2014 for the basic reproduction number and the data after September 12th 2014 for estimating the control effectiveness. The jump of the case data between day 100 and day 200 is due to a catch up in data monitoring and reporting in Liberia [64].

3.3 Control strategies evaluation

This section further studies the effectiveness of possible control interventions on Ebola propagation. The analysis is conducted from two perspectives: one is to find parameters to which the basic reproduction number is sensitive and the other is to investigate the timing of interventions and changes in possible control parameters based on final size and cumulative cases. The results could be helpful in guiding interventions in future Ebola outbreaks.

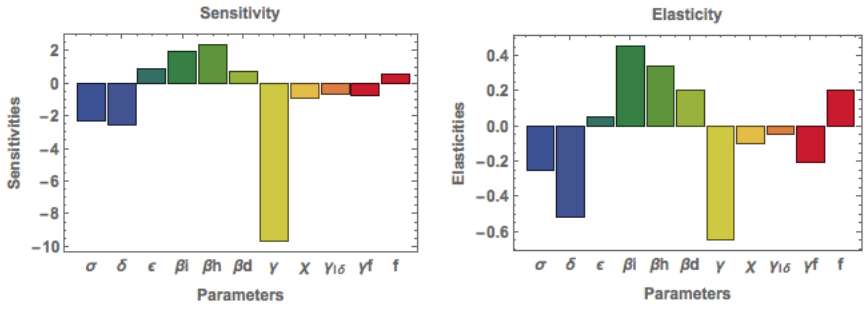

Fig. 3.5. Local sensitivity and elasticity analysis of $\mathcal{R}_0$ with respect to epidemiological parameters in Table 3.1. Sensitivity analysis is about the change in $\mathcal{R}_0$ and elasticity analysis is about the proportional change in $\mathcal{R}_0$.

3.3.1 Sensitivity analysis of basic reproduction number

We performed local sensitivity and elasticity analysis with respect to epidemiological parameters in Table 3.1. This analysis represents how changes (or proportional changes) in $\mathcal{R}_0$ are associated with changes (or proportional changes) in different parameters at their given values. Results are shown in Figure 3.5. The most sensitive biological parameters are the progression rate of severely symptomatic infections γ, and two parameters for asymptomatic (or mildly symptomatic) infections, i.e., the proportions with moderately symptomatic infections through the latent period δ and of asymptomatic infections σ. This shows that asymptomatic and moderately symp-

tomatic infections are crucial in the reproduction number. The figure also offers clues about how $\mathcal{R}_0$ might be reduced efficiently. The reduction in community transmission rate β_I is most influential, followed by reductions in hospital β_H and post-death transmission β_D. This tells us that, if transmission in community can be controlled, it would be very effective in reducing the reproduction number. Then hospital and post-death transmission follow.

We also investigate interaction effects as the local sensitivity analysis is about one-on-one linear relationships between individual parameters and the reproduction number. Figure 3.6 shows the dependence of $\mathcal{R}_0$ on moderate symptom related parameters. The left figure shows that $\mathcal{R}_0$ is not sensitive to the fraction of asymptomatic infections $(1-\sigma)\delta$ when ε is small, but as ε increases $\mathcal{R}_0$ becomes more sensitive to the fraction of asymptomatic infections $(1-\sigma)\delta$. The right figure shows similarly that $\mathcal{R}_0$ becomes more sensitive to the infectious period for moderately symptomatic infections as ε increases. This explains that, if the transmission rate of those moderately symptomatic is small, then other parameters related to the reproduction number become less influential.

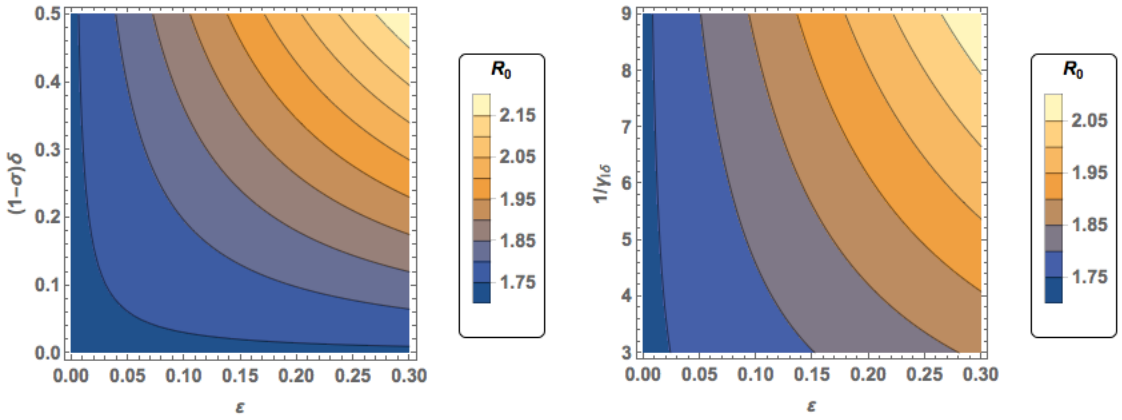

Fig. 3.6. Contour plots of $\mathcal{R}_0$ and moderate symptom related parameters. (a) the reduced infectivity of moderate relative to severe infection ε and the proportion with moderate symptoms $(1-\sigma)\delta$; (b) the reduced infectivity of moderate relative to severe symptoms ε and the infectious period of the moderate symptoms $1/\gamma_\delta$.

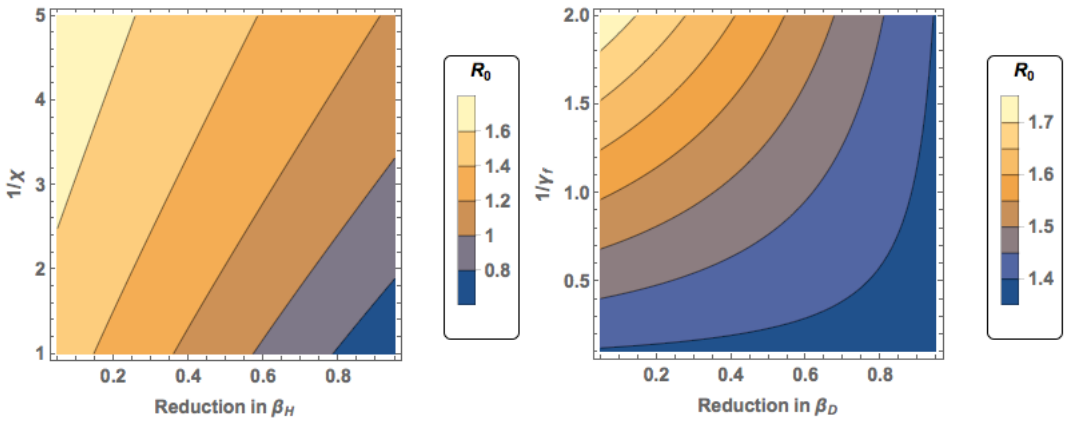

Fig. 3.7. Contour plots $\mathcal{R}_0$ and control by reducing hospital transmission (reduction in β_H and time from onset to hospitalization $1/\chi$) and post-death transmission (reduction in β_D and time from death to burial $1/\gamma_f$).

The basic reproduction number $\mathcal{R}_0$ could be reduced through hospital transmission and post-death transmission. This is shown in Figure 3.7, where the left figure shows control via hospital transmission, i.e., reduction in β_H, and the time from disease onset to hospitalization $(1/\chi)$. $\mathcal{R}_0$ is effectively decreased by early hospitalization if the transmission rate in hospital is reduced. But if this transmission rate is not reduced, then early hospitalization would not be effective in controlling the reproduction number. Early hospitalization might be achieved by contact-tracing and reduction in transmission rate in β_H might be achieved by increasing the effectiveness of isolation in hospital and use of personal protective equipment (PPE). This suggests that to control $\mathcal{R}_0$ effectively, both contact-tracing and isolation must work together. The right figure shows control via post-death transmission, i.e., reduction in β_D and time from death to burial $1/\gamma_f$. This figure shows that reducing β_D or reducing $1/\gamma_f$ is effective early, but becomes less effective as either of the two is controlled. It is not possible to make $\mathcal{R}_0$ less than 1 by controlling only post-death transmission.

To further investigate how to control the reproduction number $\mathcal{R}_0$ effectively, Figure 3.8 shows combinations of reduction in hospital and post-death transmission

rates β_H and β_D under different levels of reduction in the community transmission rate β_I (0%, 10%, 20% and 30%). First, the four sub-figures show that $\mathcal{R}_0$ is more sensitive to reduction in β_H than reduction in β_D. This means that control of the hospital transmission rate is more effective than the post-death transmission rate. This is more achievable in realty by strictly implementing isolation and increasing use of personal protective equipment by healthcare workers. Second, the four sub-figures show that reducing $\mathcal{R}_0$ below 1 is most probable by control of hospital and post-death transmission with some reduction in community transmission. If community transmission is not reduced (0 reduction in β_I), then it is very difficult to reduce $\mathcal{R}_0$ below 1 by controlling the transmission rates β_H and β_D. It is only possible to reduce $\mathcal{R}_0$ below 1 if β_H has been reduced at least by 65% (vertical dashed line) and β_D has been reduced at least by 45% (horizontal dashed line). In fact, one needs to further reduce β_I and β_H to make $\mathcal{R}_0$ below than 1 in the upper left triangle bounded above the thick line. However, it becomes more probable to reduce $\mathcal{R}_0$ below 1 by decreasing transmission rates β_H and β_D, with the reduction in community transmission rate β_I by from 0% to 30%. Then the required reduction in β_H becomes more achievable, from 65% to 28%, and the required reduction in β_D is from 45% to 0%. Therefore, to reduce the reproduction number $\mathcal{R}_0$ below 1, all three transmission rates for community, hospital and post-death must be reduced together.

Global sensitivity and uncertainty analysis is conducted through Latin hypercube sampling (LHS) and partial rank correlation coefficients (PRCC). The uncertainty analysis uses the Latin hypercube sampling method to sample the parameters of the reproduction number $\mathcal{R}_0$ [45] (see Section 1.4, Chapter for more detail). The size of Latin hyper cube samples is set at $\mathtt{N} = 2000$ in this section. The parameter ranges are listed in Table 3.2. Some statistics about the basic reproduction number $\mathcal{R}_0$ are obtained from the samples, mean 1.83, median 1.80, and standard deviation 0.34, and the 95% upper bound is 2.42. For the components of $\mathcal{R}_0$, $\mathcal{R}_0^I$ has mean 0.774, median 0.762, and standard deviation 0.152, $\mathcal{R}_0^H$ has mean 0.677, median 0.654, and standard deviation 0.134, $\mathcal{R}_0^D$ has mean 0.34, median 0.334, and standard deviation

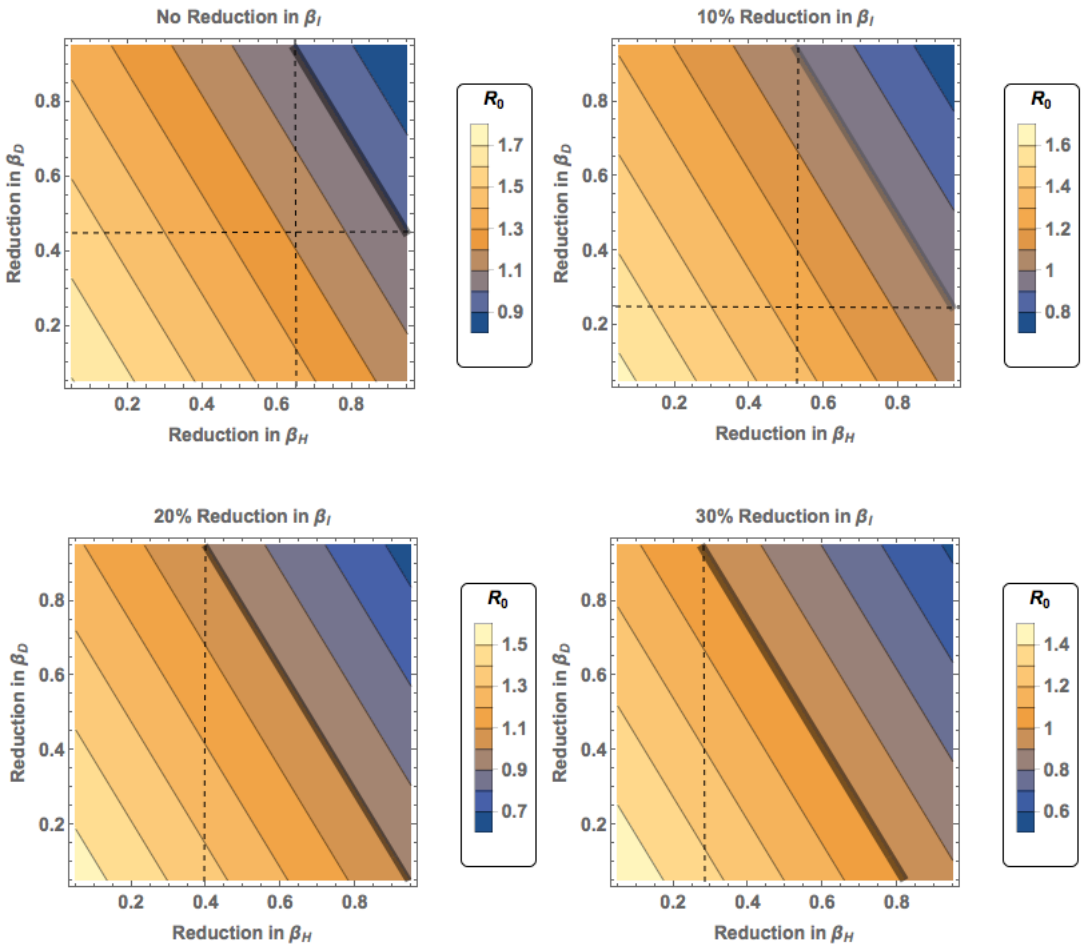

Fig. 3.8. $\mathcal{R}_0$ and the reduction in hospital transmission rate β_H and in post-death transmission rate β_D under different levels of reduction in community transmission rate β_I by 0%, 10%, 20% and 30%. The thick lines in each sub-figure corresponds to $\mathcal{R}_0$=1.

0.078, and $\mathcal{R}_0^{I_\delta}$ has mean 0.049, median 0.034, and standard deviation 0.045. The sample distributions of $\mathcal{R}_0$ and its components are shown in Figures 3.9 and 3.10. The empirical distribution of $\mathcal{R}_0$ is shown in Figure 3.11, which also includes the proportions of each component of $\mathcal{R}_0$ as $\mathcal{R}_0$ samples are sorted. This shows that the probability of $\mathcal{R}_0 > 1$ is equal to 1, which means that the outbreak will occur when an index patient is introduced to the population. The most important component of $\mathcal{R}_0$ is the community, then hospital and post-death transmission, and finally transmission through those with moderately symptomatic infections.

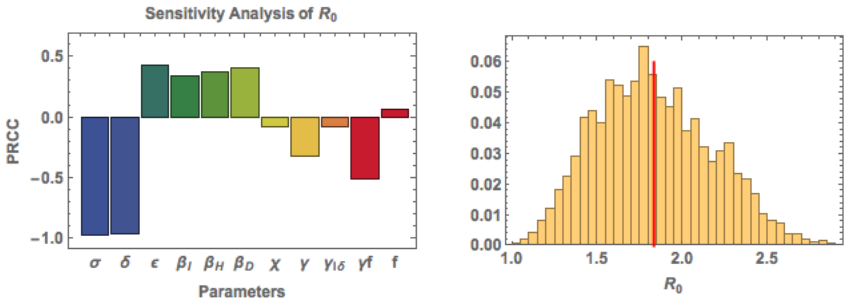

Fig. 3.9. Global sensitivity and uncertainty analysis of $\mathcal{R}_0$ with respect to epidemiological parameters in Table 3.1.

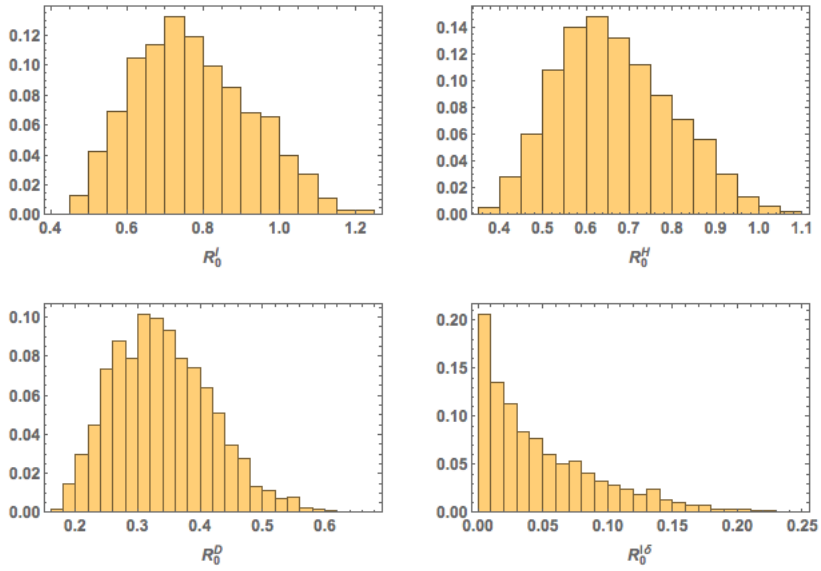

Fig. 3.10. Histograms of the components of $\mathcal{R}_0$.

The global sensitivity analysis applies the partial rank correlation coefficient (PRCC) to assessing pairwise relations between parameters and the reproduction number $\mathcal{R}_C$ after removing the influence of other parameters (see Section 1.4, Chapter 1). PRCC identifies and measures the statistical influence, specifically the monotonicity, of the parameters on $\mathcal{R}_0$. Figure 3.9 shows the influence of asymptomatic (σ) as well as asymptomatic infections (δ and ε) on $\mathcal{R}_0$. It also shows that post-death transmission

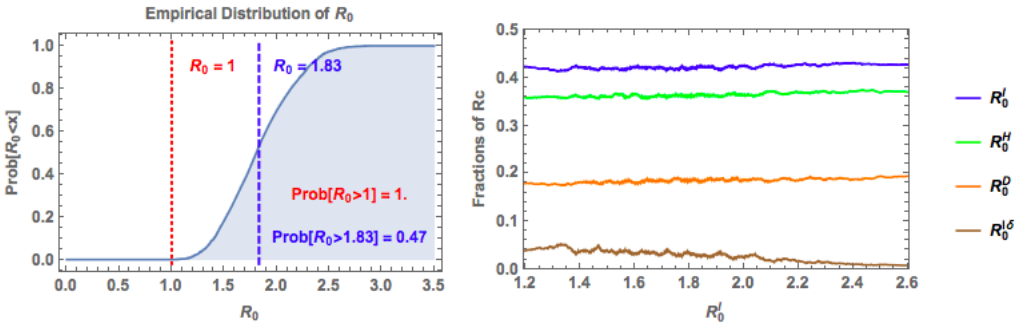

Fig. 3.11. Empirical distribution of $\mathcal{R}_0$ and components of $\mathcal{R}_0$.

(β_D and γ_f) is important, but the effects of community and hospital transmission (β_I and β_H) are similar.

3.3.2 The effects of intervention timing

The timing of interventions is critical for disease control, and early effective interventions usually reduce the final outbreak size. With the same interventions, if the timing is three weeks earlier, then more than 50% cases are prevented. On the other hand, if the timing is three weeks later, then final size could triple (See Figure 3.12 (a)). The peak sizes and times with different intervention timing are shown in Figure 3.12 (b). The epidemics reach their peaks shortly (around 10 days) after implementation of interventions. The peak size could be decreased by 63% or increased by 169% due to earlier or later interventions.

The predicted cumulative cases vary among different combinations of asymptomatic and moderately symptomatic infections (see Figure 3.13). For early intervention, models with 20% asymptomatic and 30% moderately symptomatic and models with 0% asymptomatic and 50% moderately symptomatic infections provide larger estimates than models with 0% asymptomatic and 0% moderately symptomatic infections and models with 50% asymptomatic and 0% moderately symptomatic infections. However, late intervention switches the order of predictions. This shows that the pre-

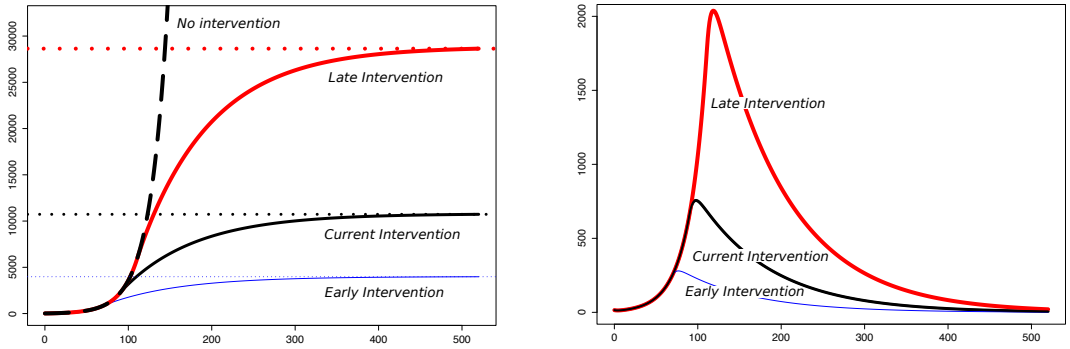

(a) Cumulative cases with different timing of intervention.

(b) Epidemic curves with different timing of intervention.

Fig. 3.12. Timing of the interventions. The lower blue thin curves correspond to three weeks earlier implementation, the middle black curves correspond to the actual time of implementation, and the top red thick curves corresponds to three weeks later implementation. The exponential growth dashed curve in sub-figure (a) corresponds to no control.

diction from models without moderately symptomatic infection are more sensitive to the timing of intervention and might exaggerate their effects. This is also shown further by varying the timing of controls in Figure 3.14. The final size as a function of intervention timing is obtained by fitting a regression line to the log transformed final size, and the equation is

$$FS(t) = FS(t_0)exp(k(t - t_0))$$

with k=0.0470, 0.0440, 0.0531 and 0.0536 for (a-d), where t_0 corresponds to September 12, 2014, and $FS(t_0)$ corresponds to the actual final size with intervention at t_0. Using this formula, it is easy to estimate the effects of intervention timing on final size. This might be useful in intervention policy-making.

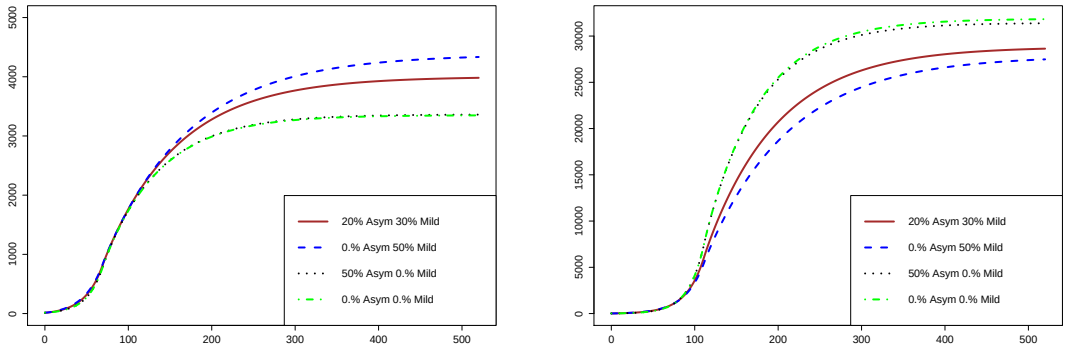

(a) Cumulative cases with 3 weeks earlier implementation.

(b) Cumulative cases with 3 weeks later implementation.

Fig. 3.13. Early and late interventions.

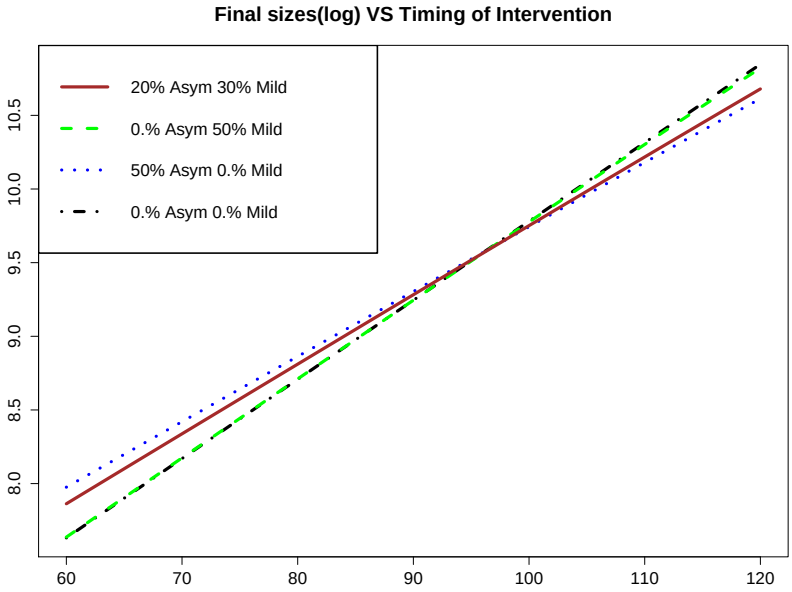

Fig. 3.14. Final sizes depend on the timing of the interventions.

3.3.3 Control parameters and their effects on the time course

To assess the importance of control measures for future outbreaks based on the 2014-15 Liberia outbreak, time course sensitivity is conducted through Latin hyper-

cube sampling of the control parameters and partial rank correlation coefficients. (See Figure 3.15) The timing of intervention T ranges from 3 weeks earlier than the current timing to 3 weeks later. The reductions in β_I, β_H and β_D , i.e., z_I, z_H and z_D, range from 0 to 30%, 50% to 90%, 30% to 70%, respectively. The reduction in the time from onset to hospitalization z_χ ranges from 0 to 60%. The PRCC curves of control parameters are similar and close to zero before implementation of control measures. Once control measures are implemented, the PRCC curves of different control parameters quickly go to relatively stable values. The first PRCC curve approaching 1 is the timing of control measures, which is positively correlated with cumulative cases. This means that the later the implementation of control measures, the larger the outbreak. Early implementation of control measures is very important in the exponential growth phase of the outbreak. Later on, the influence of intervention timing wanes. All other control measures are negatively correlated with the outbreak, which means that implementing them mitigates the outbreak. The most influential measures are hospital transmission z_H, i.e., effectiveness of isolation in hospitals, and the time from onset to hospitalization z_χ, which could be reduced by contact-tracing and educating the public about Ebola. Contact-tracing and raising public awareness could also affect the next most influential parameter, the community transmission rate β_I. The PRCC of the reduction of β_D is the smallest, but proper burials might be the most easily implemented control measure.

3.4 Discussion

To crudely account for the spectrum of symptoms of Ebola infection, assumptions for the newly developed model are based on biological findings about Ebola infections with mild, moderate and severe symptoms. First, those mildly or asymptomatic directly from the susceptible class have very little if any viral replication, which is controlled rapidly by virtue of genetic resistance or immunity from prior infection with a related virus. Therefore, they are probably not infectious due to their low

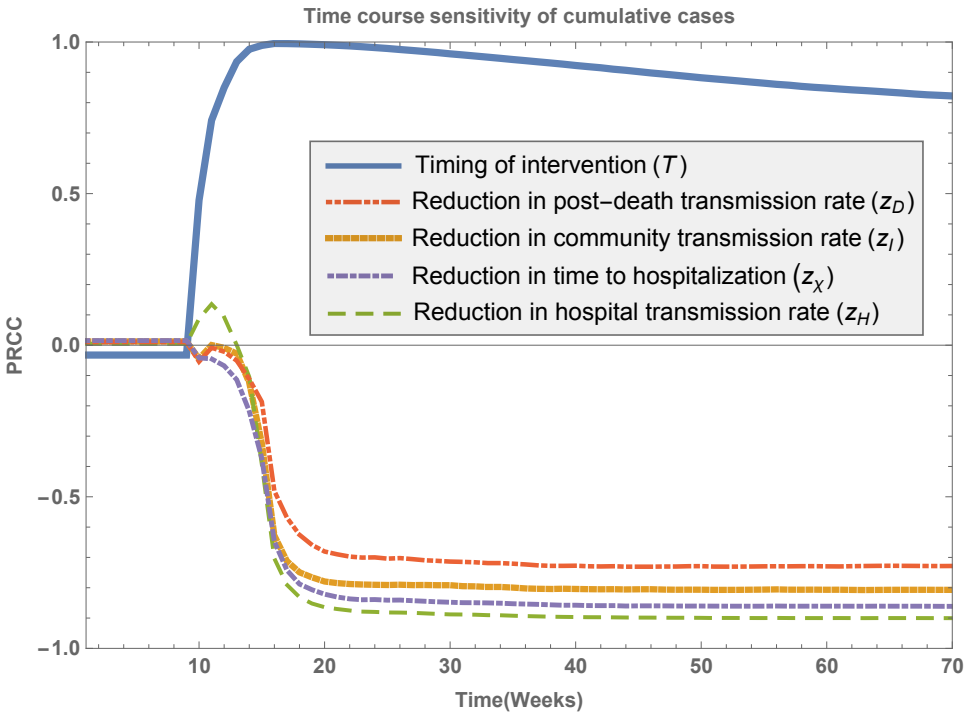

Fig. 3.15. Time course sensitivity with respect to control parameters.

viral load. Secondly, those with moderately symptomatic infections from the exposed class have some virus replication. However, viral replication is controlled due to strong innate immunity plus successful adaptive immunity. These individuals are not very infectious even though they have moderately symptomatic infections, because they have limited amount of viruses circulating within their bodies. Third, those from the exposed class with severe symptoms have higher virus load and therefore are more infectious than the moderately symptomatic cases. Based on the estimate of Bellan et al. [54] (Asymptomatic infection accounts for 50% of the total infection with lower bound 20%), the fraction asymptomatic is 20%, moderately symptomatic is 30% and severely symptomatic is 50%. Various other combinations of asymptomatic and moderately symptomatic infections are considered as well.

The model developed in this chapter extends one of the models in [48], which has multiple sub-stages of infectious and hospitalized individuals, based on the assumption of Gamma distributed disease progression (the infectious period). The formulation and its underlying assumptions are clearly shown via integral-differential equations and their reduction to ordinary differential equations in [48]. The merit of this model is that it allows the infection history to pass over even after hospitalization. This is important in determining the times of recovery and death, especially when there is no treatment with effective medicines. The Gamma assumption also provides a realistic infectious period, and infectious individuals recover or die in the later stage of the infection, but not sooner.

The results show the importance of considering a spectrum of symptoms. First, the estimated basic reproduction number for this model is 1.83, consistent with WHO's estimate independent of compartmental modeling. Without considering mildly and moderately symptomatic infections, reproduction number estimates can be inflated as shown by disabling these states in this model. However, uncertainty about the prevalence of asymptomatic and mildly symptomatic infections could lead to reproduction numbers from 1.32 to 2.57. This suggests the need for studies of the full spectrum of symptoms. Second, interventions are estimated to be more effective when ignoring the full spectrum of symptoms. Models with different levels of infectivity provide more reasonable estimates of the effectiveness of interventions. Without considering asymptomatic and moderately symptomatic infections, extra credit is given to implemented control measures. In addition, the timing of interventions is of great importance to mitigate final epidemic size. Because final size is an exponential function of the time of intervention, early interventions could significantly reduce epidemic size. An empirical regression equation linking final size and timing of interventions could be useful for policy-making. It is also observed that the model with only typical infections provides more dramatic changes in final size with respect to intervention timing compared to the model with a full spectrum of symptoms.

Control strategies are also studied through sensitivity analysis. Local sensitivity and elasticity analyses show that the most effective way to control the reproduction number is by reducing transmission in the community, followed by reductions in hospital and post-death transmission. This is consistent with the estimated magnitudes of reproduction numbers due to each transmission component. The analysis also shows the importance of moderately symptomatic and asymptomatic infection to the basic reproduction number. In real applications, various combination of different interventions are implemented at the same time. Different combinations are evaluated in this chapter. The combination of contact-tracing and effective isolation in hospital is more effective than implementation of these interventions separately. With a certain reduction in community transmission, mitigating the outbreak by control of hospital and post-death transmission becomes more achievable. A time course sensitivity analysis is conducted to show how sensitive cumulative cases is to control parameter changes at different times. The timing of interventions shows waning effects on cumulative cases, while all other controls show constant effectiveness.

It is necessary to stratify infections by severity of clinical symptoms in modeling. This permits reasonable estimates of the reproduction number and effectiveness of control measures, especially when infected persons present with various symptoms. More epidemiological investigation of asymptomatic and moderately symptomatic infections of Ebola will be helpful to estimate their fractions of the total infection and infectivity. These are crucial to more useful modeling of future outbreaks.

4. VACCINE PREVENTIBLE DISEASES MODELS - DESIGNING AND EVALUATING CONTROL STRATEGIES FOR MIGRATING POPULATIONS

The work presented in this chapter was done in collaboration with Feng, Hernandez-Ceron and Zhao. Most of the results and ideas in this chapter have been accepted for publication as a book chapter [65]. I contribute several parts of the manuscript but not exclusively, including model formulation and analysis as well as the writing of the manuscript.

4.1 Introduction

Most epidemiological models simply assume that the population under study is homogeneous. However, this assumption might not be accurate because people are clustered and form different residential patches. One of typical structures consists of urban, peri-urban and rural patches, where patches are connected when people migrates. Most of the time rural residents migrate to urban/peri-urban areas for better economic opportunities. This rural to urban migration might be seasonal, as people from rural patch seek temporal employment in cities in non-farming seasons and return homes in growing seasons.

These patches are different in population density, and therefore residents of different patches have contact rates, which leads to the possibility that infectious diseases are long-lasting may be epidemic in rural, but endemic in urban/peri-urban areas. In such case, rural residents are less likely to be immune than urban people of the same age. Together with births, rural-urban migration thus increases the proportions of urban or peri-urban populations that are susceptible to infection by the pathogens causing these diseases. Jos Cassio de Moraes et al. [66] argue that–insofar as the cov-

erage required to prevent outbreaks is lower in rural than urban areas – rural-urban migration motivates regional versus local design of optimal vaccination programs.

In this chapter we developed a system of long-term and short-term models with three sub-populations consisting of urban, peri-urban, and rural populations. One of the main differences between these sub-populations is their density (and immunity, naturally acquired or vaccine-induced). The model system is constructed to include not only the usual mixing between the three sub-populations (deterministic) but also seasonally-driven migrations of individuals from rural to urban areas (stochastic). In addition to routine vaccination within each patch, supplementary vaccination may be used to mitigate the consequences of the migration.

Compared to deterministic models describing the expected effects of various immunization policies, stochastic models enable to capture the inherent randomness of contact between susceptible and infectious people. They also allow us to examine the distribution of possible outcomes and compare the likelihood of certain results across immunization policies. When the threat of a disease outbreak cannot be eliminated entirely, it may be possible to contain those to specific desired levels. For example, stochastic simulations are conducted to analyze the likelihood of containing outbreaks to a prescribed final or peak size. Perhaps the goal is a below 5% risk of the disease spreading to more than that threshold level, because the policies necessary to eliminate that final 5% are prohibitively expensive or unrealistic to implement. In such cases, stochastic models can provide more insights than deterministic ones, which are demonstrated in this chapter.

Many researchers have been studied effects of spatial movement of humans on the spread and control of infectious diseases in different settings. For example, [31,67,68] study international spread of Ebola virus via air travel, and the efficacy of control measures including travel restrictions or exit and entry screening of travelers. They provide important quantitative information about the benefits and associated costs of screening and restriction of travel, which can be very helpful for policy-making. The study presented in this chapter aims at assessing the role of vaccinating migrants from

a rural area at their entry (e.g. bus stops, train stations, etc.) to urban and peri-urban areas, where disease transmission rates can be much higher due to greater population densities. Results in this study suggest that such a difference in population densities can have important implications for disease outbreaks and vaccination strategies.

This chapter is organized as follows: Section 4.2 elaborates the models for long term and short term, and simulates the models in various situations. Section 4.3 studies the impacts of different possible vaccination policies. Section 4.4 is devoted to discussion.

4.2 Models and analysis

The objective of this study is to identify the best short-term vaccination policy to mitigate outbreaks. Therefore, our focus is on an short-term stochastic epidemic model without demographics, i.e., neither births nor deaths. However, long-term vaccination policy influences the population immunity among different patches. This is captured by a long-term deterministic endemic model. For each sub-population, the steady-state distribution of the epidemiological classes is computed and passed to the short-term model via its initial conditions. We adopt discrete-time models following the approach of Lloyd et al. [69].

4.2.1 The long-term endemic model

The long term model consists of six epidemiological classes for each of urban, peri-urban, and rural populations. Let M_i, V_i, S_i, E_i, I_i and R_i denote individuals with maternal immunity, individuals with temporary immunity due to vaccination, susceptible individuals, exposed or latent, infectious, and those who have recovered from infection (and are immune), respectively, where the subscripts $i = 1, 2, 3$ correspond to urban, peri-urban, and rural populations, respectively. Temporary immunity is considered in both V and M classes. Birth and death rates within each patch are

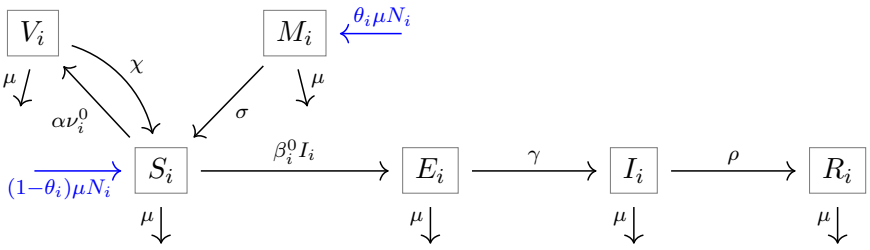

Fig. 4.1. Transition diagram for the long-term endemic model. The blue arrow to M_i represent the new born with maternal immunity while the other to S_i represent the new born without maternal immunity.

assumed to be equal so that the total population remains constant. A transition diagram of the long-term MVSEIR model is shown in Figure 4.1.

The long-term model is given by

$$\begin{aligned}
M_i(n+1) &= \theta_i\mu_i N_i + (1-\mu_i)(1-\sigma)M_i(n)\\
V_i(n+1) &= \alpha\nu_i^0(1-\mu_i)e^{-\beta_i^0\frac{I_i(n)}{N_i}}S_i(n) + (1-\mu_i)(1-\chi)V_i(n)\\
S_i(n+1) &= (1-\theta_i)\mu_i N_i + (1-\mu_i)(1-\alpha\nu_i^0)e^{-\beta_i^0\frac{I_i(n)}{N_i}}S_i(n)\\
&\quad +\sigma(1-\mu_i)M_i(n) + \chi(1-\mu_i)V_i(n)\\
E_i(n+1) &= (1-\mu_i)(1-e^{-\beta_i^0\frac{I_i(n)}{N_i}})S_i(n) + (1-\mu_i)(1-\gamma)E_i(n)\\
I_i(n+1) &= (1-\mu_i)\gamma E_i(n) + (1-\mu_i)(1-\rho)I_i(n)\\
R_i(n+1) &= (1-\mu_i)\rho I_i(n) + (1-\mu_i)R_i(n), \quad i=1,2,3,
\end{aligned} \tag{4.1}$$

where $N_i = M_i + V_i + S_i + E_i + I_i + R_i$. For patch i, θ_i is the proportion of newborns with maternal immunity, μ_i is the daily per-capita birth and death probability ($1/\mu_i$ is the average lifespan, based on Geometric distribution) in patch i, σ is the daily probability of immunity loss due to maternal antibodies ($1/\sigma$ is the average period of maternal immunity); α is the vaccine efficacy, ν_i^0 is the daily probability of being vaccinated, β_i^0 is the daily transmission rate, $1/\chi$ is the duration of immunity due to vaccination, $1/\gamma$ and $1/\rho$ are the average periods of latency and infection, respectively. The probability of infection for a susceptible individual in patch i, $e^{-\beta_i^0\frac{I_i}{N_i}}$, has the

same form as in [35, 36, 69, 70]. All parameters and their meanings are listed in Table 4.1.

Table 4.1.
Parameters in the long-term model (4.1) for patch i ($i = 1, 2, 3$). The subscripts $i = 1, 2, 3$ correspond to urban, peri-urban, rural patches, respectively.

Symbol	Description	Value (patch 1, 2, 3)
θ_i	Fraction of newborns with maternal immunity	(0.7, 0.7, 0.7)
$1/\mu_i$	Lifespan	$(70, 70, 68)$ years
$1/\sigma$	Duration of maternal immunity	6 months
$1/\chi$	Duration of vaccine-induced immunity	60 years
α	Vaccine efficacy	92% – 95%
ν_i^0	Daily probability of being vaccinated	determined by p_i
β_i^0	Daily transmission rate	(1.4, 1.1, 0.85)
$\mathcal{R}_{vi}$	Effective reproduction number (long-term)	(1.25, 1.16, 1.03)
$\mathcal{R}_{0i}$	Basic reproduction number (long-term)	(9.79, 7.70, 5.95)
$1/\gamma$	Latent period	7 days
$1/\rho$	Infectious period	7 days
N	Total population size $= N_1 + N_2 + N_3$	$(0.125N, 0.2N, 0.675N)$

The parameter values listed in Table 4.1 are based on measles, and the three sub-populations have a similar spatial structure to the urban, peri-urban and rural populations in São Paulo, Brazil. Some parameter values are selected from the literature while others are calculated or estimated from available data. For example, given the long-term vaccination policy of vaccinating $p_i = 0.9$ of susceptibles within 10 years, the daily probability ν_i^0 of being vaccinated can be determined from using the

relationship $1-p_i=(1-\nu_i^0)^{10\times 360}$. Also, knowing the basic reproduction number $\mathcal{R}_{0i}$ and all other parameter values except β_i, we can estimate β_i. Using these parameter values, we can numerically compute the steady-state values of each epidemiological class, which then can be used in stochastic simulations of the short-term model.

Because the long-term model is used to determine the local population immunity within each patch under the long term routine vaccination policy, no interactions between patches are modeled. Even though the interactions between patches are ignored, it is difficult to obtain an explicit expression for the non-trivial steady state of the system for sub-population i. Numerical computations of these steady states will be used for short-term simulations. Nevertheless, the effective reproduction number for sub-population i, denoted by $\mathcal{R}_{vi}$, can be computed (see Appendix) and is given by

$$\mathcal{R}_{vi}=\left(\frac{(1-\mu_i)\gamma}{1-(1-\mu_i)(1-\gamma)}\right)\left(\frac{\beta_i^0(1-\mu_i)}{1-(1-\mu_i)(1-\rho)}\right)\frac{S_i^0}{N_i}, \tag{4.2}$$

in which the first factor is the probability that a newly infected individual survives the latent period, the second factor is the number of new infections that a typical infectious individual produces during the entire infectious period in a completely susceptible population, and the third factor is the fraction of the susceptible population i at the disease-free equilibrium. The susceptible fraction and the immunized fraction by routine vaccination (see Appendix in this chapter) at the disease-free equilibrium are

$$\frac{S_i^0}{N_i}=\frac{\left[(1-\theta_i)+\theta_i\frac{\sigma(1-\mu_i)}{1-(1-\mu_i)(1-\sigma)}\right]\mu_i}{1-(1-\mu_i)(1-\alpha\nu_i^0)-\frac{\chi(1-\mu_i)\alpha\nu_i^0(1-\mu_i)}{1-(1-\mu_i)(1-\chi)}},\quad \frac{V_i^0}{N_i}=\frac{\alpha\nu_i^0(1-\mu_i)S_i^0/N_i}{1-(1-\mu_i)(1-\chi)}. \tag{4.3}$$

The expressions in (4.2) and (4.3) jointly illustrate how the effective reproduction number $\mathcal{R}_{vi}$, the population susceptibility S_i^0/N_i and level of immunity V_i^0/N_i depend on vaccination at rate ν_i^0, which depends on immunization policies of patches and therefore may differ among the three patches.

Similarly, it is clear that the endemic equilibrium of patch i,

$$\hat{E}_i=(\hat{M}_i,\hat{V}_i,\hat{E}_i,\hat{I}_i,\hat{R}_i),\quad i=1,2,3, \tag{4.4}$$

depends on transmission rate β_i^0 in addition to vaccination rate ν_i^0. This may lead to susceptibility of the rural population much higher than that of the urban population due to vaccination coverage and population density (lower densities corresponds to smaller values of β_i^0 through contact rates). Consequently, migrants from rural to urban or peri-urban might significantly increase the likelihood of an outbreak (see [66]). The long-term steady state values of the components in $\hat{E}_i$ will are computed and passed to the short-term model via initial conditions. The simulations of the long-term model is shown in Figure 4.2.

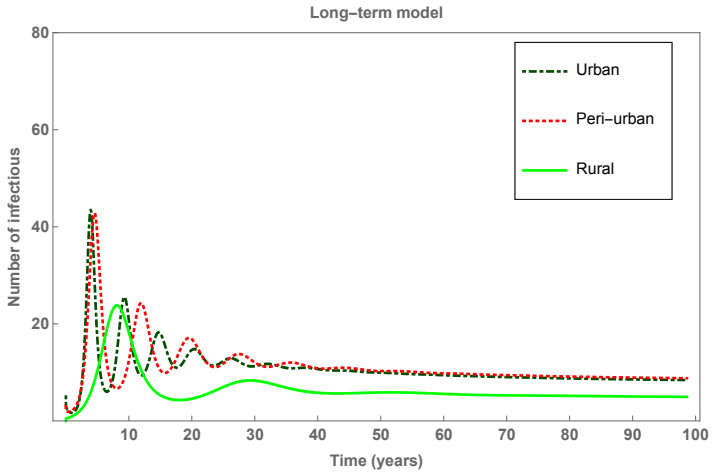

Fig. 4.2. Long-term dynamics of the model (4.1) for each of the three patches when rural-urban migration is ignored.

4.2.2 The short-term model

The short-term stochastic model focuses on mitigating a single outbreak during one season. It ignores the demographic processes (i.e., birth and death), as well as the vaccination/immunity loss considered in the long-term model. In this case, the individuals in the V, M, and R classes are all considered immune and grouped in the same compartment, denoted by R for each patch. Disease transmission and migration between patches for the short-term model are shown in Figure 4.3.

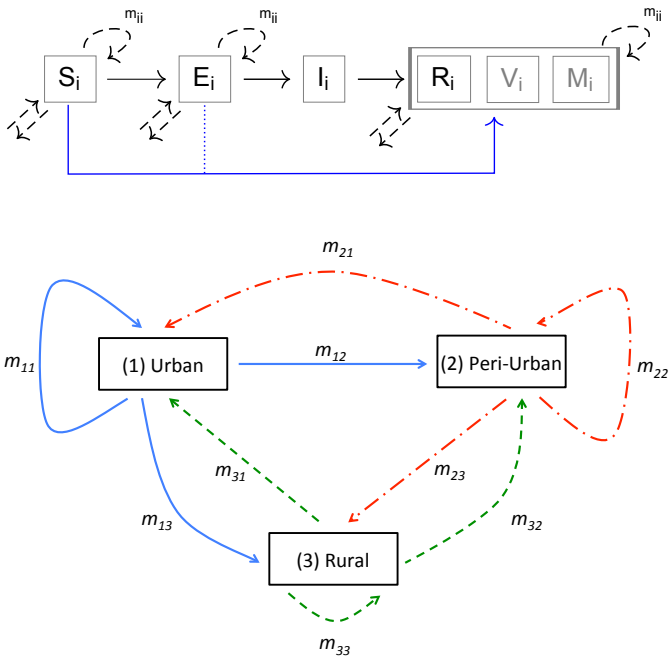

Fig. 4.3. A disease transmission diagram for the short-term model (top) and a depiction of the movement between the three patches (bottom). The dashed arrows in the top diagram represent migration. The parameter m_{ij} represents the daily per capita migration probability from patch i to patch j.

The stochasticity is considered following the approach in [69]. The short-term model is given by:

$$
\begin{aligned}
S_i(n+1) &= \sum_{j=1}^{3} m_{ji}(n) S_j(n) e^{-\lambda_j(n)} (1 - \eta_{ji}(n)) \\
E_i(n+1) &= \sum_{j=1}^{3} m_{ji}(n) S_j(n) \left[1 - e^{-\lambda_j(n)}\right] + \sum_{j=1}^{3} (1-\gamma) m_{ji}(n) E_j(n) \\
I_i(n+1) &= \sum_{j=1}^{3} \gamma m_{ji}(n) E_j(n) + (1-\rho) I_i(n) \\
R_i(n+1) &= \rho I_i(n) + \sum_{j=1}^{3} m_{ji}(n) R_j(n) \\
V_i^s(n+1) &= \sum_{j=1}^{3} m_{ji}(n) S_j(n) e^{-\lambda_j(n)} \eta_{ji}(n) + \sum_{j=1}^{3} m_{ji}(n) V_j^s(n), \quad i = 1, 2, 3,
\end{aligned}
\tag{4.5}
$$

where V_i^s denotes the individuals in patch i who are vaccinated due to the routine vaccination program as well as supplemental efforts; $m_{ij}(n)$ is the time-dependent exiting probability from patch i to patch j at time step n (see the migration diagram in Figure 4.3); η_{ij} represents the combined routine and supplementary vaccination; γ and ρ have the same meanings as in the long-term model (4.1). The force of infection, λ_i is given by

$$\lambda_i(n) = \beta a_i \sum_{j=1}^{3} c_{ij} \frac{I_j(n)}{N_j(n)}, \quad i = 1, 2, 3. \tag{4.6}$$

Here, the c_{ij} represent casual mixing between patches i and j, which we consider to be preferential and are given by

$$c_{ij} = \varepsilon_i \delta_{ij} + (1 - \varepsilon_i) f_j, \quad f_j = \frac{(1 - \varepsilon_j) a_j N_j}{\sum_k (1 - \varepsilon_k) a_k N_k}, \tag{4.7}$$

where a_i denotes the number of contacts per day in patch i, and $N_i(n) = S_i(n) + E_i(n) + I_i(n) + R_i(n) + V_i^s(n)$ is the total population in patch i at time n. Note that the M_i and V_i classes of the long-term model are included in the R_i class in the short-term model. The parameter ε_i denotes the proportion of contacts of patch i reserved for the same patch. The rest $1 - \varepsilon_i$ of contacts are distributed proportionately among all patches including i. The parameter a_i denotes the per-capita number of contacts in population i, and the balance equation $a_i N_i c_{ij} = a_j N_j c_{ji}$ must be satisfied. That is, the total number of contacts from individuals in patch i with individuals in patch j must equal to the total contacts of individuals in patch j with those in patch i.

We remark that, although $N_i(n)$ may change with time n when migration rates are not zero, the balance equation will always hold as long as c_{ij} are defined as in (4.7). We also remark that, although vaccinations are also given to individuals in the E_i class (assuming that no testing will be done before vaccinating), these individuals will remain in the E_i class assuming vaccination for them is in effective, which is why this process need not to be explicitly modeled. However, the wasted vaccines are included in determining the actual doses consumption.

To evaluate the effect of various short-term vaccination programs, particularly those involving migrants, it is important to obtain reasonable parameter values for

the migration probabilities m_{ij}. Although these parameters are chosen to be time-invariant constants in many patch models, it is not appropriate here as the migration considered in this chapter is driven by seasonally-available job opportunities, and migrants will return to their home patch within one year. To capture this seasonally varying pattern, we consider piecewise-constant m_{ij} values as described below.

For demonstration purposes, consider the case in which a proportion of rural individuals will move to urban and peri-urban for jobs during a fixed period of time in a year and return to their rural homes afterwards; there is no migration between patches during the rest of the year. Let $M = (m_{ij})$ denote the 3×3 migration matrices. Denote by M_{ru}, M_{ur}, and M_0 the matrices for the migration from rural to urban/peri-urban, the migration from urban/peri-urban back to rural, and no migration, respectively, during the corresponding periods of a year.

To parameterize the migration matrix M_{ru}, we assume that the migration season lasts for d days, and that a fraction l_3 of the rural population move to the urban/peri-urban patches, of which a fraction q_1 go to the urban patch and fraction q_2 go to the peri-urban patch. Then $1 - l_3 = m_{33}^d$ or

$$m_{33} = (1 - l_3)^{\frac{1}{d}}. \tag{4.8}$$

Note that $m_{31} + m_{32} + m_{33} = 1$ and that

$$q_1 = \frac{m_{31}}{m_{31} + m_{32}}, \quad q_2 = \frac{m_{32}}{m_{31} + m_{32}}.$$

It follows that

$$m_{31} = q_1(1 - m_{33}), \quad m_{32} = q_2(1 - m_{33}). \tag{4.9}$$

Thus, the matrix M_{ru} is given by

$$M_{ru} = \begin{bmatrix} 1 & 0 & 0 \\ 0 & 1 & 0 \\ q_1[1 - (1 - l_3)^{\frac{1}{d}}] & q_2[1 - (1 - l_3)^{\frac{1}{d}}] & (1 - l_3)^{\frac{1}{d}} \end{bmatrix}. \tag{4.10}$$

For the matrix M_{ur} for migrants returning from urban/peri-urban to rural, let $n_i = N_i/(N_1 + N_2 + N_3)$ denote the ratio of sub-population N_i of patch i to the total

population N. Let l_i $(i = 1, 2)$ denote the ratios of rural migrants in patch i to the total population in patches i ($i = 1, 2$ for urban and peri-urban, respectively). Then

$$l_i = \frac{n_3 l_3 q_i}{n_i + n_3 l_3 q_i} = 1 - m_{ii}^d, \quad i = 1, 2, \tag{4.11}$$

and thus,

$$m_{11} = (1 - l_1)^{\frac{1}{d}}, \quad m_{22} = (1 - l_2)^{\frac{1}{d}}.$$

Noticing that $m_{21} = m_{31} = m_{12} = m_{32} = 0$, $m_{33} = 1$, and $\sum_{j=1}^{3} m_{ij} = 1$ $(i = 1, 2, 3)$, we have

$$M_{ur} = \begin{bmatrix} (1 - l_1)^{\frac{1}{d}} & 0 & 1 - (1 - l_1)^{\frac{1}{d}} \\ 0 & (1 - l_2)^{\frac{1}{d}} & 1 - (1 - l_2)^{\frac{1}{d}} \\ 0 & 0 & 1 \end{bmatrix}, \tag{4.12}$$

where l_1 and l_2 are determined in (4.11). The no-migration matrix M_0 is simply the identity matrix I_3.

4.2.3 Stochastic simulations of the short-term model

For simulations of the short-term model, we use the migration matrices given in (4.10) and (4.12) with $(n_1, n_2, n_3) = (0.125, 0.2, 0.675)$, $l_3 = 0.25$, $q_1 = 0.3$, $q_2 = 0.7$, and $d = 90$ days. This means 25% of the rural population migrate, to rural and peri-urban patches with 30% and 70% proportions, respectively. The values of l_2 and l_3 can be determined by (4.11). For the mixing matrix, the preferential parameters (ε_i) are chosen to be $(0.95, 0.9, 0.95)$, which assumes that the peri-urban residents have a higher probability of having contacts with people from the other two patches. The per capita contact rates or activity levels for the three sub-populations are chosen to be $(8, 5, 2)$ based on the assumption that the activity level for disease transmission is correlated with population density. The probability of infection per contact is assumed to be $\beta = 0.23$. The initial values for the short-term model are based on the immunity level of each patch estimated from long-term models, which are assumed to be 90%, 87%, 83% of the total population equal to 1 million in the simulations.

One focus of the short-term vaccination policy is to vaccinate migrants from patches where density is lower (e.g., rural patch) who are entering patches with higher density (urban or peri-urban). We assume that it is possible to vaccinate these immigrants (e.g., at bus stations) if needed. This policy (i.e., vaccinate migrants only) is compared to other policies including vaccinating (besides routine local vaccination) additional local populations. To identify a better vaccination strategy, we examine several measures including final epidemic and peak sizes of potential outbreaks. Because of the costs associated with vaccination programs, identification of the best policy will consider the total number of doses required to achieve a prescribed goal under the specific measures mentioned above.

We conducted simulations in both the deterministic and stochastic settings. Figure 4.4 shows the deterministic (left) and stochastic (right) outcomes of the short-term model in the absence of supplemental vaccinations. We examine how the outbreak can be affected by various vaccination policies. We compare outbreak (final and peak) sizes over a fixed period of time, one year in this case.

For ease of reference, we use the term "final size" to denote the number of infections over the fixed period in each patch, and use the term "total final size" to denote the final size over all three patches. Similarly, the total peak size denotes the peak size over the three patches. The measures used for comparison include the total final size, total peak size, and total number of vaccine doses used. For the deterministic outcome shown in Figure 4.4 (left) the total final size is 12044, which is about 12% of the total population, the total peak size is 540, and the total number of vaccine doses is zero (as this is the case of no supplemental vaccinations).

For stochastic simulations of the short-term model, events (e.g., migration, being vaccinated, etc.) occur based on their corresponding probabilities. In these simulations, for each fixed set of parameter values, the trajectories can be dramatically different, as illustrated in Figure 4.4 for identical parameter values. This figure illustrates various levels of outbreaks in the three patches. It demonstrates the result of 20 realizations for the case of no supplementary vaccination. Each of the trajectories

shows the total number of infectious individuals in all three patches at time t. We observe that these epidemic curves exhibit various final epidemic as well as peak sizes. The mean of the total final sizes is 1.2%, and the mean of the total peak sizes is 564.

The final and peak sizes of each of the 20 realizations are plotted in Figure 4.5. as well as the mean values for the total final size and peak size among the 20 realizations (the dashed lines). Plots A and B illustrate the final size and peak size, respectively, and plot C shows the peak sizes in each patch. The dot-dashed, dotted and dashed lines mark the mean values of the peak sizes for urban, peri-urban and rural patches, respectively. In the peak sizes in each patch shown in plot C, we observe large variations, particularly in the urban patch, which vary between 150 and 515 with a mean value of about 400 (marked by the dot-dashed line). The mean peak sizes in the peri-urban and rural patches are 150 and 50, respectively.

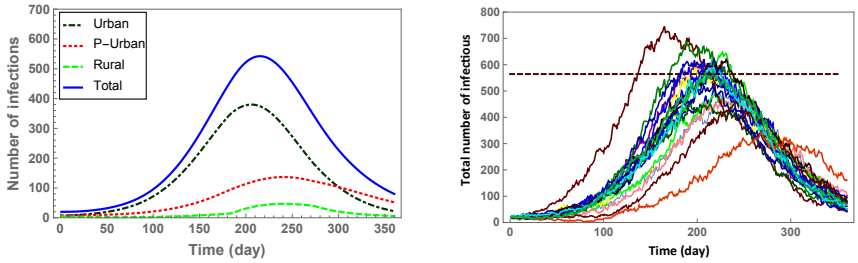

Fig. 4.4. Deterministic (left) and stochastic (right) simulations of the short-term model (4.5) over one year in the absence of supplementary vaccinations. The left figure shows the epidemic curves in the urban (dot-dashed), peri-urban (dotted), and rural patches (dashed), as well as the total number of infectious individuals in all three patches (solid). The right figure shows the epidemic curves from 20 stochastic realizations, each of which shows the total number of infectious individuals in all three patches. The dashed line indicates the mean of the total peak sizes (564).

4.3 Impact of vaccination policies on short-term outbreaks

We can compare different ways of distributing supplemental vaccines to identify the best vaccination strategy. For local populations, we incorporate supplementary vaccination in the short-term model via initial conditions by moving the corresponding fraction of susceptible individuals (S_i) in patch i to the vaccinated class V_i^s. For migrants, supplementary vaccination is reflected in the daily vaccination probability η_{ji} of individuals migrating from patch j to patch i ($j \neq i$). Because we are focusing on migrations from rural to urban and peri-urban patches, we have $\eta_{ji} = 0$ for all i, j except η_{31} and η_{32}.

For ease of reference, let

$$\mathbf{h}_{\text{loc}} = (h_{\text{loc1}}, h_{\text{loc2}}, h_{\text{loc3}}), \quad \mathbf{h}_{\text{mig}} = (h_{\text{mig1}}, h_{\text{mig2}}),$$

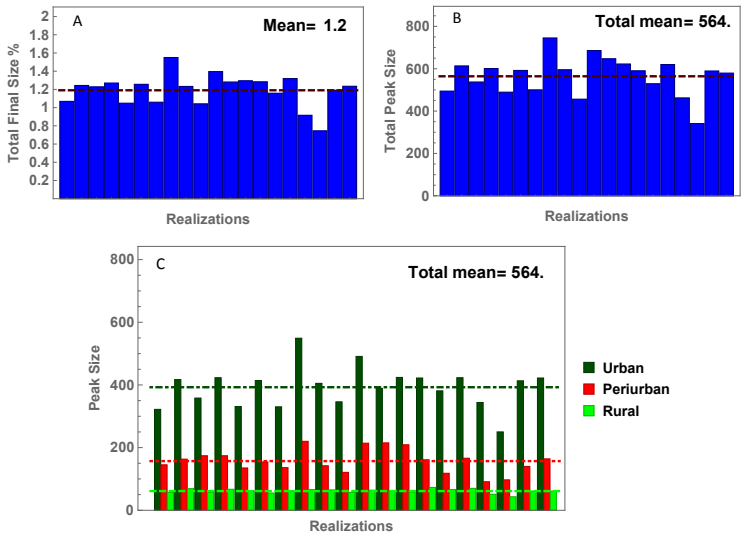

Fig. 4.5. Total final size (A) and peak size (B) from the 20 realizations of stochastic simulations shown in Figure 4.4. Peak sizes in the three patches are shown in C. The dashed lines mark the mean values over the 20 realizations.

where h_{loc1}, h_{loc2} and h_{loc3} denote the probabilities of local individuals in urban, peri-urban and rural, respectively, receiving supplementary vaccinations, and h_{mig1} and h_{mig2} denote the vaccination probabilities for migrants. We consider three types of supplementary vaccination:

Policy I. Vaccinate local populations only, i.e., $\mathbf{h}_{\text{loc}} > 0$ and $\mathbf{h}_{\text{mig}} = 0$;

Policy II. Vaccinate migrants only, i.e., $\mathbf{h}_{\text{loc}} = 0$, and $\mathbf{h}_{\text{mig}} > 0$;

Policy III. Vaccinate both local people and migrants, i.e., $\mathbf{h}_{\text{loc}} > 0$, $\mathbf{h}_{\text{mig}} > 0$.

Introduce the following vector notation

$$\mathbf{u} = (1, 1, 1), \quad \mathbf{v} = (a_1, a_2, a_3), \quad \mathbf{w} = (1, 1), \quad \mathbf{z} = (a_1, a_2), \tag{4.13}$$

where $a_i > 0$ are the activity levels in population i. For ease of reference, we define several terms based on the properties of $\mathbf{h}_{\text{loc}}$ and $\mathbf{h}_{\text{mig}}$ ($k_i > 0$ are constants):

(i) Homogeneous policy I (or Hom I) is a program with $\mathbf{h}_{\text{loc}} = k_1\mathbf{u}$, $\mathbf{h}_{\text{mig}} = 0$.

(ii) Heterogeneous policy I (or Het I) is a program with $\mathbf{h}_{\text{loc}} = k_2\mathbf{v}$, $\mathbf{h}_{\text{mig}} = 0$.

(iii) Homogeneous policy II (or Hom II) is a program with $\mathbf{h}_{\text{mig}} = k_3\mathbf{w}$, $\mathbf{h}_{\text{loc}} = 0$.

(iv) Heterogeneous policy II (or Het II) is a program with $\mathbf{h}_{\text{mig}} = k_4\mathbf{z}$, $\mathbf{h}_{\text{loc}} = 0$.

(v) Heterogeneous policy III (or Het III) is a program with $\mathbf{h}_{\text{loc}} > 0$, $\mathbf{h}_{\text{mig}} > 0$, and they are not multiples of $\mathbf{u}$ or $\mathbf{w}$.

We will compare both homogeneous and heterogeneous coverages. In addition to the cases mentioned above, we may also consider other heterogeneous programs for which $\mathbf{h}_{\text{mig}}$ is a non-zero multiple of neither $\mathbf{w}$ nor $\mathbf{z}$.

Figure 4.6 compares the outcomes of four vaccination programs under policies I and II. The activity levels are the same as in Figures 4.4 and 4.5 (i.e., $a_1 = 8, a_2 = 5, a_3 = 2$). In this case, $\mathbf{v} = (8, 5, 2)$ and $\mathbf{z} = (8, 5)$. Rows 1 and 2 are for policy I

with homogeneous coverage $\mathbf{h}_{\text{loc}} = 0.01\mathbf{u}$ (A1 and B1) and heterogeneous coverage $\mathbf{h}_{\text{loc}} = 0.0332\mathbf{v}$ (A2 and B2), and rows 3 and 4 are for policy II with homogeneous coverage $\mathbf{h}_{\text{mig}} = 0.547\mathbf{w}$ (A3 and B3) and heterogeneous coverage $\mathbf{h}_{\text{mig}} = 0.092\mathbf{z}$ (A4 and B4). For ease of comparison, the results are also summarized in Table 4.2 (see (a)–(d)). The h values are chosen such that all four programs described in rows (a)-(d) use a similar total number of vaccine doses: 15227, 15244, 15131 and 15091, respectively. However, the outcomes of these four programs are very different. The mean total final sizes are 0.47% , 0.14%, 0.14% and 0.07% of the population, respectively, and the mean total peak sizes are 190, 57, 55 and 36, respectively. This suggests that heterogeneous policy II is most effective among the four programs in terms of reducing total final and peak sizes, while using fewer vaccine doses.

Table 4.2.
Comparison of policies I and II under homogeneous and heterogeneous coverages. Hom: Homogeneous policy. Het: Heterogeneous policy. Vectors $\mathbf{u}, \mathbf{v}, \mathbf{w}, \mathbf{z}$ are defined in (4.13).

Policy type	Values	Mean final size	Mean peak size	Mean total doses	Figure
None	$\mathbf{h}_{\text{loc}} = \mathbf{h}_{\text{mig}} = 0$	1.21%	564	0	Figure 4.5
(a) Hom I	$\mathbf{h}_{\text{loc}} = 0.1\mathbf{u}$	0.47%	190	15227	Figure 4.6 (A1, B1)
(b) Het I	$\mathbf{h}_{\text{loc}} = 0.0332\mathbf{v}$	0.14%	57	15244	Figure 4.6 (A2, B2)
(c) Hom II	$\mathbf{h}_{\text{mig}} = 0.547\mathbf{w}$	0.14%	55	15131	Figure 4.6 (A3, B3)
(d) Het II	$\mathbf{h}_{\text{mig}} = 0.092\mathbf{z}$	0.07%	36	15091	Figure 4.6 (A4, B4)
(e) Het I	$\mathbf{h}_{\text{loc}} = 0.01\mathbf{v}$	0.74%	324	4591	Figure 4.8 (A1, B1)
(f) Hom II	$\mathbf{h}_{\text{mig}} = 0.16\mathbf{w}$	0.75%	316	4180	Figure 4.8 (A2, B2)

Although the mean values presented in Figure 4.6 provide useful information, further insights can be obtained by examining the distribution of possible events

shown in the stochastic results. Particularly important to policy decisions is the likelihood that the final size of an outbreak may exceed some prescribed level of severity under various vaccination programs. Figure 4.7 compares the four programs shown in Figure 4.6 in terms of the frequencies of the 100 realizations (which is analogous to likelihood in a single outbreak) under each policy that corresponds to the final sizes being below some hypothetical prescribed thresholds. We observe that the homogeneous policy I with $\mathbf{h}_{\text{loc}} = 0.1\mathbf{u}$ is less likely to reduce the final size to be below 0.2% of the total population, while the heterogeneous policy II with

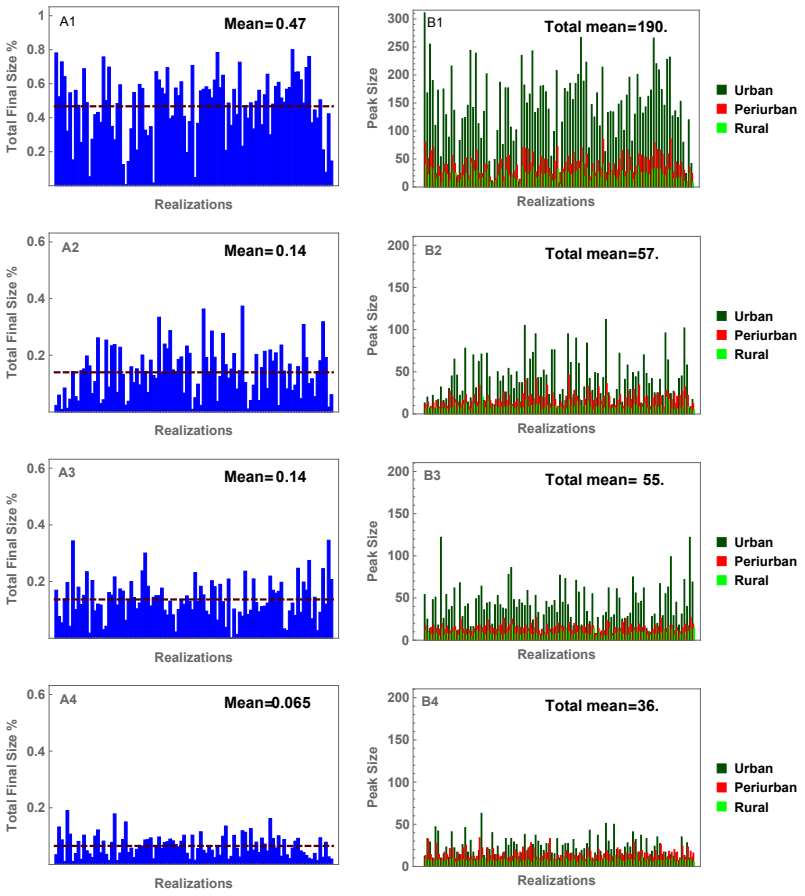

Fig. 4.6. Results of 100 stochastic realizations of the short-term model under homogeneous or heterogeneous policies I and II. See text for detailed descriptions.

$\mathbf{h}_{\text{mig}} = 0.092\mathbf{z}$ is most likely (with a 80% chance) to contain the final size to be below 0.1%. The middle two programs (heterogeneous policy I with $\mathbf{h}_{\text{loc}} = 0.0332\mathbf{v}$ and homogeneous policy II with $\mathbf{h}_{\text{mig}} = 0.092\mathbf{z}$) have very similar likelihood for all threshold levels. Similarly, the heterogeneous policy II has a much higher likelihood than other three policies to contain the urban peak size to be below 25 or 50.

From Figure 4.6, we also observe that, under the similar number of total vaccine doses, the heterogeneous policy II (A2 and B2) and homogeneous policy I (A3 and B3)

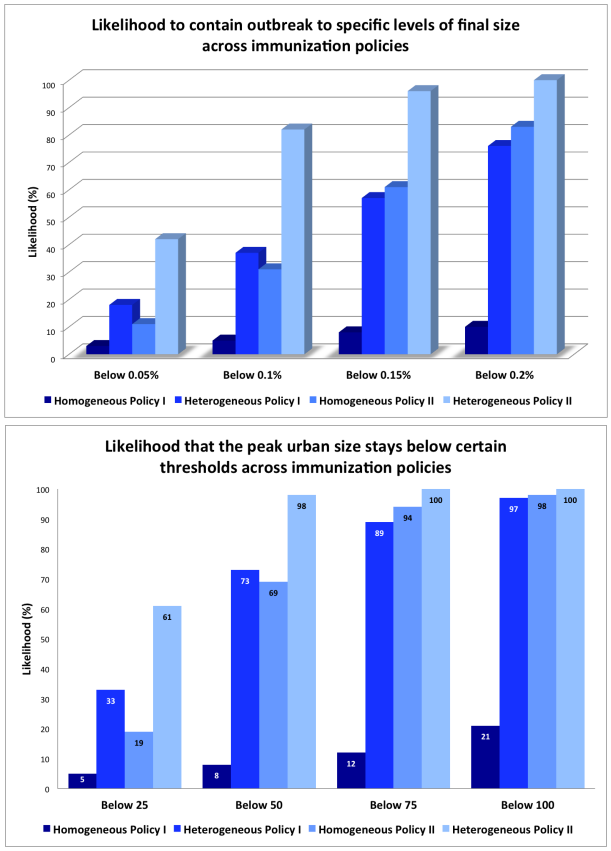

Fig. 4.7. Likelihood that the final size of an epidemic may exceed some prescribed level of severity (top) or the likelihood that the peak size in urban is below certain thresholds (bottom) under the four vaccination programs presented in Figure 4.6 based on 100 stochastic realizations. The four policies correspond to the vaccination programs shown in A1–A4 in Figure 4.6 or cases (a)–(d) in Table 4.2.

have similar effects in reducing the final and peak sizes. Many of our simulations under other parameter values illustrate similar features. One such example is demonstrated in Figure 4.8. The vaccination programs are represented by $\mathbf{h}_{\text{loc}} = 0.01\mathbf{v}$ (Figures 4.8 (A1 and B1)) and $\mathbf{h}_{\text{mig}} = 0.15\mathbf{w}$ (A2 and B2). The average total numbers of vaccine doses over 20 realizations in these two cases are similar with 4591 in A1 and B1, and 4180 in A2 and B2. We observe that the mean final and peak sizes under these two programs are also similar: the mean total final sizes are 0.74% and 0.75%, and the mean total peak sizes are 324 and 325. These comparison results are also listed in Table 4.2. From these and many other simulations, we observe that homogeneous policy I is least effective and heterogeneous policy II is most effective in terms of reducing the total final and peak sizes with a similar number of vaccine doses. However, it needs to be pointed out that the conclusion that heterogeneous policy II is more effective depends critically on the relative activity levels a_i $(i = 1, 2, 3)$.

We can also compare policies to identify the best strategy in the sense of using the fewest vaccine doses under a prescribed upper bound for the total final size. One such

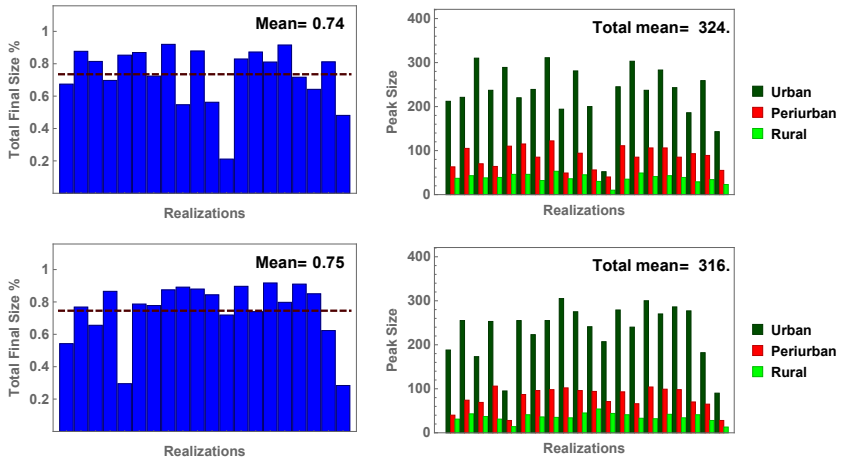

Fig. 4.8. Similar to Figure 4.6 except the values of h_i. A1 and B1 are for the heterogeneous policy I with $\mathbf{h}_{\text{loc}} = 0.01\mathbf{v}$, and A2 and B2 are for the homogeneous policy II with $\mathbf{h}_{\text{mig}} = 0.15\mathbf{w}$. Similar numbers of vaccine doses, 4591 (top) and 4180 (bottom), were used.

example is presented in Table 4.3. All parameter values are the same as in Table 4.2 except for the h_i values. The results presented in Table 4.3, however, are computed from the deterministic model. In rows (a)-(c), the three vaccination programs lead to the same total final size (0.43%), but the number of vaccine doses required differ with program (c) being the most effective policy (6896 doses versus 9183 in (a) and 8905 in (b)). Similarly, the vaccination policies represented in (d)-(f) lead to the same final size (0.19%) but the option (f) of heterogeneous policy II uses the least vaccine doses (10673 versus 13774 in (d) and 13915 in (e)).

Table 4.3.
Comparison of policy I and policy II (equal final size with fewer vaccine doses). Hom: Homogeneous policy. Het: Heterogeneous policy. Vectors $\mathbf{v}, \mathbf{w}, \mathbf{z}$ are defined in (4.13).

Policy type	Values	Mean final size	Mean peak size	Mean total doses
(a) Het I	$\mathbf{h}_{\text{loc}} = 0.02\mathbf{v}$	**0.43%**	147	9183
(b) Hom II	$\mathbf{h}_{\text{mig}} = 0.32\mathbf{w}$	**0.43%**	144	8905
(c) Het II	$\mathbf{h}_{\text{mig}} = 0.042\mathbf{z}$	**0.43%**	142	6896
(d) Het I	$\mathbf{h}_{\text{loc}} = 0.03\mathbf{v}$	**0.19%**	55	13774
(e) Hom II	$\mathbf{h}_{\text{mig}} = 0.5\mathbf{w}$	**0.19%**	54	13915
(f) Het II	$\mathbf{h}_{\text{mig}} = 0.065\mathbf{z}$	**0.19%**	54	10673

To explore the effects of policy III, in which supplementary vaccination is given to both local populations and migrants, many factors can influence the allocation of supplementary vaccines among sub-groups, including the costs associated with vaccine distribution and administration. We present in Figure 4.9 several scenarios based on two main objectives. One is to identify the policy that uses the least vaccine doses to contain the final size at the same (or similar) level, and another is to identify a policy that reduces the final size the most with the same (or similar) vaccine doses.

We compared various vaccination policies for local and migrant populations, including both homogeneous and heterogeneous coverages. Figure 4.9 (A1) is a baseline scenario, which corresponds to the combination of homogeneous local coverage with $\mathbf{h}_{\text{loc}} = 0.02\mathbf{u}$ and homogeneous migrant coverage with $\mathbf{h}_{\text{mig}} = 0.028\mathbf{z}$. It shows 20 realizations of the stochastic simulations. The top panel is for the case when local vaccinations are homogeneous with $\mathbf{h}_{\text{loc}} = 0.02\mathbf{u}$, and the bottom B panel is for the case of heterogeneous local coverage with $\mathbf{h}_{\text{loc}} = 0.07\mathbf{v}$. The six cases are for different coverages in migrants: homogeneous with $\mathbf{h}_{\text{mig}} = 0.2\mathbf{w}$ (A1); heterogeneous with $\mathbf{h}_{\text{mig}} = 0.28\mathbf{z}$ (A2); heterogeneous with $\mathbf{h}_{\text{mig}} = (0.54, 0.054)$ (A3); homogeneous with $\mathbf{h}_{\text{mig}} = 0.192\mathbf{w}$ (B1); heterogeneous with $\mathbf{h}_{\text{mig}} = 0.2\mathbf{z}$ (B2); and heterogeneous with $\mathbf{h}_{\text{mig}} = (0.52, 0.052)$ (B3). In each plot, the mean total final size and the mean total number of vaccine doses are listed. We observe again that, with the same or similar vaccine doses (e.g., see A1, A3, B1 and B3)), heterogeneous coverage (A3 and B3) will likely lead to a lower final size than homogeneous coverage (A1). The greater effectiveness can be represented either by a lower final size with similar vaccine doses (A1 versus A3, or B1 versus B3) or by a lower number of vaccine doses when final sizes are similar (A1 versus A2, or B1 versus B2).

We need to point out that the assessments presented above are based only on the final and peak epidemic sizes or the number of vaccine doses needed to achieve a prescribed epidemic size. When other factors are considered, such as economic costs related to vaccinating local populations versus migrants, the conclusions might differ. In addition, parameter values may affect the relative effectiveness of these programs, including population density, migration patterns, infectious period, and others.

4.4 Discussion

The objective of this chapter is to evaluate vaccination policies for a vaccine-preventable disease using a meta-population model that explicitly incorporates migration between patches. This is an extension of the model considered in [66], in

which migrations are modeled implicitly. In the short-term model (4.5), seasonal spatial movements from one patch to another are included to capture the migration from rural to urban or peri-urban for employment opportunities and return home afterwards. The main findings of the study suggest that (because of the significant difference in population density, which directly influences the contact rate, affecting the rate of disease transmission), vaccinating migrants can be a very important means of preventing outbreaks. Particularly, heterogeneous coverages among migrants are likely the most effective vaccination strategies.

The model outcomes are generated by both deterministic and stochastic simulations. Various vaccination programs are compared in terms of three measures: number of vaccine doses used, final epidemic size, and peak epidemic size (either within individual patches or over all three patches). Deterministic simulations help identify suitable vaccination scenarios for comparison, and stochastic simulations with multiple realizations provide a range of possibilities in terms of epidemic sizes, for which

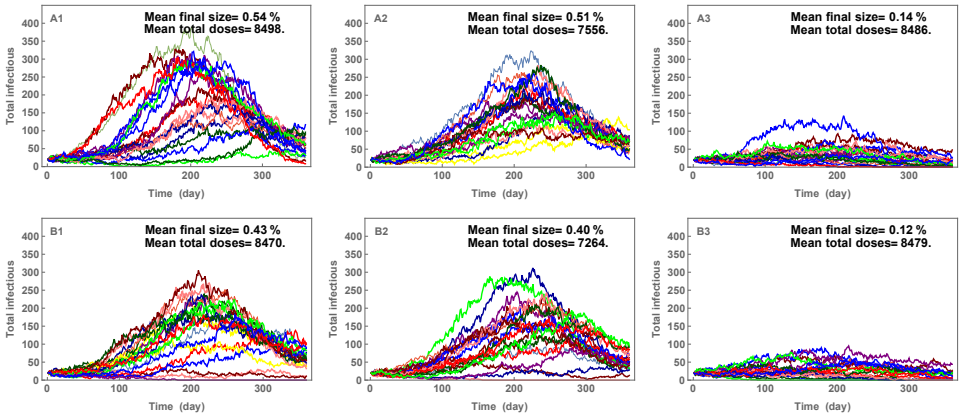

Fig. 4.9. Comparison of six scenarios under policy III. It shows the epidemic curves from 20 stochastic realizations in each scenario. The top panel is for the case when the local vaccinations are homogeneous with $\mathbf{h}_{\text{loc}} = 0.02\mathbf{u}$, whereas the bottom panel is for the heterogeneous local coverage with $\mathbf{h}_{\text{loc}} = 0.07\mathbf{v}$. The six cases are for different coverages in migrants. See the text for detailed information.

the mean value of each measure also provides useful insights into possible outcomes of various vaccination policies.

Our comparisons focused on identifying the best vaccination strategy based on two objectives: Objective 1 is to apply fewer vaccine doses while bringing the epidemic size below a prescribed level, and Objective 2 is to reduce the outbreak size the most with a given number of vaccine doses. Three types of vaccination policies are considered in terms of the allocation of supplementary vaccines: policy I involves vaccinating only local populations; policy II involves vaccinating only migrants; and policy III involves combined vaccinations of both local and migrant populations. In all comparisons, we considered homogeneous and heterogeneous vaccination coverages in either local populations or migrants or both. One of the main results is that, in the case when the heterogeneity in population density is significant, the best vaccination strategy likely involves heterogeneous coverages among migrants. For example, Figure 4.6(A1–A4) and the cases (a-d) in Table 4.2 present four policies that use similar vaccine doses. The homogeneous policy I (A1 and (a)) corresponds to a much higher final size than the other three policies, while the heterogeneous policy II (A4 and (d)) leads to the lowest final size. The results presented in Table 4.3 show two cases in which heterogeneous policy II is more effective then heterogeneous policy I in terms of using fewer doses while leading to similar final sizes.

In most cases, heterogeneous coverages are taken to be proportional to the activity levels $\mathbf{v} = (a_1, a_2, a_3)$, which are related to the population densities in urban, peri-urban and rural patches (i.e., $\mathbf{h}_{\text{loc}} = k\mathbf{v}$ or $\mathbf{h}_{\text{mig}} = k'\mathbf{z}$ for some positive constants k and k'). Results are shown for $\mathbf{v} = (a_1, a_2, a_3) = (8, 5, 2)$. For the set of parameter values used, simulation results show that the selection of vaccination policies should be guided by the objectives of outbreak prevention, and that for the evaluation of certain types of policy goals, stochastic models can provide more useful insights than deterministic ones. For example, based on 100 realizations from stochastic simulations of the short-term model (4.5) presented in Figure 4.6 or the corresponding scenarios listed in (a)–(d) in Table 4.2, it is shown in Figure 4.7 that the heterogeneous policy I

is more likely than the homogeneous policy II to contain the outbreak within a small size (e.g., final size below 0.05% or 0.1%, or urban peak size below 20 or 50), but that homogeneous policy II is more likely than the heterogeneous policy I to contain the outbreak within a medium to larger size (e.g., final size below 0.15% or 0.2%, or urban peak size below 75 or 100). This illustrates that, while the deterministic model implies that these two vaccination policies are essentially identical, the stochastic model reveals meaningful differences.

It is important to emphasize that the conclusion that heterogeneous coverages among migrants are more effective is critically dependent on heterogeneity in contact and migration rates. If these heterogeneities are not very strong, vaccinating local populations could be more effective than vaccinating migrants. Which vaccination strategies are most effective may also depend on other characteristics of the population such as immunity (see [71]).

4.5 Appendix

This section includes the derivation of the reproduction numbers $\mathcal{R}_{vi}$ for the long-term model (4.1). Denote the disease-free equilibrium by $U_i^0 = (M_i^0, V_i^0, S_i^0, E_i^0, I_i^0, R_i^0)$, $i = 1, 2, 3$. Then U^0 is obtained by solving the following equation with $E_i^0 = I_i^0 = R_i^0 = 0$:

$$\begin{aligned} M_i &= \theta_i\mu_i N_i + (1-\mu_i)(1-\sigma)M_i \\ V_i &= \alpha\nu_i^0(1-\mu_i)S_i(n) + (1-\mu_i)(1-\chi)V_i \\ S_i &= (1-\theta_i)\mu_i N_i + (1-\mu_i)(1-\alpha\nu_i^0)S_i + \sigma(1-\mu_i)M_i(n) + \chi(1-\mu_i)V_i, \end{aligned}$$

given N_i are constants. It gives

$$\frac{M_i^0}{N_i} = \frac{\theta_i\mu_i}{1-(1-\mu_i)(1-\sigma)}, \quad \frac{S_i^0}{N_i} = \frac{\left[(1-\theta_i) + \theta_i\frac{\sigma(1-\mu_i)}{1-(1-\mu_i)(1-\sigma)}\right]\mu_i}{1-(1-\mu_i)(1-\alpha\nu_i^0) - \chi(1-\mu_i)\frac{\alpha\nu_i^0(1-\mu_i)}{1-(1-\mu_i)(1-\chi)}},$$

$$\frac{V_i^0}{N_i} = \frac{\alpha\nu_i^0(1-\mu_i)}{1-(1-\mu_i)(1-\chi)} \frac{\left[(1-\theta_i) + \theta_i\frac{\sigma(1-\mu_i)}{1-(1-\mu_i)(1-\sigma)}\right]\mu_i}{1-(1-\mu_i)(1-\alpha\nu_i^0) - \chi(1-\mu_i)\frac{\alpha\nu_i^0(1-\mu_i)}{1-(1-\mu_i)(1-\chi)}}.$$

To compute the reproduction number, we follow the method outlined in [36]. The Jacobian matrix at U_i^0 can be written in the form $F + T$, where

$$F = \begin{bmatrix} 0 & (1-\mu_i)\beta_i^0 \frac{S_i^0}{N_i} \\ 0 & 0 \end{bmatrix}, \qquad T = \begin{bmatrix} (1-\mu_i)(1-\gamma) & 0 \\ (1-\mu_i)\gamma & (1-\mu_i)(1-\rho) \end{bmatrix}.$$

Then

$$(1-T)^{-1} = \begin{bmatrix} \frac{1}{1-(1-\mu_i)(1-\gamma)} & 0 \\ \frac{(1-\mu_i)\gamma}{(1-(1-\mu_i)(1-\gamma))} \frac{1}{(1-(1-\mu_i)(1-\rho))} & \frac{1}{1-(1-\mu_i)(1-\rho)} \end{bmatrix},$$

and

$$F(1-T)^{-1} = \begin{bmatrix} \frac{(1-\mu_i)\gamma}{1-(1-\mu_i)(1-\gamma)} \frac{(1-\mu_i)\beta_i^0(S_i^0/N_i)}{1-(1-\mu_i)(1-\rho)} & \frac{(1-\mu_i)\beta_i^0(S_i^0/N_i)}{1-(1-\mu_i)(1-\rho)} \\ 0 & 0 \end{bmatrix}.$$

Therefore,

$$\mathcal{R}_{vi} = \varrho(F(1-T)^{-1}) = \frac{(1-\mu_i)\gamma}{1-(1-\mu_i)(1-\gamma)} \frac{(1-\mu_i)\beta_i^0(S_i^0/N_i)}{1-(1-\mu_i)(1-\rho)},$$

where $\frac{(1-\mu_i)\gamma}{1-(1-\mu_i)(1-\gamma)}$ is the probability that an infected individual survives the latent period, and $\frac{(1-\mu_i)\beta_i^0(S_i^0/N_i)}{1-(1-\mu_i)(1-\rho)}$ is the expected number of new infections that an infectious individual can generate during the entire infectious period in a population where the fraction of susceptibles is S_i^0/N_i.

5. SUMMARY

This thesis consists of several models for Ebola virus disease and vaccine preventable infectious diseases. These models are motivated, developed and studied to answer the driving questions in epidemiology:

- What are the underlying assumptions of the Legrand model, which has been widely used in modeling Ebola outbreaks?
- What difference does it make if the spectrum of Ebola symptoms are not considered?
- How do we design efficient vaccination plans to mitigate the vaccine preventible disease epidemics if migration between patches differing in density is considered?

Through Chapter 2 to 4 in this thesis, these questions are addressed using different mathematical tools including systems of ordinary differential equations, integro-differential equations as well as deterministic and stochastic discrete models. The results may be helpful for providing insights into consequences of the underlying assumptions, disease transmission dynamics and evaluation of disease control strategies.

Chapter 2 studies the assumptions underlying the widely used Legrand model. The Legrand model has been applied to major Ebola outbreaks in Africa by various researchers, and many other Ebola models are based on it. The Legrand model includes transmission in community, hospital and funeral based on a system of ordinary differential equations. However, in its original formulation, several intermediate parameters are introduced without direct epidemiological meanings, hindering the interpretation and further applications. In this chapter, a much simpler but equivalent formulation is provided that helps researchers to understand the parametrization of this model. This complex formulation also disguises how mathematical processes are

related to epidemiological ones for infectious individuals, including hospitalization, recovery and death. It is difficult to determine the dependence or independence of these processes. Three alternative models are developed with clear assumptions about these processes, one of which simplifies to the Legrand model. The three models also include more realistic Gamma distributed sojourns, whereas the Legrand model assumes exponential sojourns. Comparison of these models shows that the underlying assumptions are important in evaluating control strategies.

Chapter 3 also develops a mathematical model to crudely account for the wide spectrum of Ebola symptoms. Even 13% of infected individuals do not experience the most common symptom, fever, in the recent West Africa outbreak. This suggests that asymptomatic (mild) and moderate symptoms of Ebola infection are possible as observed in previous outbreaks. Model II in chapter 2 is extended to include the Ebola infection with asymptomatic (mild) and moderate symptoms. The model is calibrated to the Liberia outbreak and captures the observed dynamics. If we disable the infection with asymptomatic (mild) and moderate symptoms, the model overestimates the reproduction numbers and effectiveness of interventions. Sensitivity analyses of the model are used to evaluate possible control strategies. It is shown that modeling the spectrum of Ebola symptoms is important regarding policy-making.

Chapter 4 develops models to design and evaluate public health policies for vaccine-preventable diseases. Unlike models assuming homogeneous mixing, the model in this chapter explicitly includes a spatial structure of urban, peri-urban and rural patches. A deterministic discrete model is used to determine the immunity levels of patches in the long-term, finding that the rural patch has lower immunity than urban/peri-urban patches. Thus, seasonal migration of rural residents between rural and urban/peri-urban patches may change the immunity levels of patches dynamically. This increases chances of outbreaks in urban patch as more susceptible people migrate to urban area from rural area and therefore it decreases the immunity level of urban patch. A short-term stochastic model captures migration as well as disease transmission. It is also used to compare different short-term vaccination policies to mitigate the recurrent

outbreaks. The results help public health officials to ensure the best possible use of available vaccines.

REFERENCES

REFERENCES

[1] "WHO Statement on the 1st meeting of the IHR Emergency Committee on the 2014 Ebola outbreak in West Africa," http://www.who.int/mediacentre/news/statements/2014/ebola-20140808/en/, [Online; accessed 2016-02-03].

[2] "One year into the Ebola epidemic: a deadly, tenacious and unforgiving virus," http://www.who.int/csr/disease/ebola/one-year-report/introduction/en/, [Online; accessed 2016-02-03].

[3] "WHO | Ebola virus disease," http://www.who.int/mediacentre/factsheets/fs103/en/, [Online; accessed 2016-04-03].

[4] S. K. Singh and D. Ruzek, *Viral Hemorrhagic Fevers*. CRC Press, Jul. 2013.

[5] "Ebola haemorrhagic fever in Zaire, 1976," *Bull World Health Organ*, vol. 56, no. 2, pp. 271–293, 1978.

[6] E. T. W. Bowen, G. Lloyd, W. J. Harris, G. S. Platt, A. Baskerville, and E. E. Vella, "Originally published as Volume 1, Issue 8011viral HÆMORRHAGIC FEVER IN SOUTHERN SUDAN AND NORTHERN ZAIRE," *The Lancet*, vol. 309, no. 8011, pp. 571–573, Mar. 1977.

[7] H. Feldmann and T. W. Geisbert, "Ebola haemorrhagic fever," *Lancet*, vol. 377, no. 9768, pp. 849–862, Mar. 2011.

[8] M. D. Van Kerkhove, A. I. Bento, H. L. Mills, N. M. Ferguson, and C. A. Donnelly, "A review of epidemiological parameters from Ebola outbreaks to inform early public health decision-making," *Scientific Data*, vol. 2, p. 150019, May 2015.

[9] G. Chowell and H. Nishiura, "Transmission dynamics and control of Ebola virus disease (EVD): a review," *BMC medicine*, vol. 12, no. 1, p. 196, 2014.

[10] E. M. Leroy, B. Kumulungui, X. Pourrut, P. Rouquet, A. Hassanin, P. Yaba, A. Délicat, J. T. Paweska, J.-P. Gonzalez, and R. Swanepoel, "Fruit bats as reservoirs of Ebola virus," *Nature*, vol. 438, no. 7068, pp. 575–576, Dec. 2005.

[11] X. Pourrut, A. Délicat, P. E. Rollin, T. G. Ksiazek, J.-P. Gonzalez, and E. M. Leroy, "Spatial and temporal patterns of Zaire ebolavirus antibody prevalence in the possible reservoir bat species," *J. Infect. Dis.*, vol. 196 Suppl 2, pp. S176–183, Nov. 2007.

[12] "Preliminary study finds that Ebola virus fragments can persist in the semen of some survivors for at least nine months | CDC Online Newsroom | CDC," http://www.cdc.gov/media/releases/2015/p1014-ebola-virus.html, [Online; accessed 2016-04-12].

[13] "Recommendations for Breastfeeding/Infant Feeding in the Context of Ebola | Ebola Hemorrhagic Fever | CDC," http://www.cdc.gov/vhf/ebola/hcp/recommendations-breastfeeding-infant-feeding-ebola.html, [Online; accessed 2016-04-12].

[14] WHO Ebola Response Team, "Ebola Virus Disease in West Africa — The First 9 Months of the Epidemic and Forward Projections," *New England Journal of Medicine*, vol. 371, no. 16, pp. 1481–1495, Oct. 2014.

[15] S. Baize, D. Pannetier, L. Oestereich, T. Rieger, L. Koivogui, N. Magassouba, B. Soropogui, M. S. Sow, S. Keïta, H. De Clerck, A. Tiffany, G. Dominguez, M. Loua, A. Traoré, M. Kolié, E. R. Malano, E. Heleze, A. Bocquin, S. Mély, H. Raoul, V. Caro, D. Cadar, M. Gabriel, M. Pahlmann, D. Tappe, J. Schmidt-Chanasit, B. Impouma, A. K. Diallo, P. Formenty, M. Van Herp, and S. Günther, "Emergence of Zaire Ebola virus disease in Guinea," *N. Engl. J. Med.*, vol. 371, no. 15, pp. 1418–1425, Oct. 2014.

[16] "Ebola Situation Reports," http://apps.who.int/ebola/ebola-situation-reports, [Online; accessed 2016-02-15].

[17] S. F. Dowell, R. Mukunu, T. G. Ksiazek, A. S. Khan, P. E. Rollin, and C. J. Peters, "Transmission of Ebola hemorrhagic fever: a study of risk factors in family members, Kikwit, Democratic Republic of the Congo, 1995. Commission de Lutte contre les Epidémies à Kikwit," *J. Infect. Dis.*, vol. 179 Suppl 1, pp. S87–91, Feb. 1999.

[18] T. H. Roels, A. S. Bloom, J. Buffington, G. L. Muhungu, W. R. Mac Kenzie, A. S. Khan, R. Ndambi, D. L. Noah, H. R. Rolka, C. J. Peters, and T. G. Ksiazek, "Ebola hemorrhagic fever, Kikwit, Democratic Republic of the Congo, 1995: risk factors for patients without a reported exposure," *J. Infect. Dis.*, vol. 179 Suppl 1, pp. S92–97, Feb. 1999.

[19] B. S. Hewlett and R. P. Amola, "Cultural Contexts of Ebola in Northern Uganda," *Emerg Infect Dis*, vol. 9, no. 10, pp. 1242–1248, Oct. 2003.

[20] J. Legrand, R. F. Grais, P. Y. Boelle, A. J. Valleron, and A. Flahault, "Understanding the dynamics of Ebola epidemics," *Epidemiol. Infect.*, vol. 135, no. 4, pp. 610–621, May 2007.

[21] C. L. Althaus, "Estimating the Reproduction Number of Ebola Virus (EBOV) During the 2014 Outbreak in West Africa," *PLoS Currents*, 2014.

[22] A. Khan, M. Naveed, M. Dur-e Ahmad, and M. Imran, "Estimating the basic reproductive ratio for the Ebola outbreak in Liberia and Sierra Leone," *Infect Dis Poverty*, vol. 4, Feb. 2015.

[23] J. S. Weitz and J. Dushoff, "Modeling Post-death Transmission of Ebola: Challenges for Inference and Opportunities for Control," *Scientific Reports*, vol. 5, p. 8751, Mar. 2015.

[24] A. Camacho, A. J. Kucharski, S. Funk, J. Breman, P. Piot, and W. J. Edmunds, "Potential for large outbreaks of Ebola virus disease," *Epidemics*, vol. 9, pp. 70–78, Dec. 2014.

[25] C. M. Rivers, E. T. Lofgren, M. Marathe, S. Eubank, and B. L. Lewis, "Modeling the Impact of Interventions on an Epidemic of Ebola in Sierra Leone and Liberia," *PLoS Curr*, vol. 6, Nov. 2014.

[26] A. Pandey, K. E. Atkins, J. Medlock, N. Wenzel, J. P. Townsend, J. E. Childs, T. G. Nyenswah, M. L. Ndeffo-Mbah, and A. P. Galvani, "Strategies for containing Ebola in West Africa," *Science*, vol. 346, no. 6212, pp. 991–995, Nov. 2014.

[27] R. T. Heffernan, B. Pambo, R. J. Hatchett, P. A. Leman, R. Swanepoel, and R. W. Ryder, "Low Seroprevalence of IgG Antibodies to Ebola Virus in an Epidemic Zone: Ogooué-Ivindo Region, Northeastern Gabon, 1997," *J Infect Dis.*, vol. 191, no. 6, pp. 964–968, Mar. 2005.

[28] E. M. Leroy, S. Baize, V. E. Volchkov, S. P. Fisher-Hoch, M.-C. Georges-Courbot, J. Lansoud-Soukate, M. Capron, P. Debré, A. J. Georges, and J. B. McCormick, "Human asymptomatic Ebola infection and strong inflammatory response," *The Lancet*, vol. 355, no. 9222, pp. 2210–2215, Jun. 2000.

[29] G. Chowell, N. W. Hengartner, C. Castillo-Chavez, P. W. Fenimore, and J. M. Hyman, "The basic reproductive number of Ebola and the effects of public health measures: the cases of Congo and Uganda," *Journal of Theoretical Biology*, vol. 229, no. 1, pp. 119–126, Jul. 2004.

[30] P. E. Lekone and B. F. Finkenstädt, "Statistical Inference in a Stochastic Epidemic SEIR Model with Control Intervention: Ebola as a Case Study," *Biometrics*, vol. 62, no. 4, pp. 1170–1177, Dec. 2006.

[31] M. F. C. Gomes, A. Pastore Piontti, L. Rossi, D. Chao, I. Longini, M. E. Halloran, and A. Vespignani, "Assessing the International Spreading Risk Associated with the 2014 West African Ebola Outbreak," *PLoS Currents*, 2014.

[32] M. Barbarossa, A. Dénes, G. Kiss, Y. Nakata, G. Röst, and Z. Vizi, "Transmission Dynamics and Final Epidemic Size of Ebola Virus Disease Outbreaks with Varying Interventions," *PLoS ONE*, vol. 10, no. 7, p. e0131398, Jul. 2015.

[33] P. van den Driessche and J. Watmough, "Reproduction numbers and subthreshold endemic equilibria for compartmental models of disease transmission," *Mathematical Biosciences*, vol. 180, no. 1–2, pp. 29–48, Nov. 2002.

[34] Z. Feng, D. Xu, and H. Zhao, "Epidemiological Models with Non-Exponentially Distributed Disease Stages and Applications to Disease Control," *Bull. Math. Biol.*, vol. 69, no. 5, pp. 1511–1536, Jan. 2007.

[35] N. Hernandez-Ceron, Z. Feng, and C. Castillo-Chavez, "Discrete Epidemic Models with Arbitrary Stage Distributions and Applications to Disease Control," *Bull Math Biol*, vol. 75, no. 10, pp. 1716–1746, Jun. 2013.

[36] N. Hernández-Cerón, Z. Feng, and P. v. d. Driessche, "Reproduction numbers for discrete-time epidemic models with arbitrary stage distributions," *Journal of Difference Equations and Applications*, vol. 19, no. 10, pp. 1671–1693, Oct. 2013.

[37] H. W. Hethcote and D. W. Tudor, "Integral equation models for endemic infectious diseases," *J. Math. Biology*, vol. 9, no. 1, pp. 37–47, Mar. 1980.

[38] A. L. Lloyd, "Destabilization of epidemic models with the inclusion of realistic distributions of infectious periods," *Proceedings of the Royal Society B: Biological Sciences*, vol. 268, no. 1470, pp. 985–993, May 2001.

[39] H. J. Wearing, P. Rohani, and M. J. Keeling, "Appropriate Models for the Management of Infectious Diseases," *PLOS Med*, vol. 2, no. 7, p. e174, Jul. 2005.

[40] H. Smith, "Distributed Delay Equations and the Linear Chain Trick," in *An Introduction to Delay Differential Equations with Applications to the Life Sciences*, ser. Texts in Applied Mathematics. Springer New York, 2011, no. 57, pp. 119–130, dOI: 10.1007/978-1-4419-7646-8_7.

[41] R. Sheldon and others, *A first course in probability*. Pearson Education India, 2002.

[42] E. Vynnycky and R. White, *An Introduction to Infectious Disease Modelling*. OUP Oxford, May 2010.

[43] B. M. Bolker, *Ecological models and data in R*. Princeton University Press, 2008.

[44] J. Wu, R. Dhingra, M. Gambhir, and J. V. Remais, "Sensitivity analysis of infectious disease models: methods, advances and their application," *Journal of The Royal Society Interface*, vol. 10, no. 86, p. 20121018, Sep. 2013.

[45] M. A. Sanchez and S. M. Blower, "Uncertainty and Sensitivity Analysis of the Basic Reproductive Rate: Tuberculosis as an Example," *Am. J. Epidemiol.*, vol. 145, no. 12, pp. 1127–1137, Jun. 1997.

[46] S. Marino, I. B. Hogue, C. J. Ray, and D. E. Kirschner, "A methodology for performing global uncertainty and sensitivity analysis in systems biology," *Journal of Theoretical Biology*, vol. 254, no. 1, pp. 178–196, Sep. 2008.

[47] I. M. Sobol, "Global sensitivity indices for nonlinear mathematical models and their Monte Carlo estimates," *Mathematics and Computers in Simulation*, vol. 55, no. 1–3, pp. 271–280, Feb. 2001.

[48] Z. Feng, Y. Zheng, N. Hernandez-Ceron, J. Glasser, and A. Hill, "Mathematical models of Ebola - Consequences of underlying assumptions," *Mathematical Biosciences, Accepted*, 2016.

[49] N. MacDonald, *Time Lags in Biological Models*. Springer Berlin Heidelberg, 1978.

[50] A. L. Lloyd, "Realistic Distributions of Infectious Periods in Epidemic Models: Changing Patterns of Persistence and Dynamics," *Theoretical Population Biology*, vol. 60, no. 1, pp. 59–71, Aug. 2001.

[51] J. A. Lewnard, M. L. Ndeffo Mbah, J. A. Alfaro-Murillo, F. L. Altice, L. Bawo, T. G. Nyenswah, and A. P. Galvani, "Dynamics and control of Ebola virus transmission in Montserrado, Liberia: a mathematical modelling analysis," *The Lancet Infectious Diseases*, vol. 14, no. 12, pp. 1189–1195, Dec. 2014.

[52] G. Webb, C. Browne, X. Huo, O. Seydi, M. Seydi, and P. Magal, "A Model of the 2014 Ebola Epidemic in West Africa with Contact Tracing," *PLoS Currents*, 2015.

[53] C. Browne, H. Gulbudak, and G. Webb, "Modeling contact tracing in outbreaks with application to Ebola," *Journal of Theoretical Biology*, vol. 384, pp. 33–49, Nov. 2015.

[54] S. E. Bellan, J. R. C. Pulliam, J. Dushoff, and L. A. Meyers, "Ebola control: effect of asymptomatic infection and acquired immunity," *The Lancet*, vol. 384, no. 9953, pp. 1499–1500, Oct. 2014.

[55] J. Audet and G. P. Kobinger, "Immune evasion in ebolavirus infections," *Viral Immunol.*, vol. 28, no. 1, pp. 10–18, Feb. 2015.

[56] G. Wong, G. P. Kobinger, and X. Qiu, "Characterization of host immune responses in Ebola virus infections," *Expert Review of Clinical Immunology*, vol. 10, no. 6, pp. 781–790, Jun. 2014.

[57] C. A. Zampieri, N. J. Sullivan, and G. J. Nabel, "Immunopathology of highly virulent pathogens: insights from Ebola virus," *Nat. Immunol.*, vol. 8, no. 11, pp. 1159–1164, Nov. 2007.

[58] A. Sobarzo, D. E. Ochayon, J. J. Lutwama, S. Balinandi, O. Guttman, R. S. Marks, A. I. Kuehne, J. M. Dye, V. Yavelsky, E. C. Lewis, and L. Lobel, "Persistent Immune Responses after Ebola Virus Infection," *New England Journal of Medicine*, vol. 369, no. 5, pp. 492–493, Aug. 2013.

[59] S. J. Chapman and A. V. S. Hill, "Human genetic susceptibility to infectious disease," *Nat Rev Genet*, vol. 13, no. 3, pp. 175–188, Mar. 2012.

[60] A. L. Rasmussen, A. Okumura, M. T. Ferris, R. Green, F. Feldmann, S. M. Kelly, D. P. Scott, D. Safronetz, E. Haddock, R. LaCasse, M. J. Thomas, P. Sova, V. S. Carter, J. M. Weiss, D. R. Miller, G. D. Shaw, M. J. Korth, M. T. Heise, R. S. Baric, F. Villena, H. Feldmann, and M. G. Katze, "Host genetic diversity enables Ebola hemorrhagic fever pathogenesis and resistance," *Science*, vol. 346, no. 6212, pp. 987–991, Nov. 2014.

[61] A. Sanchez, K. E. Wagoner, and P. E. Rollin, "Sequence-based human leukocyte antigen-B typing of patients infected with Ebola virus in Uganda in 2000: identification of alleles associated with fatal and nonfatal disease outcomes," *J. Infect. Dis.*, vol. 196 Suppl 2, pp. S329–336, Nov. 2007.

[62] "Evidence for Declining Numbers of Ebola Cases - Montserrado County, Liberia, June - October 2014," http://www.cdc.gov/mmwr/preview/mmwrhtml/mm63e1114a2.htm, [Online; accessed 2016-02-29].

[63] "2014 Ebola Outbreak in West Africa - Reported Cases Graphs Ebola Hemorrhagic Fever, CDC," http://www.cdc.gov/vhf/ebola/outbreaks/2014-west-africa/cumulative-cases-graphs.html, [Online; accessed 2016-01-23].

[64] "Liberia Ebola Situation Report no. 58," http://www.unicef.org/appeals/files/UNICEF_Liberia_SitRep_29_October_2014.pdf, Oct. 2014, [Online; accessed 2016-03-28].

[65] Z. Feng, Y. Zheng, N. Hernandez-Ceron, and H. Zhao, "Designing public health policies to mitigate the adverse consequences of rural-urban migration via metapopulation modeling," in *Mathematical modeling for emerging and re-emerging infectious diseases, Chowell-Puente, C., Hyman, J.M. (Eds.)*. Springer-Verlag, 2015 (To appear), 2015.

[66] J. deMoraes, M. Camargo, M. deMello, B. Hersh, and J. Glasser, "The 1997 Measles Outbreak in Metropolitan So Paulo, Brazil: Strategic Implications of Increasing Urbanization. Chapter 8," in *Mathematical modeling for emerging and re-emerging infectious diseases, Chowell-Puente, C., Hyman, J.M. (Eds.)*. Springer-Verlag, 2015 (To appear), 2015.

[67] I. I. Bogoch, M. I. Creatore, M. S. Cetron, J. S. Brownstein, N. Pesik, J. Miniota, T. Tam, W. Hu, A. Nicolucci, S. Ahmed, J. W. Yoon, I. Berry, S. I. Hay, A. Anema, A. J. Tatem, D. MacFadden, M. German, and K. Khan, "Assessment of the potential for international dissemination of Ebola virus via commercial air travel during the 2014 west African outbreak," *The Lancet*, vol. 385, no. 9962, pp. 29–35, Jan. 2015.

[68] C. Poletto, M. Gomes, A. Pastore y Piontti, L. Rossi, L. Bioglio, D. Chao, I. Longini, M. Halloran, V. Colizza, and A. Vespignani, "Assessing the impact of travel restrictions on international spread of the 2014 West African Ebola epidemic," *Eurosurveillance*, vol. 19, no. 42, p. 20936, Oct. 2014.

[69] J. O. Lloyd-Smith, A. P. Galvani, and W. M. Getz, "Curtailing transmission of severe acute respiratory syndrome within a community and its hospital," *Proceedings of the Royal Society of London B: Biological Sciences*, vol. 270, no. 1528, pp. 1979–1989, Oct. 2003.

[70] F. Brauer, Z. Feng, and C. Castillo-Chavez, "Discrete epidemic models," *Math Biosci Eng*, vol. 7, no. 1, pp. 1–15, Jan. 2010.

[71] Z. Feng, A. N. Hill, P. J. Smith, and J. W. Glasser, "An elaboration of theory about preventing outbreaks in homogeneous populations to include heterogeneity or preferential mixing," *J. Theor. Biol.*, vol. 386, pp. 177–187, Dec. 2015.

VITA

VITA

Yiqiang Zheng was born in Shenyang, China. He graduated from Jilin University, Changchun, China, with his Bachelor of Science Degree in Mathematics and Applied Mathematics in June of 2007 and his Master of Science Degree in Applied Mathematics in June of 2009. In August of 2009, he started his Doctor of Philosophy degree in Mathematical Biology at Purdue University under the supervision of Professor Zhilan Feng. During his study at Purdue University, he also obtained his Master of Science Degree in Applied Statistics in the May of 2015.